

Self-Assembly of DNA Containing Non-nucleosidic Polyaromatic Building Blocks

Inauguraldissertation
der Philosophisch-naturwissenschaftlichen Fakultät
der Universität Bern

vorgelegt von
Florent Samain
aus Frankreich

Leiter der Arbeit:
Prof. Dr. R. Häner
Departement für Chemie und Biochemie der Universität Bern

Self-Assembly of DNA Containing Non-nucleosidic Polyaromatic Building Blocks

Inauguraldissertation
der Philosophisch-naturwissenschaftlichen Fakultät
der Universität Bern

vorgelegt von
Florent Samain
aus Frankreich

Leiter der Arbeit:
Prof. Dr. R. Häner
Departement für Chemie und Biochemie der Universität Bern

Von der Philosophisch-naturwissenschaftlichen Fakultät angenommen.

Bern, den 30. May 2008

Der Dekan:
Prof. Dr. P. Messerli

This work was supported by the University of Bern and the Swiss National Science Foundation.

Acknowledgements

Many people have influenced my life and my work in Bern and I would like to take this opportunity to thank them.

First of all, I am very thankful to Prof. Dr. Robert Häner and Dr. Vladimir Malinovskii. Not only did they supervise my work, but they also gave me the necessary support to complete it successfully. Discussions have led to new ideas and further development of my work.

Thanks to Prof. Dr. Vladimir Chirvony and Prof. Dr. Jean-Louis Reymond for having accepted to carefully read my manuscript and evaluate my work.

The realization of this work would not have been possible without the people from MS group and *Ausgabe*. I would like to thank them too. For her help about any administrative questions, a special thank goes to Mrs Rosmarie Rohner.

My days in Bern wouldn't be the same without excellent colleagues Nicolas Bouquin and Ivan Trkulja. With their support and optimistic attitude they helped me through all the ups and downs. Thanks to: Dr. Holger Bitterman, Andre Mätzener, Daniel Wenger, Josefine Reber and the other current members of the Häner group. Thanks to the colleagues of the Renaud groups with whom I had nice moments.

Et surtout un grand merci à ma famille , à mes parents et Hubert pour leur soutien et leurs encouragements. Que tous ceux qui, de près ou de loin, directement ou indirectement et de quelque manière que ce soit, ont contribué à la réussite de cette thèse, trouvent ici l'expression de ma profonde gratitude.

List of Publications:

1. F. Samain, V. L. Malinovskii, S. M. Langenegger and R. Häner, **Spectroscopic Properties of Pyrene-Containing DNA Mimics**, *Bioorg. Med. Chem.* **2008**, *16*, 27-33.
2. V. L. Malinovskii, F. Samain and R. Häner, **Helical Arrangement of Interstrand Stacked Pyrenes in a DNA Framework**, *Angew. Chem. Int. Ed.* **2007**, *46*, 4464-4467.
3. F. Samain, V. L. Malinovskii and R. Häner, **DNA-Directed Organization of Double Helical Foldamers**, *Article in preparation*.
4. F. Samain, V. L. Malinovskii and R. Häner, **Control of Double Helical Self-Assembly by a Single DNA Base Pair**, *Article in preparation*.

« Ce que nous appelons le hasard n'est et ne peut être que la cause ignorée d'un effet connu »

Dictionnaire philosophique 1764

Voltaire

Table of Contents

<i>Summary</i>	1
1. Introduction	3
1.1 Introduction	3
1.2 Structure of DNA	4
1.3 Forces Stabilizing Nucleic Acid Structure	7
1.3.1 Hydrogen Bonds	7
1.3.2 π - π Stacking Interactions	8
1.4 Chemical Modifications of Nucleotides	9
1.4.1 Non-nucleosidic Base Surrogates	10
1.4.2 Interstrand Stacked Building Blocks	11
1.4.3 Extended Stretches of Non-nucleosidic Building Blocks	13
1.5 Nanoarchitectures	14
1.5.1 DNA Foldamers	14
1.5.2 Helically Folding Oligomers	16
1.6 Aim of the Work	21
2. Spectroscopic Properties of Pyrene-Containing DNA Mimics	26
2.1 Abstract	26
2.2 Introduction	26
2.3 Results and Discussion	27
2.3.1 Thermal Denaturation Experiments	28
2.3.2 Pyrene Containing Single Strands	30
2.3.3 Investigation of Pyrene Containing Hybrids	35
2.4 Conclusion	42
2.5 Experimental Section	43
2.6 References	45
3. Helical Arrangement of Interstrand Stacked Pyrene in a DNA Framework	48
3.1 Abstract	48
3.2 Introduction	48
3.3 Results and Discussion	49
3.4 Conclusion	61
3.5 Experimental Part	62

3.6 References	64
4. DNA Containing Extended Stretches of Pyrene Building Blocks	67
4.1 Abstract	67
4.2 Introduction	67
4.3 Results and Discussion	68
4.3.1 Thermal Denaturation Experiments	68
4.3.2 Spectroscopic Studies	71
4.4 Conclusion	80
4.5 Experimental Section	80
4.6 References	82
5. Helical Arrangement in Alternative Systems	85
5.1 Abstract	85
5.2 Introduction	85
5.3 Results and Discussion	86
5.3.1 Thermal Denaturation Experiments	86
5.3.2 Spectroscopic Studies	90
5.4 Conclusion	100
5.5 Experimental part	100
5.6 References	102
6. Conclusions and Outlook	104
Annexes	106
Annex I Properties of DNA Containing Non-nucleosidic Phenanthroline Building Blocks	106
1. Abstract	106
2. Introduction	106
3. Results and Discussion	107
4. Conclusion	110
5. Experimental Section	111
6. References	113
Annex II Solid Phase Synthesis of Oligonucleotides	114
Annex III Fluorescence Properties of Pyrene	117
Annex IV Spectrometry and Study of Duplex Formation	120

Summary

DNA plays an eminent role in the design of well-defined nanostructures. The combination of the natural oligonucleotides with, novel, synthetic building blocks lead to a large increase in the number of possible construct and applications. Furthermore, natural DNA is well known to adopt an interstrand stacking structure. Within the set of building blocks that have been used in our group (phenanthrene, phenanthroline and pyrene), the pyrene was an excellent candidate for probing the stacking interactions and self-organization of non-nucleosidic building blocks in DNA. Due to its spectroscopic properties such as longer wavelength absorption and specific fluorescence emission when two pyrenes involve in stacking interactions, we investigated properties of DNA containing stretches of non-nucleosidic pyrene moieties within single and double strands. In addition fluorescence and circular dichroism spectroscopy gave insight on structural details and the interstrand helical organization within an entirely artificial section composed of fourteen consecutive achiral pyrenes.

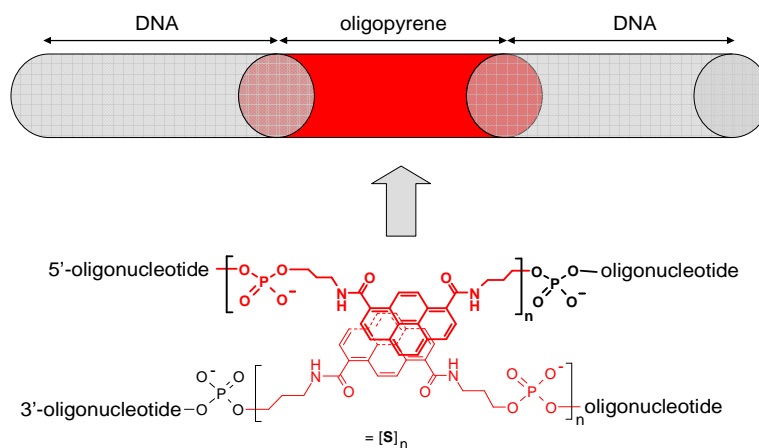


Figure 1: Schematic representation of an oligopyrene-stack embedded within a DNA duplex.

Hybrids containing one to seven pyrene building blocks per strand have been investigated in order to examine the influence of the replacement of base pairs on hybrid stability

firstly and secondly to the transition between the sandwich-type aggregation and the twisted pyrene conformation leading to a helical structure. The focus was then on using the construct in alternative systems consisting of a poly (dA)·(dT) framework and a short DNA scaffold. In addition, in order to go in more details, one hybrid containing fourteen achiral pyrene building blocks and only one G≡C base pair has been studied. It was shown that the oligopyrene strands was highly sensitive to the chiral environment of either G or C or G≡C base pair. The findings and the unique feature linked to only a G≡C base pair described in this work are very attractive for the design of novel intelligent materials and might provide the basis for applications in the area of molecular electronics, diagnostics as well as in nanotechnology.

Chapter 1. Introduction

Deoxyribonucleic acid (DNA) is a long polymer in a form of a twisted double strand (double helix) that is the major component of chromosomes and carries genetic information. DNA, which is found in all living organisms but not in some viruses, is self-replicating and is responsible for passing along hereditary characteristics from one generation to the next.

1.1 Introduction

The nucleic acid chemistry enjoyed growing interest since *Friedrich Miescher*, a Swiss Biologist who carried out the first systematic chemical studies of cell nuclei. He isolated in 1869 a phosphorus containing substance which he called “nuclein”, from the nuclei of pus cells (leukocytes) ¹. But the first direct evidence that DNA is the bearer of the genetic information came in 1944 through a discovery made by *Oswald T. Avery*, *Colin MacLeod*, and *Maclyn McCarty*². In the late 1940s, *Erwin Chargaff* and his colleagues found that the four nucleotide bases in DNA occur in different ratios in the DNAs of different organisms and that amount of certain bases are closely related.³ In the early 1950, *Rosalind Franklin* and *Maurice Wilkins* provided X-ray images that were crucial for determining the structure of DNA. By combining these informations with chemical properties of DNA and in agreement with *Chargaff's* rules, *James D. Watson* and *Francis Crick* postulated a three dimensional model in 1953 which is often said to mark the birth of modern molecular biology⁴. It consists of two helical DNA chains coiled around the same axis to form a right-handed double helix. The hydrophilic backbones of alternating deoxyribose and negatively charged phosphate groups are on the outside of the double helix, facing the surrounding water. The purine and pyrimidine bases of both strands are stacked inside the double helix, with their hydrophobic and nearly planar ring structures very close together and perpendicular to the long axis of the helix.

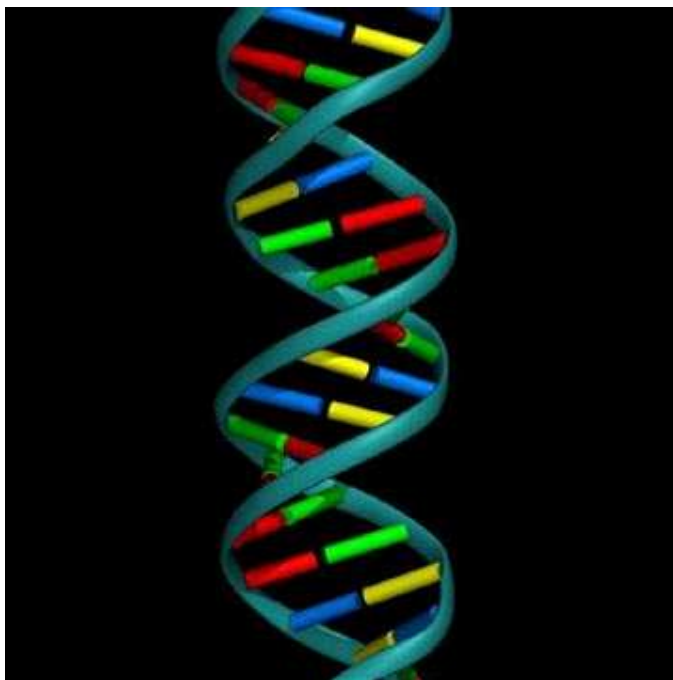


Figure 1.1 DNA double helix.⁵

In 1962, the Nobel Prize in Physiology or Medicine has been awarded to *Watson, Crick,* and *Wilkins* for their accomplishments. The Chemical methods for synthesizing nucleic acids have been developed primarily by *H. Gobind Khorana*⁶ in the 1970s followed in the 1980s by *automated DNA synthesis* which was developed by *Caruthers*⁷ and *Köster*⁸ and based on phosphoramidite chemistry. This method has been improved and nowadays a huge variety of modified types of nucleic acids can be synthesized in an automated way.

1.2 Structure of DNA

DNA is a polymer of single units called nucleotides. Each nucleotide is made up of a heterocyclic base, a pentose sugar, and a phosphate residue. There are four major nucleosides: adenine (A), thymine (T), guanine (G), and cytosine (C) (Figure 1.2). DNA has equal numbers of adenine and thymine residues ($A=T$) and guanine and cytosine residues ($G=C$). Deoxyribonucleosides are linked with each other to form a chain whose phosphates bridge the 3' and 5' positions of neighbouring ribose units. Finally two DNA single strands can form a

duplex in which the bases of one strand pair with the bases of the other strand through specific hydrogen bonds.

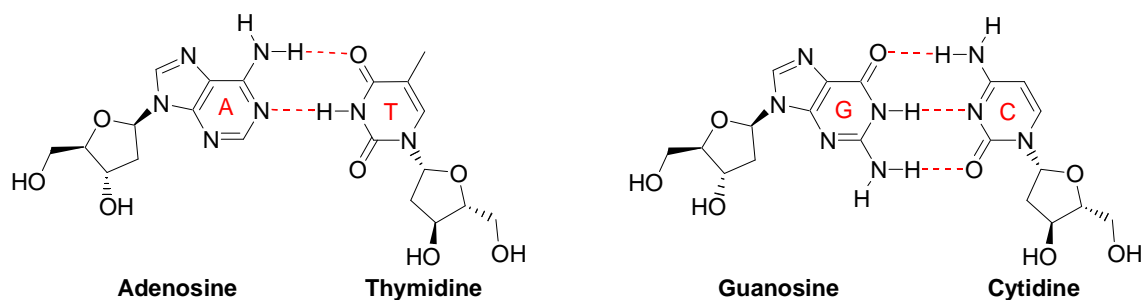


Figure 1.2 Watson-Crick base pairs, A-T and G-C.

The spatial relationship between these strands creates a major and minor groove formed by the sugar-phosphate backbone between the two strands. The grooves differ in depth and width (Figure 1.3).

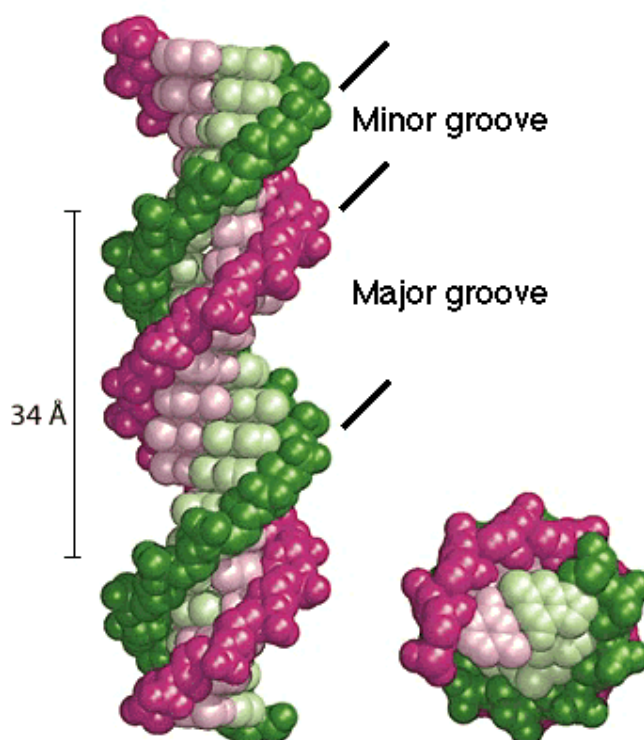


Figure 1.3 Major and Minor groove of B- DNA.⁹

Double-helical DNA can assume three major conformations: B-DNA, A-DNA, and Z-DNA. B-DNA and A-DNA form the right-handed double helix whereas Z-DNA adopts a left-handed double helix. Under dehydrating conditions, *in vitro*, B-DNA changes to A-DNA, which forms a wider and flatter right-handed helix than B-DNA. Furthermore polynucleotides with alternating purines and pyrimidines, such as poly d(G-C)·poly d(G-C), assume the Z conformation at high salt concentrations (Figure 1.4).

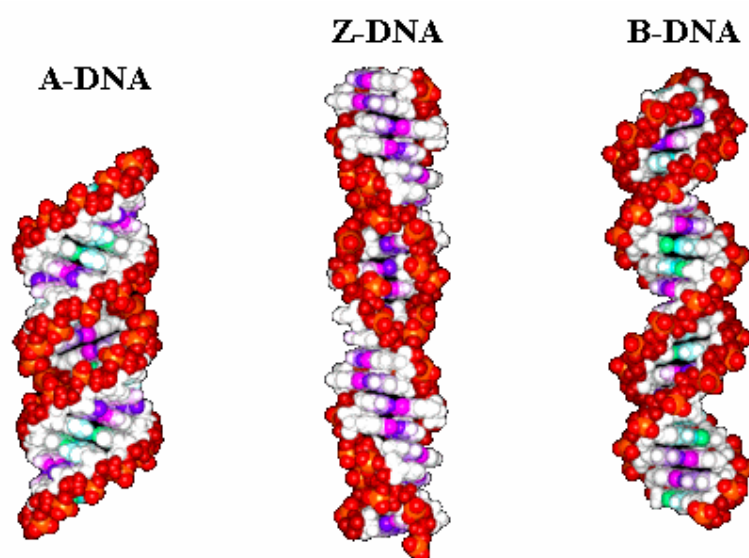


Figure 1.4 Structure of A, Z and B-DNA.¹⁰

B-DNA has 10 bases per turn whereas the A-type helix has 11 bases per turn. The major groove of B-DNA is wide and the minor groove is narrow, in A-DNA the major groove is narrow and deep and the minor groove is broad and shallow. Z-DNA has 12 base pairs, a deep minor groove and a shallow major groove. A difference between the A- and the B-duplex is also found in the sugar pucker mode (Figure 1.5). The A-DNA underlines a C3'-endo conformation whereas the B-DNA underlines a C2'-endo conformation. The structural features of ideal A-, B-, and Z-DNA are summarized in Table 1.1.

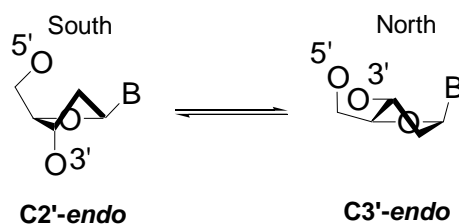


Figure 1.5 The sugar pucker modes.

Table 1.1 Comparison of helical parameters.¹¹

Entry	A-DNA	B-DNA	Z-DNA
Helicity	Right-handed	Right-handed	Left-handed
Sugar pucker	C(3')-endo	C(2')-endo	C(2')-endo in pyrimidine and C(3')-endo in purine
Number of bases per turn	11	10	12
Distance Between neighbouring base-pairs (Å)	2.9	3.3 – 3.4	3.7
Dislocation of base-pairs from the axis (Å)	4.5	-0.2 to -1.8	-2 to -3
Tilt of bases (°)	20	-6	7

1.3 Forces Stabilizing Nucleic Acid Structures

The major forces stabilizing DNA structure are of two kinds: those in the plane of the bases (horizontal) due to hydrogen bonding and those perpendiculars to the bases planes (base stacking).

1.3.1 Hydrogen Bonds

In general, a hydrogen bond is formed if a hydrogen atom H connects two atoms of higher electronegativity. These bonds can occur between molecules (intermolecularly), or within different parts of a single molecule (intramolecularly). Compared with covalent bonds and ionic bonds, hydrogen bonds are weaker; on the other hand they are stronger than van der Waals forces. They play a key role in the stabilization of nucleic acid structure. The Watson-Crick hydrogen bonds are responsible for the A-T and G-C pairing in the duplex.¹²

Furthermore nucleic acid hydrogen bonds have been the topic of numerous experimental, theoretical studies and several review articles.¹³⁻¹⁹

1.3.2 π - π Stacking Interactions

Aromatic interactions play a major role in biological systems such as: the double helical structure of DNA, stabilization of proteins and peptides, molecular recognition, the packing of aromatic molecules in crystals and many others.²⁰⁻²² But the understanding and prediction of these interactions are difficult, because unlike hydrogen bond which are characterized by an electrostatic point-to-point interaction, aromatic interactions are made up of a combination of forces including van der Waals, electrostatic, and hydrophobic interactions. The following part is an overview of these different contributions.²³

Van der Waals interactions. They are the sum of the dispersion and repulsion energies and vary with r^{-6} (r is the distance between the nuclear positions of the atoms).

Electrostatic interactions between partial atomic charges. Electronegative atoms like nitrogen and oxygen polarize the electron density of heteroatomic molecules such as nucleobases and so these atoms and neighbouring atoms are associated with partial atomic charges. These interactions vary with r^{-1} in agreement with Coulomb's law²⁴:

$$V \sim q_i q_j / r_{ij}$$

As a consequence, they are relatively long ranging effects (q_i and q_j are the magnitude of the charges and r_{ij} is their separation).

Electrostatic interactions between the charge distributions associated with the out-of-plane π -electron density. The nuclei of aromatic molecules have a characteristic charge distribution, with a positively charged σ -framework which is sandwiched between two regions of negatively charged π -electron density. These interactions vary with r^{-5} and are determined by the geometry.²¹

Electrostatic interactions between the charge distributions associated with the out of plane - electron density and the partial atomic charges. This term varies roughly with r^{-4} and is therefore quite sensitive to geometry.²⁴

Interaction of aromatic residues and solvent. These effects are commonly called solvation effects, desolvations, solvophobic forces, solvation-driven forces or hydrophobic effects. The contribution of this interaction to the π - π stacking remains a controversial debate.²⁵⁻²⁷ *Diederich et al.* found a strong linear relationship between the free enthalpy and the solvent polarity.²⁸ They deduced that water is the best solvent for apolar bonding. However *Gellman's* experiments contrast with these findings. They suggest no significant solvent-induced interactions.²⁹

1.4 Chemical Modifications of Nucleotides

Chemically modified nucleotide building blocks have been of great importance for the understanding of the mechanisms and stereochemical aspects of numerous biochemical reactions and processes are involved in.³⁰ Changes can occur on the phosphate linker, sugar backbone or the nucleobases (Figure 1.6).

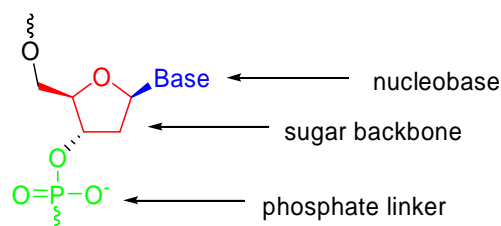


Figure1.6 Sites of possible modifications of nucleotides.

Each of these modifications results in different effects and provides a new aspect in understanding of nucleic acid chemistry and their applications. Modified phosphate linkages can improve the cell penetration or nuclease resistance. They can also modify the charge of the phosphate linkage in order to increase the stability of the DNA or RNA. The sugar modifications are of interest for the development of diagnostic probes and tools in molecular biology as well as in antisense and antigene therapy.³¹⁻³²⁻³³ Modified bases are used in order to extend the genetic code, to study the physical properties of natural bases, to analyze the

interactions between DNA and proteins or for improving the binding properties for diagnostic applications. They occur mainly through altered hydrogen-bonding patterns.^{34, 35} *Benner et al.*³⁶⁻⁴¹ have described the first example of base pairs with modified hydrogen-bonding patterns. A lot of other groups have worked on this topic. For instance *Matsuda et al* designed new base pair combinations consisting of four H-bonds as shown in Figure 1.7.⁴²

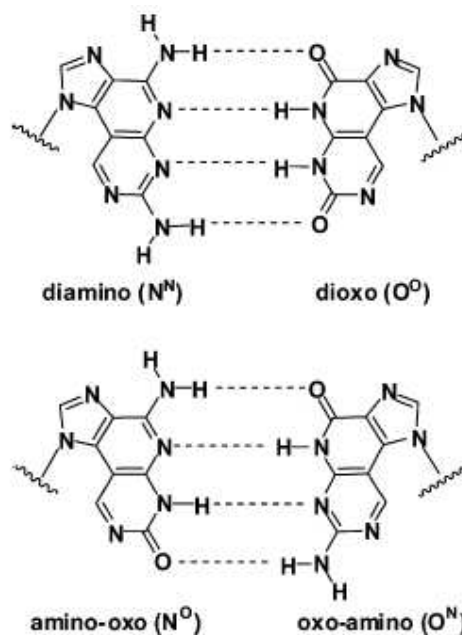


Figure 1.7 Proposed new base pairs consisting of four H-Bonds.

Furthermore, the lack of hydrogen bonding is compensated by hydrophobic bases which stabilize the DNA duplex through π - π stacking of aromatic rings.⁴³⁻⁴⁹ Studies of replication by DNA-polymerases showed that the modified bases can be replicated despite the lack of hydrogen bond complementaries.⁵⁰⁻⁵³

1.4.1 Non-Nucleosidic Base Surrogates

Besides the specificity of DNA base pairs recognition giving the chemical basis for genetics, a large new area is gaining interest consisting in the use of nucleic acids as a scaffold for the construction of molecular architectures.⁵⁴⁻⁵⁷ The advantages of using nucleic acids as objects for the designed construction of assemblies are: the ability of self-organization; their physical and chemical stability; they are amenable to a large variety of chemical, physical and

biological manipulations; nonnatural building blocks can be readily incorporated; they can be arranged for the construction of stabilized one- to three-dimensional structures.⁵⁸ Furthermore the repetitive and well defined structural features of nucleic acids and related types of oligomers render them building blocks suitable for the generation of nanometer-sized molecular structures.⁵⁹ Within this context of developing non-nucleosidic DNA-like building blocks, our group has investigated non-nucleosidic and non-hydrogen bonding building blocks.

1.4.2 Interstrand Stacked Building Blocks

One part of our research is focused on the incorporation of non-nucleosidic building blocks. Two types of aromatic derivative building blocks with flexible linker have been introduced into DNA such as phenanthrene and phenanthroline derivatives.^{47, 48} According to spectroscopic data, the polyaromatic building blocks are involved in stacking interactions (Figure 1.8).

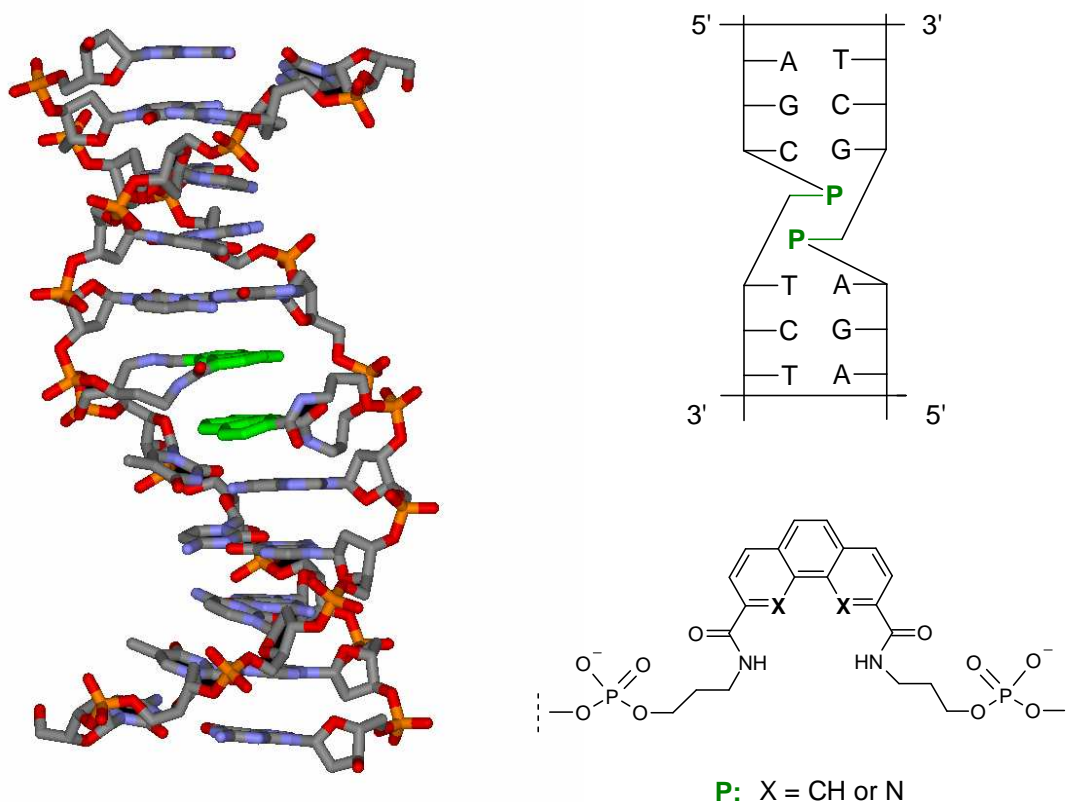


Figure 1.8 Scheme of a modified DNA duplex showing two non-nucleosidic building blocks (green) in an interstrand arrangement.⁵⁸

In addition, a third aromatic derivative with an extended π -system, pyrene was used for the same purpose. Pyrene is highly fluorescent and is known to give rise to excimer fluorescence if two molecules are stacked. This property was used to investigate the relative geometry of stretches of pyrene building blocks in the context of a DNA duplex. The spectrophysical consequence of excimer formation is the appearance of fluorescence emission with a significant red shift (up to 100 nm). In fact this was observed for the duplex in which two pyrenes are interstrand stacked (Figure 1.9).⁶⁰

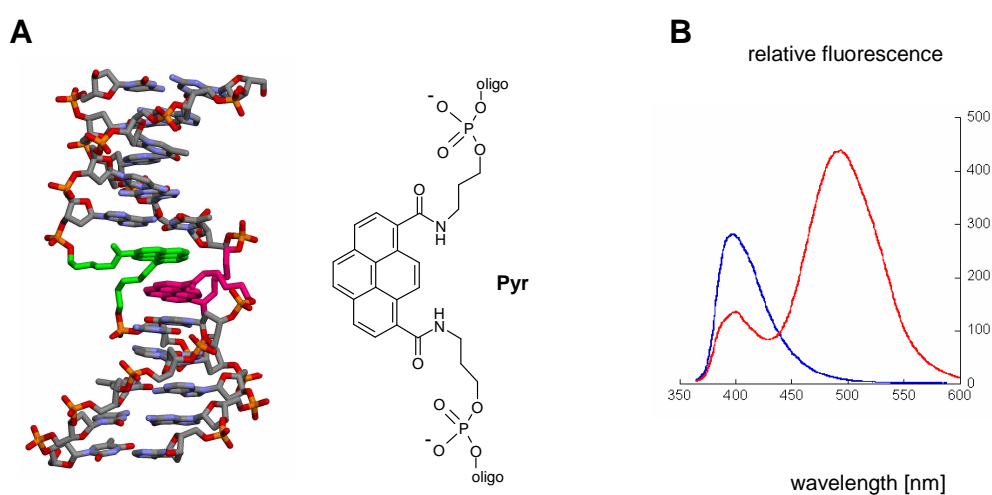


Figure 1.9 A: DNA model containing two interstrand stacked pyrenes; B: Fluorescence emission spectra of a single strand (blue) and duplex (red) containing pyrenes in opposite positions.⁵⁸

1.4.3 Extended Stretches of Non-nucleosidic Building Blocks

Replacement of two or more base pairs by non-nucleosidic phenanthrene building blocks with three carbon linkers was well tolerated having almost no influence on hybrid stability compared to an unmodified duplex. The middle part, which represents a considerable fraction of this duplex, is stabilized merely by interstrand stacking interactions, as shown by *Langenegger and Häner*.⁶¹

Molecular modeling suggests that the interstrand stacked arrangement of the phenanthrene moieties leads to a significant lengthening of the DNA (Figure 1.10). This was also supported by gel electrophoresis data.⁶¹

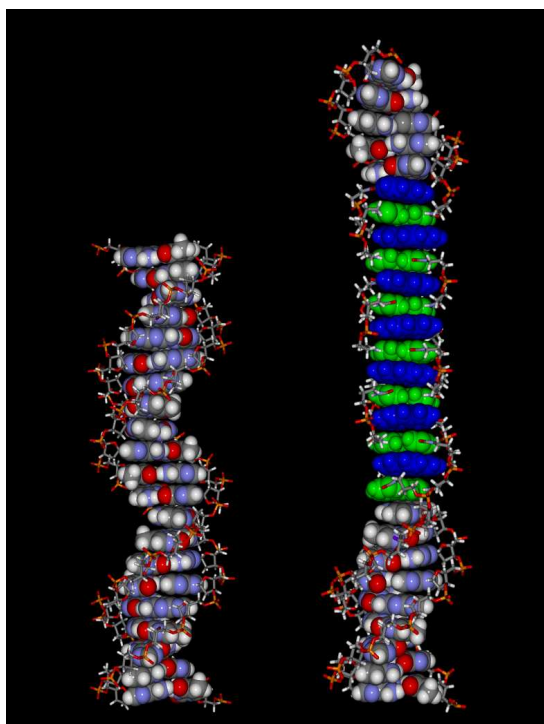


Figure 1.10 Amber-minimized models of a 21-mer DNA duplex (left) and a 21-mer DNA mimic in which seven base pairs have been replaced with phenanthrenes. The phenanthrene residues of the two strands are shown in blue and green (adopted from ⁶¹).

1.5 Nanoarchitectures

1.5.1 DNA Foldamers

Foldamers have been defined by *Gellman* as “polymers with a strong tendency to adopt a specific compact conformation” or more restrictively by *Moore* as “oligomers that fold into a conformationally ordered state in solution, the structures of which are stabilized by a collection of noncovalent interactions between nonadjacent monomer units”.⁶² Artificial folded structures, which are covered by the same definition were studied extensively long before the term foldamer was coined and include synthetic (non-natural) proteins, helical polymers, and nucleic acids, among others.

DNA which carries the genetic information relies on basic self-assembly processes: the assembly of multiple subunits into well-defined modular supramolecular devices. The

secondary structure of DNA results from hydrogen bonding between side chains. Moreover nucleic acids can be controlled to build new 3D molecular architectures with supramolecular properties. As a result and not surprisingly, DNA foldamers offer a great source of inspiration to the chemist.⁵⁵ They can potentially lead to the development of various nanometer-sized structures.

Pioneering research extending over a period of more than 15 years by *N. C. Seeman*⁶³⁻⁶⁷ has laid a foundation for the construction of structures using DNA as scaffolds, which may finally serve as frameworks for the construction of nanoelectronic devices. In fact macrocycles, DNA quadrilateral, Holliday junctions, and other structures were designed. Figure 1.11 shows a stable branched DNA junction made by DNA molecules.

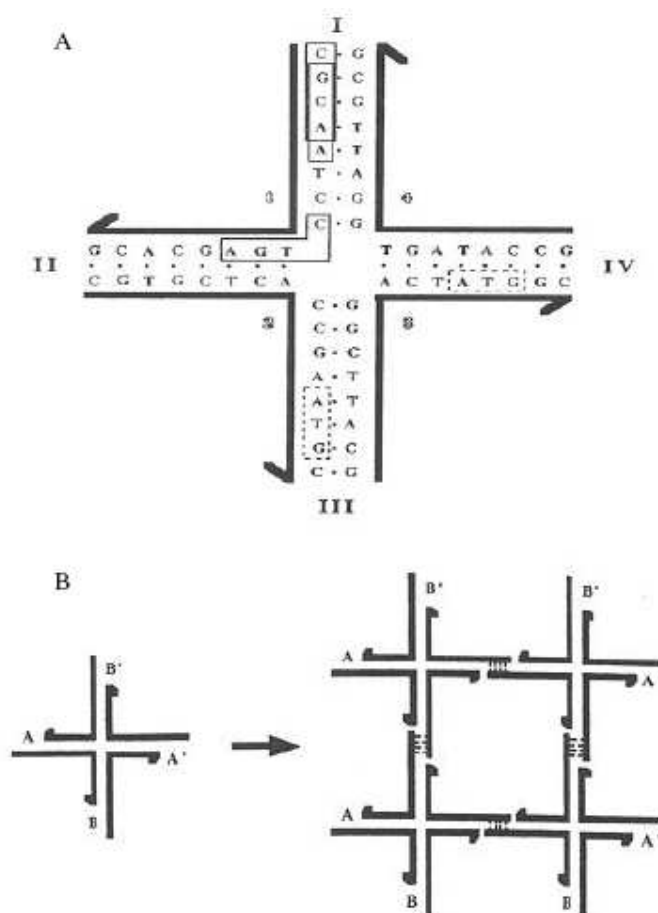


Figure 1.11 A: A four-armed stable branched junction made from DNA molecules; B: use of the branched junction to form periodic crystals.⁶⁴

There has been a huge interest in recent years to develop concepts and to design systems based on DNA molecules. Nowadays further developments have been reported in this field allowing the formation of distinct motifs from short synthetic oligonucleotides. These motifs

are then used as building blocks which can self-assemble by hybridization to form larger, two and three-dimensional elements.⁶⁸ Moreover, in order to mimic biological helices, such as the double-stranded of DNA, the design and synthesis of polymers or oligomers has attracted great attention.

1.5.2 Helically Folding Oligomers

Since the discovery of DNA double helix, the generation of helical structures that are not based on the hydrogen-bond-mediated pairing scheme of the nucleobases or related derivatives has been a highly competitive aspect in the field of molecular self-organisation.⁶⁹⁻⁷² Chemists have been looking for new molecules with the ability to form helical structures through non covalent interactions such as π -stacking, metal coordination, electrostatic interactions, and hydrogen bonds.⁷¹

For instance, in artificial analogs of DNA, the hydrogen-bond-mediated pairing scheme is replaced by metal coordination. This has been described by *Shionoya et al.* They prepared a heptanucleotide including oligomer of hydroxyl-pyridone. Upon addition of copper (II) ions, a double-stranded DNA type structure is formed (Figure 1.12).

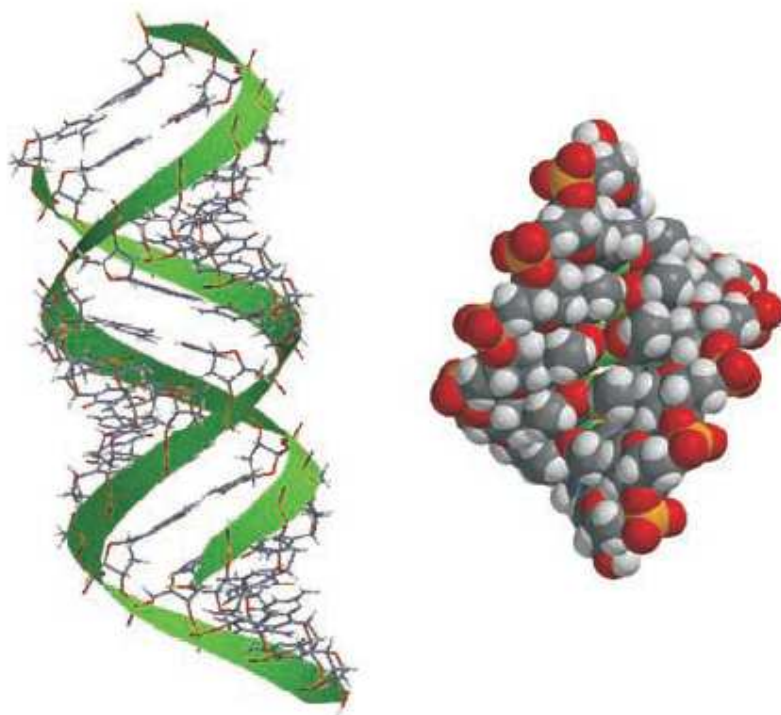


Figure 1.12 Double-stranded DNA and a CPK model of the artificial pentanuclear metalla-DNA synthesized by Shionoya et al.⁷³

Thus a large variety of synthetic foldamers or oligomers exists that are able to fold into well-defined conformations in solution. There are two classes of foldamers: single-stranded foldamers that only fold and multiple-stranded foldamers that both associate and fold. The structure of the subunits (π -conjugated systems for instance) combined with accumulation of non-covalent interactions lead to a specific folding. The major challenge is the need to control the conformation of chain molecules in solution. Recent advances in this field have provided oligomers with a high degree of conformational order.⁷²

For example *Moore and al.* have shown that *m*-phenylene ethynylene oligomers in polar solvents exhibit a unique helical conformation which involves π -stacked aromatic residues (figure 1.13).⁷⁴

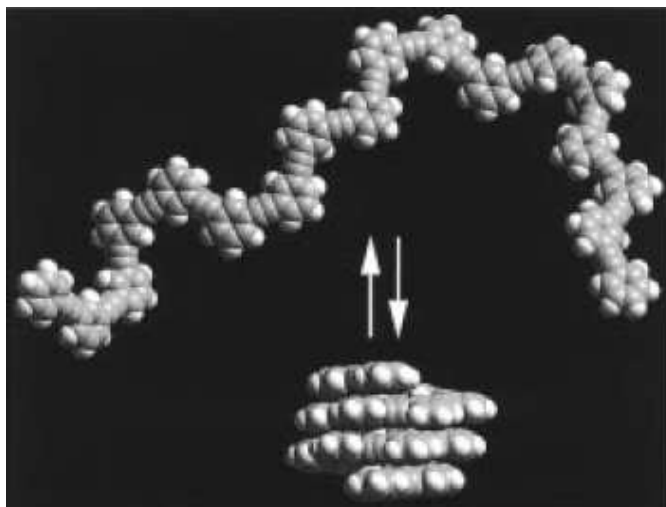


Figure 1.13 A space-filling model showing the proposed conformational equilibrium for a phenylene ethynylene oligomer. (Adopted from ⁷⁴)

Furthermore helices can also intertwine and form double-helical structures which allow much more extensive intermolecular stacking interactions (Figure 1.14). ⁷⁵

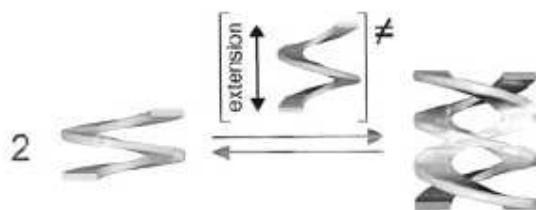


Figure 1.14 The intertwining equilibrium of helices.

A very interesting class of double helix forming foldamers is based on aromatic oligoamides as introduced by Lehn and Huc.⁷⁶ They are formed from alternating 2,6-diaminopyridines and 2,6-pyridinedicarboxylic acids. Helical conformations are induced by intramolecular hydrogen bonds. Within the double helix the two strands are held together primarily by aromatic interactions between pyridine rings located on top of each other, whereas H-bonds occur intramolecularly within each strand being responsible for the curvature of the helix (figure 1.15). ⁶²

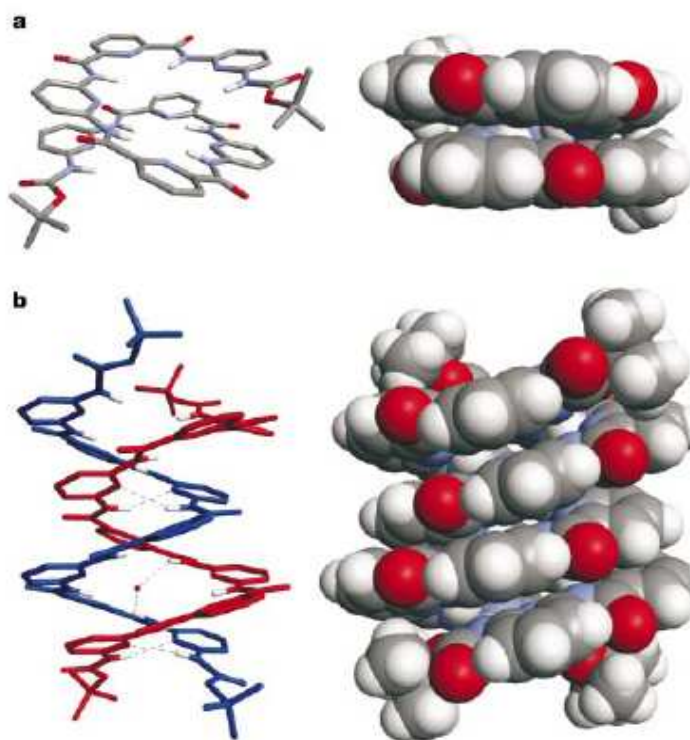


Figure 1.15 a: Single helix b: Double helix dimer. Interstrand hydrogen bonds (black dotted lines); carbon, grey; hydrogen, white; nitrogen, blue; oxygen, red. (adopted from ⁷⁶).

Another interesting and unique feature consists of conformational transition of helical oligomers called helix inversion. They may be uncontrolled and be the result of intrinsic dynamics of oligomers. They can also be triggered by external stimuli such as change in temperature, solvent or by irradiation by light.⁶² DNA is known as a biological polymer to undergo inversion of helicity driven by salt concentration and temperature. Some static helical polymers and chloral oligomers also exhibit a transition in their helicities, but their processes are not reversible. Several synthetic, dynamic helical polymers exhibit a reversible P-M (helix-helix transition) transition by changing the external conditions, such as temperature, solvent or light irradiation.⁷⁷⁻⁷⁹

Helical polyacetylenes bearing amino acids as the pendants also showed inversion of the helicity by changing the temperature or solvent, mainly resulting from the “on and off” fashion of the intramolecular hydrogen bonding between the pendant amide groups in nonpolar and polar solvents.⁸⁰⁻⁸³ Few examples of helical aromatic oligoamides bearing asymmetric centers have been also reported. In the presence of a chiral center, the right- and left-handed helices become diastereoisomers, and their proportions may differ (Figure 1.16).

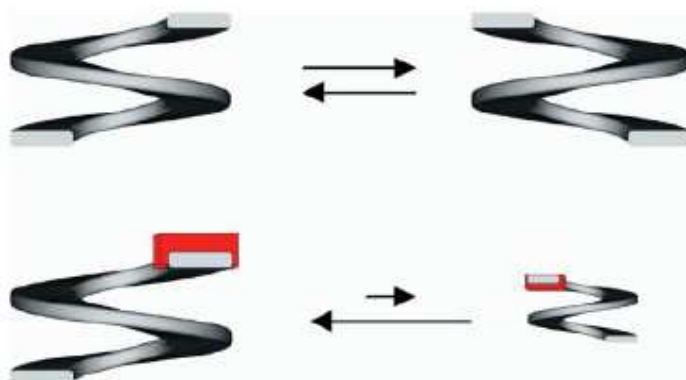


Figure 1.16 schematic representations of the equilibria between enantiomeric left- and right-handed helices (top), and between diastereoisomeric left- and right-handed helices (bottom).⁷⁵

It is also important to note that most reports describe the folding of oligomers with rather rigid structures in organic solvents.^{86, 87}

The next important and attractive challenge, which has implications for biological helices, superstructures and functions, will be not only to mimic biological helices, but also to develop supramolecular helical assemblies with a controlled helix-sense, and this may also provide a clue for the construction of advanced chiral materials.⁸⁸

1.6 Aim of the Work

Our group aims at the design and synthesis of secondary structural DNA-mimics containing non-nucleosidic, non-hydrogen bonding building blocks. We have developed various non-nucleosidic building blocks, which can be incorporated into DNA. Phenanthrene or phenanthroline derivatives with flexible linkers act as non-hydrogen bonding nucleobase surrogates (Figure 1.17). Complementary oligonucleotides containing such modifications in opposite position form stable hybrids. Moreover DNA containing extended stretches of phenanthrene building blocks has been described and reported.

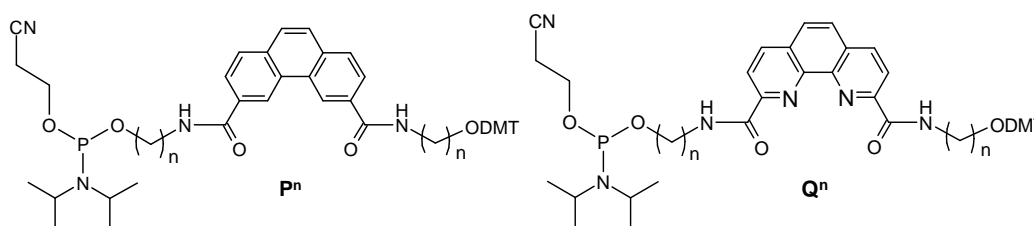


Figure 1.17 Polyaromatic building blocks Pⁿ: phenanthrene; Qⁿ: Phenanthroline.

Within the set of building blocks that have been used (phenanthrene, phenanthroline and pyrene) the pyrene molecule is an ideal candidate for probing the stacking interactions of polyaromatic building blocks in DNA due to its spectroscopic properties: long wavelength absorption, fluorescence properties (Figure 1.18).

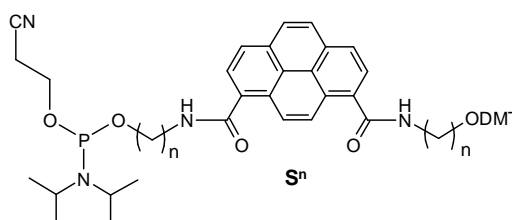
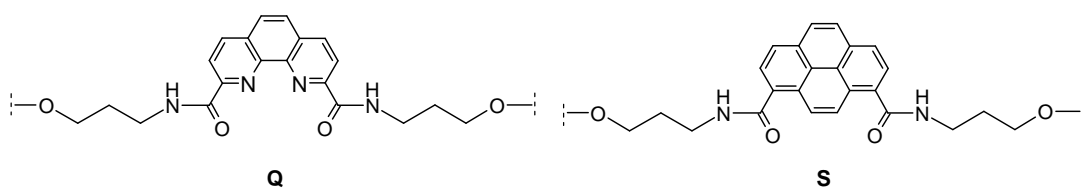


Figure 1.18 Sⁿ: Pyrene building blocks.

Consequently my work consisted in investigating DNA containing multiple phenanthroline and pyrene building blocks. The idea was to examine the influence of two or more base pairs replacement on hybrid stability firstly in case of homogeneous and secondly in case of heterogeneous hybrids. We started out with the phenanthroline and pyrene building blocks having three carbon linkers.



(5') AGC TCG GTC **XXC** GAG AGT GCA
 (3') TCG AGC CAG **XXG** CTC TCA CGT

X = Q, S

Hybrids were to be studied by thermal denaturation experiments. Furthermore fluorescence properties of oligomers containing pyrene derivatives should give insight on structural details. The behavior as well as the spectroscopic properties of DNA containing non nucleosidic phenanthroline and pyrene building blocks will be discussed.

A self-organizing system which is composed of two oligopyrene strands with achiral pyrene building blocks will be described.

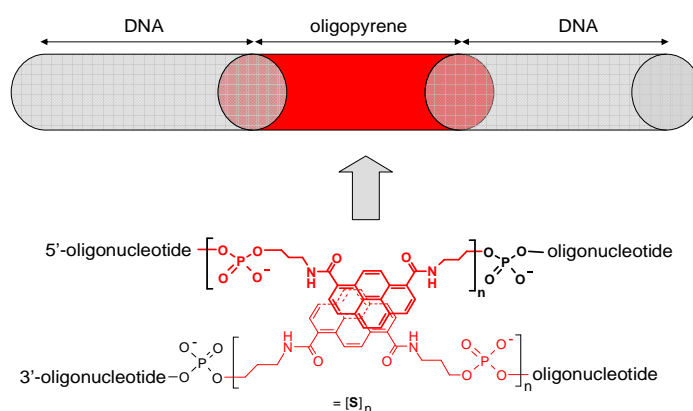


Figure 1.19 Schematic representation of an oligopyrene-stack embedded within a DNA duplex.

Moreover further area of our interest was the investigation of this helical arrangement of the pyrenes in different systems, embedded either in a poly (dA)·(dT) or in a short DNA scaffold consisting of five bases per strand and one base per strand.

References

1. Mirsky A. E. *Scientific American* **1968**, 218, 78.
2. Avery O.T., MacLeod C.M., McCarty M., *Journal of Experimental Medicine* **1944**, 79 (2), 137.
3. a) Chargaff E. *Journal of Cellular and Comparative Physiology* **1951**, 38, 41;
b) Chargaff E. *Federation Proceedings* **1951**, 10, 654.
4. a) Watson J. D., Crick F. H. C. *Nature* **1953**, 171, 737;
b) Watson J. D., Crick F. H. C. *Nature* **1953**, 171, 964.
5. <http://www.sciencemuseum.org.uk/on-line/lifecycle/135.asp>.
6. Khorana H. G., Tener G. M., Moffatt J. G., Pol E. H. *Chem. Ind. (London)* **1956**, 1523.
7. Matteucci M. D., Caruthers M. H. *J. Am. Chem. Soc.* **1981**, 103, 3185.
8. Sinha N. D., Biernat J., McManus J., Koster H. *Nucleic Acids Res.* **1984**, 12, 4539.
9. <http://138.192.68.68/bio/Courses/biochem2/DNA/DNAStructure.html>.
10. <http://www.lmb.uni-muenchen.de/groups/Biostruc/chap-08/chap-08-slides.html>.
11. Blackburn G. M., Gait M. J. *Nucleic Acids in Chemistry and Biology* **1996**., RSC Publishing.
12. Saenger W., *Principles of Nucleic Acid Structure*, Springer-Verlag, New York **1984**.
13. Guerra C. F., Bickelhaupt F. M., Snijders J. G., Baerends E. J. *J. Am. Chem. Soc.* **2000**, 122, 4117.
14. Kryachko E. S. *NATO Science Series, II: Mathematics, Physics and chemistry* **2003**, 116, 539.
15. Ogawa T., Kurita N., Sekino H., Kitao O., Tanaka S., *Chem Phys. Lett.* **2003**, 374, 271.
16. Sponer J. V., Leszczynski J., Hobza P. *THEOCHEM* **2001**, 573, 43.
17. Rueda M., Luque F. J., Orozco M. *Biopolymers* **2001**, 61, 52.

18. Dingley A. J., Masse J. E., Peterson R. D., Barfield M., Feigon J., Grzesiek S. *J. Am. Chem. Soc.* **1999**, *121*, 6019.
19. Gaffney B. L., Kung P.-P., Wang C., Jones R. A. *J. Am. Chem. Soc.* **1995**, *117*, 12281.
20. Chessari G., Hunter C. A., Blanco J. L. J., Low C. R., Vinter J. G. *NATO ASI Series, Series C: Mathematical and Physical Sciences* **1999**, 526, 331.
21. Hunter C. A. *J. Mol. Biol.* **1993**, *230*, 1025.
22. Hunter C. A. *Philosophical Transactions of the Royal Society of London, Series A: Mathematical, Physical and Engineering Sciences* **1993**, 345, 77.
23. Langenegger S. M., *Ph.D. Thesis - Department of Chemistry and Biochemistry, University of Bern – 2005*.
24. http://www.bip.bham.ac.uk/osmart/course/os_non.html.
25. Diederich F., Smithrud D. B., Sanford E. M., Wyman T. B., Ferguson S. B., Carcanague D. R., Chao I., Houk K. N. *Acta Chem. Scand.* **1992**, *46*, 205.
26. Smithrud D. B., Diederich F. *J. Am. Chem. Soc.* **1990**, *112*, 339.
27. Smithrud D. B., Wyman T. B., Diederich F. *J. Am. Chem. Soc.* **1991**, *113*, 5420.
28. Meyer E. A., Castellano R. K., Diederich F. *Angew. Chem. Int. Ed.* **2003**, *42*, 1210.
29. Gellman S. H., Haque T. S., Newcomb L. F. *Biophys. J.* **1996**, *71*, 3523.
30. Mathis G., *Ph.D. Thesis – Department of Chemistry and Biochemistry, University of Bern – 2004*.
31. De Mesmaeker A., Haener R., Martin P., Moser H. E. *Acc. Chem. Res.* **1995**, *28*, 366.
32. Prevot-Halter I., Leumann C. J. *Bioorg. Med. Chem. Lett.* **1999**, *9*, 2657.
33. Buchini S., Leumann C. J. *Curr. Opin. Chem. Biol.* **2003**, *7*, 717.
34. Kool E. T. *Curr. Opin. Chem. Biol.* **2000**, *4*, 602.
35. Kool E. T. *Biopolymers* **1998**, *48*, 3.
36. Lutz M. J., Held H. A., Hottiger M., Hubscher U., Benner S. A. *Nucleic Acids Res.* **1996**, *24*, 1308.
37. Horlacher J., Hottiger M., Podust V. N., Hubscher U., Benner S. A. *Proc. Natl. Acad. Sci. USA* **1995**, *92*, 6329.
38. Lutz M. J., Horlacher J., Benner S. A. *Bioorg. Med. Chem. Lett.* **1998**, *8*, 1149.
39. Bain J. D., Switzer C., Chamberlin A. R., Benner S. A. *Nature* **1992**, *356*, 537.
40. Piccirilli J. A., Krauch T., Moroney S. E., Benner S. A., *Nature* **1990**, *343*, 33.

41. Sismour A. M., Lutz, S., Park J. H., Lutz M. J., Boyer P. L., Hughes S. H., Benner S. A. *Nucleic Acids Res.* **2004**, *32*, 728.
42. Minakawa N., Kojima N., Hikishima S., Sasaki T., Kiyosue A., Atsumi N., Ueno Y., Matsuda A. *J. Am. Chem. Soc.* **2003**, *125*, 9970.
43. Mathis G., Hunziker J. *Angew. Chem. Int. Ed.* **2002**, *41*, 3203.
44. Brotschi C., Leumann C. J. *Angew. Chem. Int. Ed.* **2003**, *42*, 1655.
45. Brotschi C., Mathis G., Leumann C. J. *Chem. Eur. J.* **2005**, *11*, 1911.
46. Guckian K. M., Krugh T. R., Kool E. T. *Nature Struct. Biol.* **1998**, *5*, 954.
47. Langenegger S. M., Häner R., *Helv. Chim. Acta* **2002**, *85*, 3414.
48. Langenegger S. M., Häner R., *Tetrahedron Lett.* **2004**, *45*, 9273.
49. Moran S., Ren R. X., Kool E. T., *Proc. Natl. Acad. Sci. USA* **1997**, *94*, 10506.
50. Fa M., Radeghieri A., Henry A. A., Romesberg F. E., *J. Am. Chem. Soc.* **2004**, *126*, 1748.
51. Henry A. A., Olsen A. G., Matsuda S., Yu C., Geierstange B. H., Romesberg F. E., *J. Am. Chem. Soc.* **2004**, 6923.
52. Berger M., Wu Y., Ogawa A. K., McMinn D. L., Schultz P. G., Romesberg F. E., *Nucleic Acids Res.* **2000**, *28*, 2911.
53. Henry A. A., Yu C., Romesberg F. E. *J. Am. Chem. Soc.* **2003**, *125*, 9638.
54. Seeman N. C., *Nature* **2003**, *421*, 427.
55. Bashir R., *Superlattices and Microstructures* **2001**, *29*, 1.
56. Shih W. M., Quispe J. D., Joyce G. F., *Nature* **2004**, *427*, 618.
57. Mirkin C. A., *Inorg. Chem.* **2000**, *39*, 2258.
58. Langenegger S. M., Bianke G., Tona R., Häner R., *Chimia* **2005**, *59*, 794.
59. Wengel J., *Org. Biomol. Chem.* **2004**, *2*, 277.
60. Langenegger S. M., Häner R., *Chem. Commun.* **2004**, 2792.
61. Langenegger S. M., Häner R., *ChemBioChem* **2005**, *6*, 2149.
62. Hecht S., Huc I., *Foldamers: Structure, properties, and Applications*, Wiley-VCH, **2007**.
63. Seeman N. C., *J. Theor. Biol.* **1982**, *99*, 237.
64. Seeman N. C., *The use of branched DNA for nanoscale fabrication*, *Nanotechnology* **1991**, 149.
65. Seeman N. C., Zhang Y., Chen J., *J. Vac. Sci. Technol.* **1993**, *A12*, 1895.
66. Winfree E., Liu F., Wenzler L., Seeman N. C., *Nature* **1998**, *394*, 539.
67. Seeman N. C., *Annu. Rev. Biophys. Biomol. Struct.* **1998**, *27*, 225.

68. Feldkamp U., Niemeyer C. M., *Angew. Chem. Int. Ed.* **2006**, *45*, 1856.
69. Piguet C., Bernardinelli G., Hopfgartner G., *Chem Rev.* **1997**, *97*, 2005.
70. Gellman S. H., *Acc. Chem. Res.* **1998**, *31*, 173.
71. Rowan A. E., Nolte R. J. M., *Angew. Chem. Int. Ed.* **1998**, *37*, 63.
72. Hill D. J., Mio M. J., Prince R. B., Hughes T. S., Moore J. S., *Chem Rev.* **2001**, *101*, 3893.
73. Albrecht M., *Angew. Chem.* **2005**, *117*, 6606; *Angew. Chem. Int. Ed.* **2005**, *44*, 6448.
74. Prince R. B., Saven J. G., Wolynes P. G., Moore J. S., *J. Am. Chem. Soc.* **1999**, *121*, 3114.
75. Huc I., *Eur. J. Org. Chem.* **2004**, 17.
76. Berl V., Huc I., Khoury R., Krische M., Lehn J.-M., *Nature* **2000**, *407*, 720.
77. Okamoto Y., Mohri H., Nakano T., Hatada K., *J. Am. Chem. Soc.* **1989**, *111*, 5952.
78. Ute K., Hirose K., Kashimoto H., Nakayama H., Hatada K., Vogl O., *Polym J.* **1993**, *25*, 1175.
79. Ute K., Hirose K., Kashimoto H., Vogl O., *J. Am. Chem. Soc.* **1991**, *113*, 6305.
80. Lam J. W. Y., Tang B. Z., *Acc. Chem. Res.* **2005**, *38*, 745.
81. Zhao H., Sanda F., Masuda T., *J. Polym. Sci., Part A; Polym. Chem.* **2005**, *43*, 5168.
82. Okoshi K., Sakajiri K., Kumaki J., Yashima E., *Macromolecules* **2005**, *38*, 4061.
83. Cheuk K. K. L., Lam J. W. Y., Chen J., Lai L. M., Tang B. Z., *Macromolecules* **2003**, *36*, 5947.
84. Yu Q., Baroni T. E., Liable-sands L., Rheingold A. L., Borovik A. S., *Tetrahedron Lett.* **1998**, *39*, 6831.
85. Dolain C., Maurizot V., Huc I., *Angew. Chem. Int. Ed.* **2003**, *42*, 2737.
86. Semetey V., Moustakas D., Whitesides G. M., *Angew. Chem. Int. Ed.* **2006**, *45*, 588.
87. Gawronski J., Gawronska K., Grajewski J., Kacprzak K., Rychlewska U., *Chem. Commun.* **2002**, 582.
88. Elemans J. A. A. W., Rowan A. E., Nolte R. J. M., *J. Mater. Chem.* **2003**, *13*, 2661.

Chapter 2: Spectroscopic Properties of Pyrene-containing DNA Mimics

Published in:

F. Samain, V. L. Malinovskii, S. M. Langenegger, R. Häner, *Bioorg. Med. Chem.* **2008**, *16*, 27-33.

2.1 Abstract

DNA mimics containing non-nucleosidic pyrene building blocks are described. The modified oligomers form stable hybrids, although a slight reduction in hybrid stability is observed. The nature of the interaction between the pyrene residues in single and double stranded oligomers is analyzed spectroscopically. Intra- and interstrand stacking interactions of pyrenes is monitored by UV-absorbance as well as fluorescence spectroscopy. Excimer formation is observed in both single stands and double stranded hybrids. In general, intrastrand excimers show fluorescence emission at shorter wavelengths (approx. 5-10nm) than excimers formed by interstrand interactions. The existence of two different forms of excimers (intra- vs. interstrand) is also revealed in temperature dependent UV absorbance spectra.

2.2 Introduction

Modified oligonucleotides enjoy widespread interest as diagnostic and research tools.^{1,2} In addition, the generation of defined molecular architectures using nucleic acid like building blocks is a research topic of high interest.³⁻⁸ The repetitive and well-defined structural features of nucleic acids and related types of oligomers renders them valuable building blocks for the generation of nanometer-sized structures.⁹ The combination of the natural nucleotides with novel, synthetic building blocks leads to a large increase in the number of possible constructs and applications.^{10,11} Recently, we reported the synthesis and properties

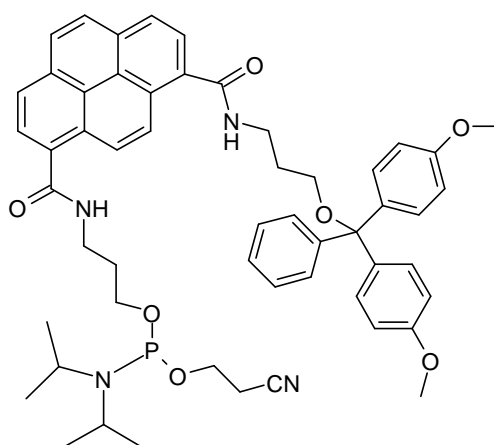
of non-nucleosidic, phenanthrene-based building blocks and their incorporation into DNA.^{12,13} These building blocks can serve as base surrogates allowing hybridisation of complementary strands without significant destabilisation of the duplex. Replacement of two or more base pairs by non-nucleosidic phenanthrene building blocks was well tolerated having almost no influence on hybrid stability compared to an unmodified duplex.¹⁴ Based on spectroscopic data, a model of interstrand stacked polyaromatic building blocks was derived. Interstrand stacking of such non-nucleosidic polyaromatic building blocks was subsequently shown by excimer formation¹⁵ of pyrenes placed in opposite positions.¹⁶ Interstrand stacking arrangement of a similar type of non-nucleosidic pyrene building blocks was shown by NMR investigations.¹⁷ Furthermore, natural DNA is also known to adopt an interstrand stacking structure, the *i-motif*, which is formed by association of stretches of two or more cytidines involving base intercalation.¹⁸ Due to their spectroscopic properties, the use of pyrene building blocks is interesting with regard to the fluorescence features of the resulting oligomers and the hybrids they form.¹⁹⁻³⁵ Some notable examples of extra-helical arrangement of pyrenes along the backbones of DNA^{19,35} and RNA²⁰ have been described recently. The absorption spectrum of pyrene overlaps only partially with oligonucleotide absorption and the fluorescence is strongly dependent on local changes. Within the set of building blocks that we have been using (phenanthrene, phenanthroline^{36,37} and pyrene) the pyrene molecule is, thus, an ideal candidate for probing the stacking interactions of polyaromatic building blocks in DNA. Here, we report the synthesis and spectroscopic investigation of DNA mimics containing multiple pyrene building blocks.

2.3 Results and Discussion

Along with geometrical constraints of the sugar phosphate backbone, stacking interactions and hydrogen bonding are the most important factors responsible for the self organization of single stranded nucleic acids into double helical structures.³⁸⁻⁴⁰ The type of modified DNA described here is based on the use of extended aromatic systems with non-nucleosidic linkers. In this system, the stacking properties can be considered as the main

factor for stabilization of secondary structures. Due to their hydrophobic nature, stacking interactions of *pyrene-pyrene* and/or *base-pyrene* are expected to play an important role not only in duplex but also in single strands in polar medium. Aggregation of pyrenes in aqueous solutions have been a topic of intensive investigation in the past and was reviewed by Winnik.¹⁵ The findings serve as an excellent basis for interpretation of pyrenes embedded in an oligonucleotide based system.

The required pyrene building block with a three-carbon linker (Scheme 2.1) has been synthesized according to a published procedure.¹⁶ Then the phosphoramidite pyrene derivative was used for the synthesis of oligonucleotides. Assembly of oligomers involved in automated oligonucleotide synthesis, the crude oligomers were purified by reverse phase HPLC and their identity was verified by mass spectrometry.



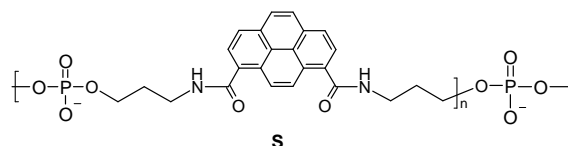
Scheme 2.1 Phosphoramidite pyrene building block.

2.3.1 Thermal denaturation experiments

Before investigation of the spectroscopic properties of pyrene containing oligomers, the stability of hybrids was tested by thermal denaturation. The data are summarized in Table 2.1. Oligonucleotides **1** and **2** serve as controls and oligomers **3-8** contain between one and three pyrene building blocks per single strand.

Table 2.1 Influence of non-nucleosidic pyrene building blocks on hybrid stability.

Oligo	duplex	T_m (°C)	ΔT_m	ΔT_m per modification
1	(5') AGC TCG GTC ATC GAG AGT GCA	69.5	-	-
2	(3') TCG AGC CAG TAG CTC TCA CGT			
3	(5') AGC TCG GTC ASC GAG AGT GCA	68.9	-0.6	-0.6
4	(3') TCG AGC CAG TSG CTC TCA CGT			
5	(5') AGC TCG GTC SSC GAG AGT GCA	66.2	-3.3	-1.7
6	(3') TCG AGC CAG SSG CTC TCA CGT			
7	(5') AGC TCG GTS SSC GAG AGT GCA	63.8	-5.7	-1.9
8	(3') TCG AGC CAS SSG CTC TCA CGT			



Conditions: 1.0 μ M each strand, 10 mM Tris-HCl buffer (pH 7.4) and 100 mM NaCl; 0.5 °C/min; absorbance measured at 260 nm.

T_m values show a picture that is in agreement with previous findings with phenanthrene-modified oligomers,^{14,36} i.e. a slight decrease in hybrid stability if one to three pairs of pyrenes are placed in opposite positions in the middle of the duplex. Values for ΔT_m per modification ranging between 0.6 and 1.9°C were observed. It can be concluded that the destabilization resulting from removal of natural base pairs is largely compensated by aryl-aryl stacking interactions between the pyrene residues. T_m values were also determined at two further wavelengths (245 and 354nm, Table 2.2). The T_m s obtained at these wavelengths correlated very well with the ones at 260nm, indicating a cooperative melting process.

Table 2.2 Melting temperature determination at different wavelength (245, 260, 354nm).

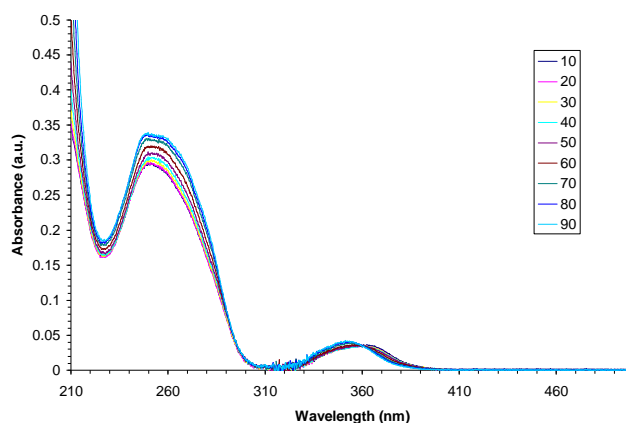
	245nm		260nm		354nm	
	T _m °C	ΔT _m °C	T _m °C	ΔT _m °C	T _m °C	ΔT _m °C
1*2	69.6	-	69.5	-	-	-
3*4	68.6	-1	68.9	-0.6	68.4	-
5*6	67.4	-2.2	66.2	-3.3	67.1	-
7*8	64.1	-5.5	63.8	-5.7	64.7	-

Conditons 1.0 μM each strand, 10 mM Tris-HCl buffer (pH 7.4) and 100 mM NaCl; 0.5 °C/min.

2.3.2 Pyrene Containing Single Strands

We next performed a set of temperature-dependend UV-VIS and fluorescence experiments with single stranded oligonucleotides to investigate the intramolecular interactions of pyrenes. Representative data are shown in Figures 2.1 and 2.2, respectively. Interactions between pyrene-base(s) can be seen clearly from the temperature-dependent experiments (Figure 2.1).

a)



b)

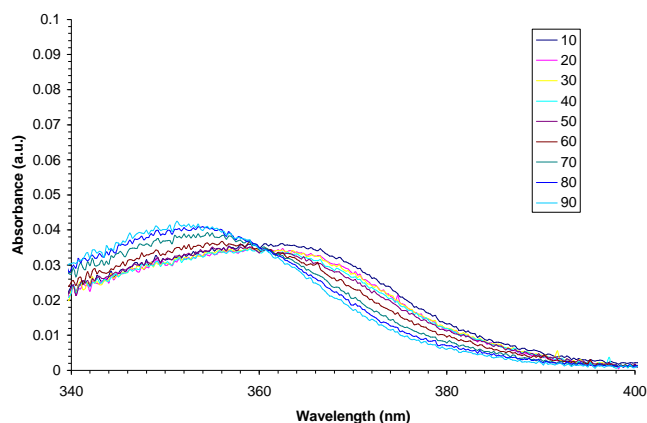
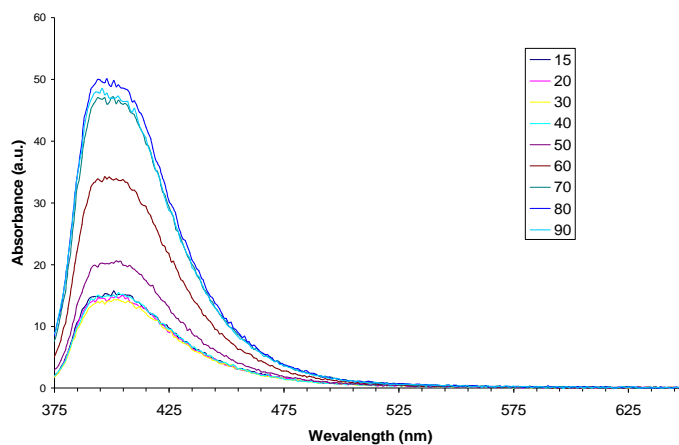


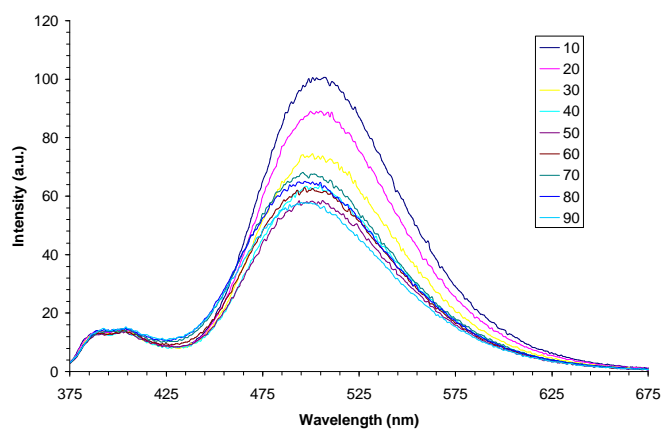
Figure 2.1 Temperature-dependent UV-absorbance of oligomer **3** (a) showing an isosbestic point at 360nm (b); for conditions see Table 2.1.

Increasing temperatures are associated with an increase in absorbance as well as with a blue-shift in maximum absorbance in the range 300-400nm, which corresponds to pyrene absorbance. These findings are in agreement with a reduction in π -stacking with increasing temperature, since stacking of chromophores is generally accompanied with i) a decrease in the absorbance intensity (hypochromic effect), ii) a broadening of signals and iii) very often with a red shift.^{15,41} While the broadening is not so clearly detectable, the other two characteristics are obviously present: a red-shift of 10nm is observed for **3** when going from 90 to 10°C and it is concomitant with a decrease in absorbance intensity. The gradual change in temperature leads to an isosbestic point at 360nm. As expected, temperature dependent fluorescence data (Figure 2.2a) shows the monomer fluorescence (around 400nm), which is typical for pyrene monomer fluorescence.

a)



b)



c)

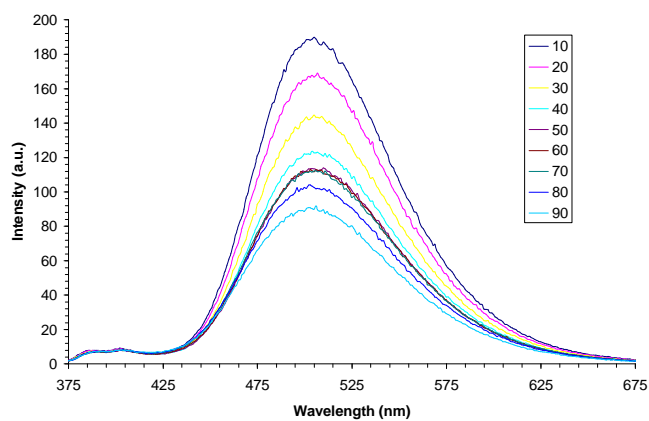


Figure 2.2 Temperature-dependent fluorescence spectra of single strands **3** (a), **5** (b) and **7** (c); for conditions, see Table 2.1.

The absence of distinct bands at longer wavelength reveals that there is no dominant intrastrand exciplex formation in single strand **3**; due to the asymmetry of the bands towards longer wavelength, exciplex can, however, not be ruled out.¹⁵ The intensity of absorbance spectra of the single strand **4** is essentially the same but fluorescence is of lower intensity (approx. 50% compared to **3**, see Figure 2.3). This is well in agreement with findings that guanine (neighboring base to pyrene in oligomer **4**, only), but not adenine or cytosine are efficient quenchers of pyrene fluorescence.⁴²

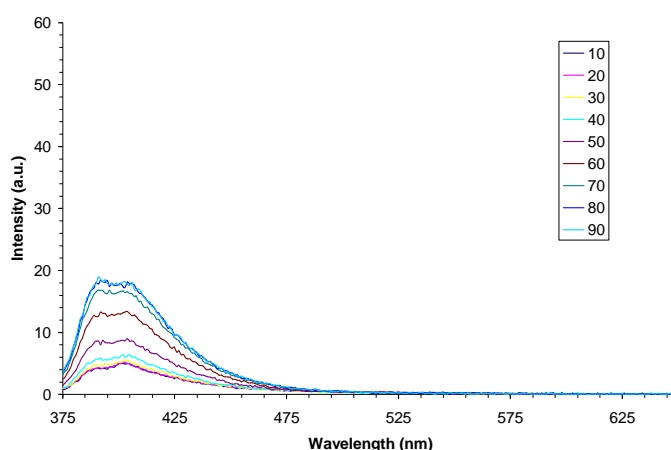
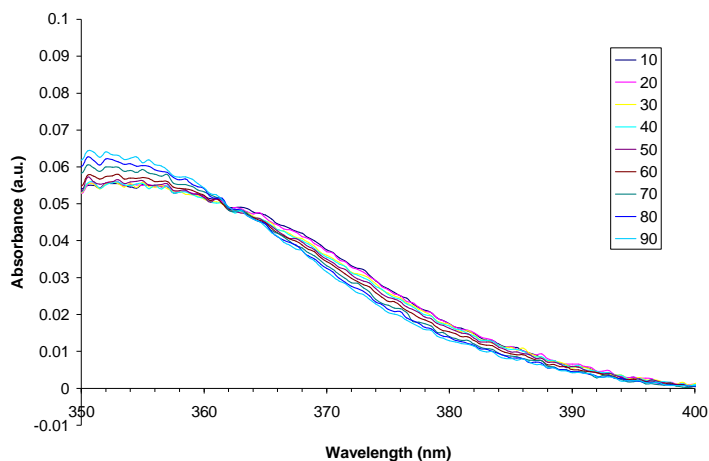


Figure 2.3 Temperature-dependent fluorescence spectra of single strand **4**.

Upon addition of further pyrenes, the possibility of observing the pyrene-pyrene interaction within single strand arises. Fluorescence data of **5** are shown in Figure 2.2 b). As expected, a strong excimer band with a maximum emission at 505nm appears while monomer fluorescence (around 400nm) is greatly reduced. This indicates strong stacking interactions between the adjacent pyrenes in the single strand. For oligomer **7**, which contains three consecutive pyrenes, this trend is even increased. The fluorescence spectrum (Figure 2.2 c) shows essentially only excimer emission at 506nm. A noteworthy difference in the two oligomers **5** and **7** exists: while a temperature dependent change of the emission maximum in **5** (from 505nm at 10°C to 498nm at 90°C) is observed, the maximum remains more or less unchanged over the same temperature range for oligomer

7. This finding is best described in terms of “static” (or dimeric in ground state) and “dynamic” (monomeric in ground state) excimers¹⁵ whereas the latter shows a blue-shifted emission in relation to the static excimer. In oligomer **5** having two pyrenes, thermal energy leads to a larger separation of the pyrenes; hence they form a dynamic excimer on irradiation. In oligomer **7** separation of all pyrenes is less likely and, hence, over the investigated temperature range the static excimer is dominating.¹⁵ As already observed with **3**, both oligomers **5** and **7** show an isosbestic point (362nm and 361nm, respectively) in the temperature-dependent absorbance spectrum (Figure 2.4).

a)



b)

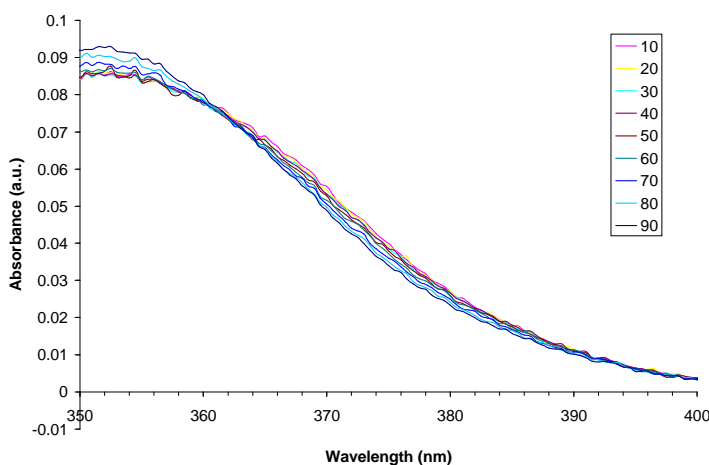
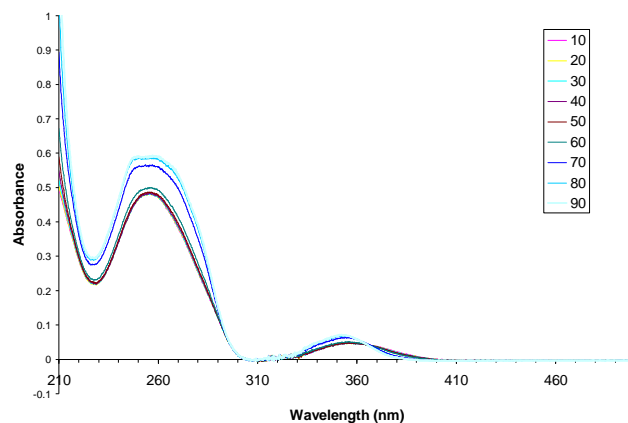


Figure 2.4 Temperature dependent UV-VIS of a) single strand **5** (isosbestic point at 362nm); b) single strand **7** (isosbestic point at 361nm).

2.3.3 Investigation of Pyrene Containing Hybrids

As described above, the pyrene unit(s) participates strongly in intrastrand stacking interactions. The question arises whether the same (intrastrand) interactions persist upon hybridization or if different (interstrand) pyrene interactions are dominant. While this question was partly answered previously for hybrid **3*4** by observation of excimer formation by interstrand stacking of two pyrenes,^{16a} the behavior of single strands containing multiple pyrenes may be different. To study this question, temperature dependent absorbance and fluorescence experiments with the different hybrids were performed. Temperature dependent fluorescence properties of pyrene of nucleic acids containing multiple, extrahelical pyrene residues has been used to study pyrene aggregation.^{19,20} The absorbance spectrum of hybrid **3*4** (Figure 2.5) shows that the two pyrene units from the single strands are involved in stacking interactions. First, the expected blue-shift is observed with increasing temperature (see Figure 2.5 b, showing the range of 320 to 400nm).⁴³ The maximum absorbance decreases from 357nm at 10°C to 352nm at 90°C. More importantly, two isosbestic points are present, indicating two different types of interaction between the pyrenes. The first isosbestic point (366nm) is formed by curves taken below the melting temperature (68.9°C, Table 2.1) can be attributed to decreasing association between the pyrenes with increasing temperature. The second isosbestic point is observed at shorter wavelength (362nm) and is formed by the curves taken above the T_m , and therefore has its origin in changes occurring within the single strands. The observed value of the blue-shifted isosbestic point correlates well with the one observed with single strand **3** alone (360nm, see above).

a)



b)

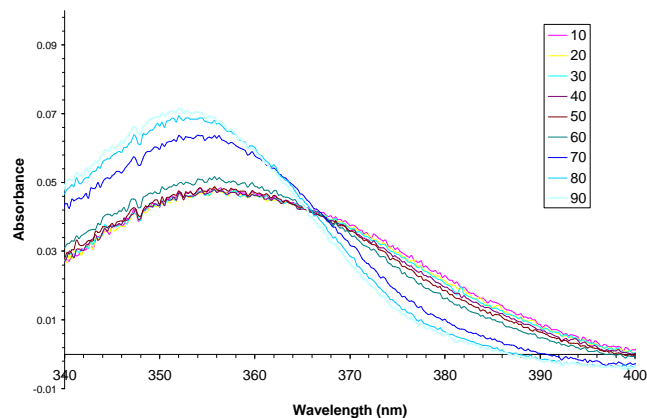


Figure 2.5 Temperature dependent absorbance spectra of hybrid 3*4 (a: full spectrum, b: enlargement of the range 340-400 nm; for conditions see Table 2.1).

The temperature dependent fluorescence spectra of hybrid 3*4 (Figure 2.6) confirm this interpretation. A strong excimer band at 500nm, arising from interstrand stacking interactions between the two pyrenes is gradually replaced by pyrene monomer emission at higher temperature. At temperatures above the T_m (68.9°C), only monomer fluorescence is observed.

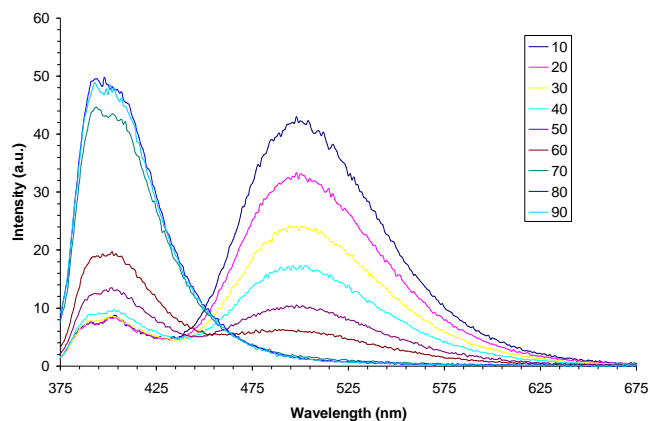
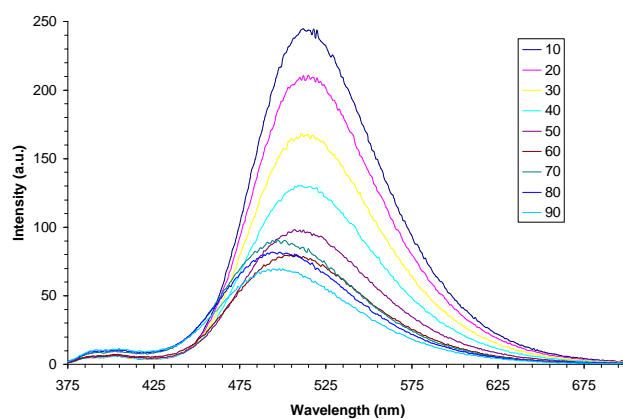


Figure 2.6 Temperature dependent fluorescence spectra of hybrid **3*4**; for conditions see Table 2.1.

As expected, the hybrids with four (**5*6**) and six (**7*8**) pyrenes show rather different temperature dependence in their fluorescence spectra (Figure 2.7) giving rise only to excimer emission also at temperatures above the T_m . Below the T_m , the emission intensity is decreasing with increasing temperature, indicating a weakening of (or a geometrical change in) the association of the pyrenes.

a)



b)

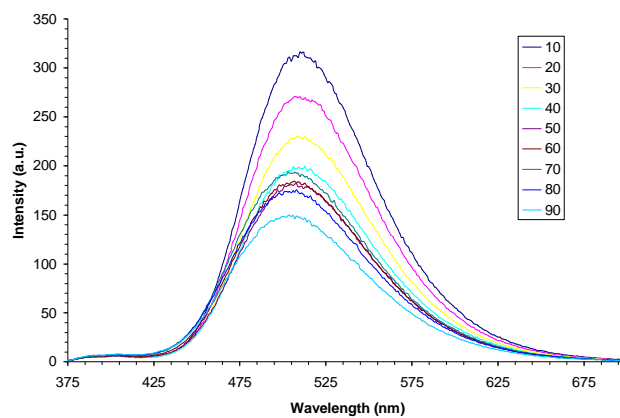


Figure 2.7 Emission spectra of hybrids 5*6 (a) and 7*8 (b); for conditions see Table 2.1.

We noticed the intensity increased slightly around the T_m before decreasing again (Figure 2.8).

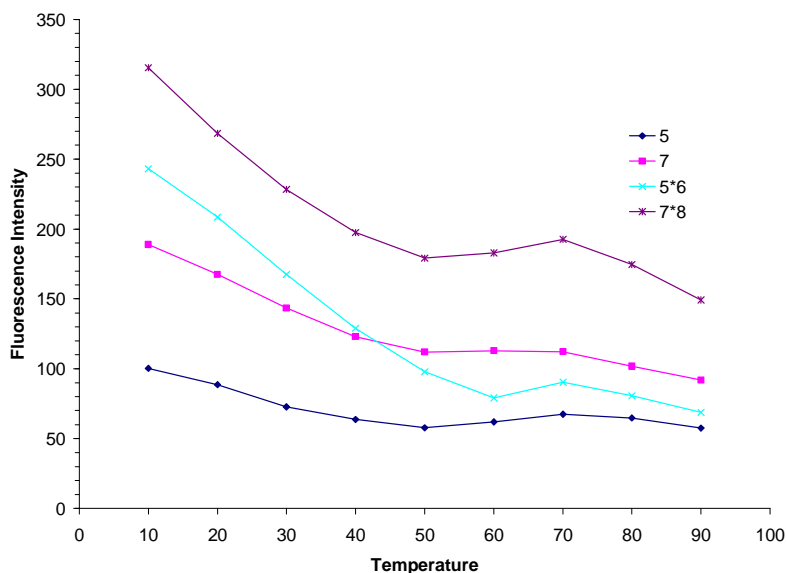
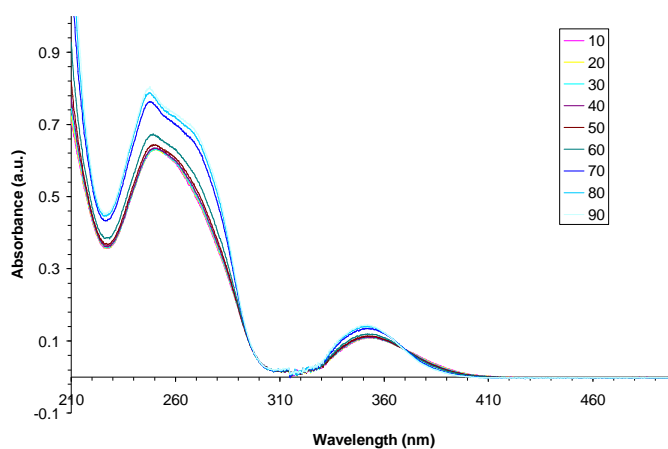


Figure 2.8 Dependence of max. excimer fluorescence intensity of single and double strands on temperature; for conditions see Table 2.1.

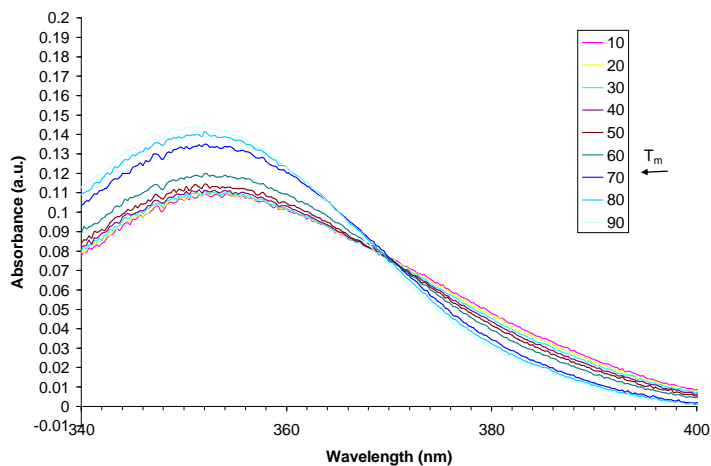
In addition, the maximum emission in the hybrids (i.e. below the T_m) is at higher wavelength than the one in the single strands (i.e. above the T_m). The changes in the

maximum emission over the temperature range investigated are from 514 to 500nm in hybrid **5*6** and 512 to 505nm in hybrid **7*8**. The temperature dependent absorbance spectra of hybrids **5*6** and **7*8** (Figure 2.9 and 2.10) are very similar to the one of hybrid **3*4**. Thus, both hybrids also show two isosbestic points representing the single and the double stranded states.

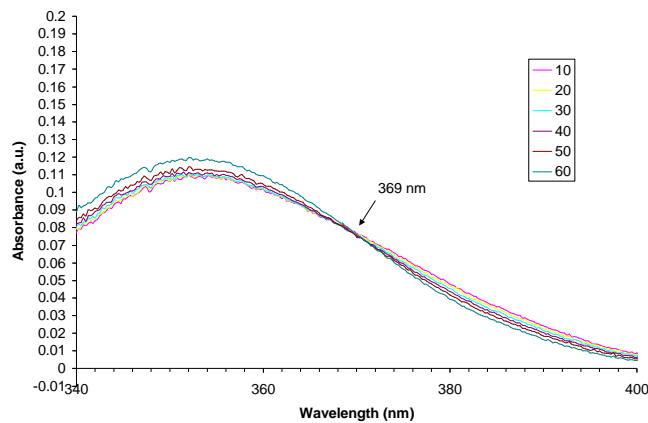
a)



b)



c)



d)

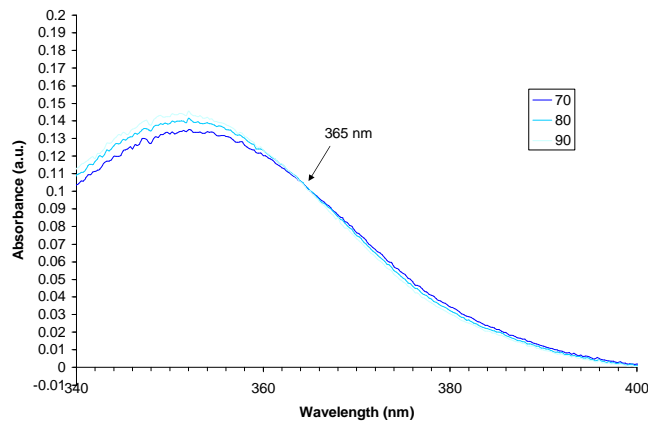
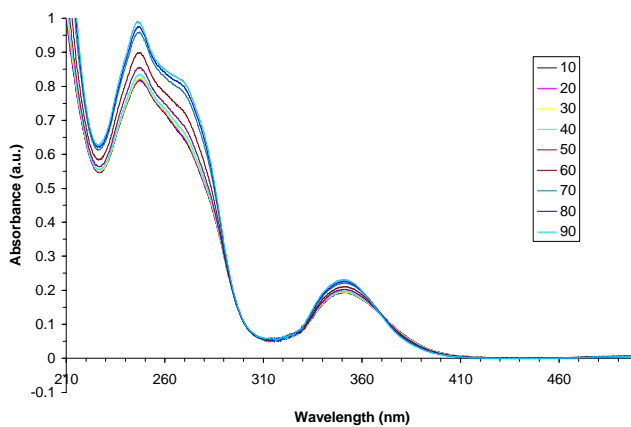
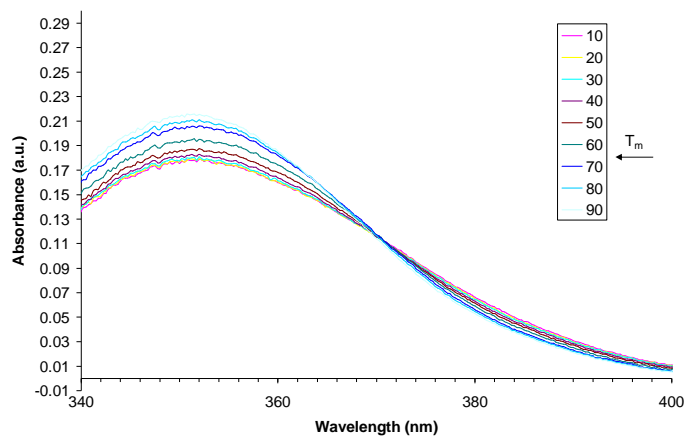


Figure 2.9 Temperature dependent UV-VIS of duplex **5*6** a) whole spectra; b) 340-400 nm pyrene absorbance extended; c, d) isobestic points at 369 and 365nm respectively; for conditions see Table 2.1.

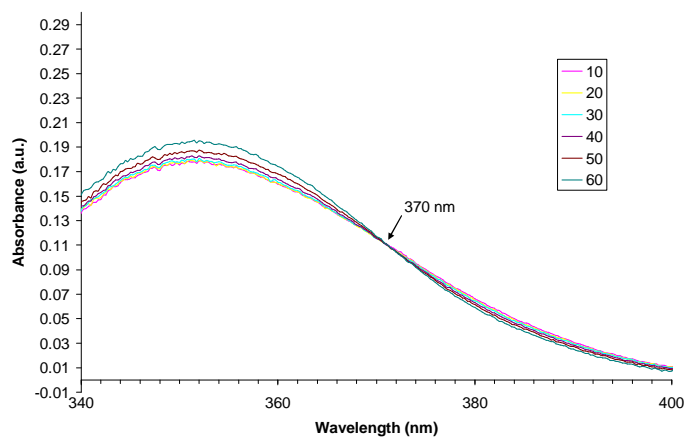
a)



b)



c)



d)

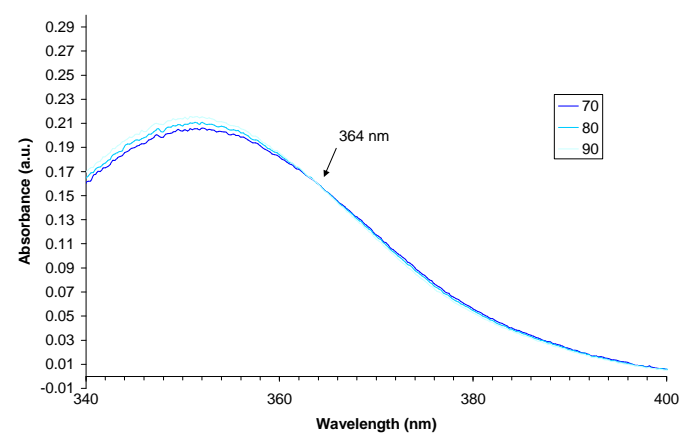


Figure 2.10 Temperature dependent UV-VIS of duplex 7*8 a) whole spectra; b) 340-400nm pyrene absorbance extended; c, d) isosbestic points at 370 and 364nm respectively; for conditions see Table 2.1.

Finally, all hybrids showed circular dichroism spectra typical for B-DNA (Figure 2.11).

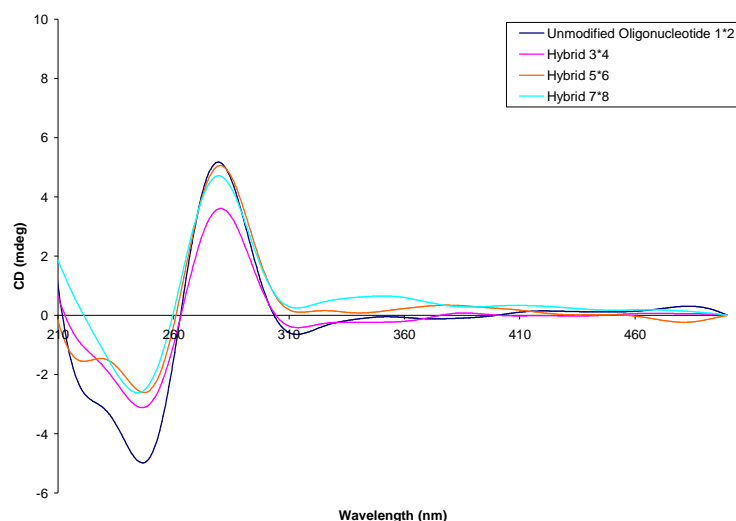


Figure 2.11 CD spectra of hybrids containing non-nucleosidic pyrene residues; for conditions see Table 2.1.

2.4 Conclusion

DNA mimics containing non-nucleosidic, polyaromatic pyrene building blocks have been investigated spectroscopically. Absorbance and emission spectra provide insight into the interactions among pyrenes or between pyrene and neighboring nucleic acid bases. Investigation of single strands showed that *intrastrand* excimer formation takes place if two or three pyrenes are placed in adjacent positions. In hybrids, interstrand excimers are formed. In general, intrastrand excimers show fluorescence emission at shorter wavelengths (498 to 505nm) than the excimers formed by interstrand interactions (505 to 514nm). The existence of two different forms of excimers (intra- vs. interstrand) is also revealed by temperature dependent UV absorbance spectra. A gradual shift of maximum absorbance is accompanied by appearance of two isosbestic points, one of which (at longer wavelength) can be attributed to interstrand stacking in the hybrid and the second

from intrastrand stacking in the single strands. Thus, as in natural single stranded nucleic acids, DNA mimics containing the type of modified building block described herein are organized by stacking interactions. Upon duplex formation, however, the DNA mimics behave differently, in that the intrastrand interactions cede to the more favorable interstrand stacking. The hybridization process of the DNA mimics is, thus, not aided - at least not to the same extent as natural DNA - by the preorganization of the single strands. In addition to giving insight into the intrastrand and interstrand interactions the described pyrene building blocks allow the design and construction of DNA mimics with interesting spectroscopic properties for applications as diagnostic tools and as novel materials.

2.5 Experimental Section

The required pyrene building block with a three-carbon linker has been synthesized according to a published procedure.^{16a} Nucleoside phosphoramidites from *Transgenomic* (Glasgow, UK) were used for oligonucleotide synthesis. Oligonucleotides **1-8** were prepared *via* automated oligonucleotide synthesis by a standard synthetic procedure ('trityl-off' mode) on a 394-DNA/RNA synthesizer (*Applied Biosystems*). Cleavage from the solid support and final deprotection was done by treatment with 30% NH₄OH solution at 55°C overnight. All oligonucleotides were purified by reverse phase HPLC (LiChrospher 100 *RP-18*, 5µm, Merck), *Bio-Tek Instruments Autosampler 560*); eluent *A* = (Et₃NH)OAc (0.1 M, pH 7.4); eluent *B* = MeCN; elution at 40°C; gradient 5 – 20% *B* over 30 min.

Molecular mass determinations of oligonucleotides were performed with a Sciex QSTAR pulsar (hybrid quadrupole time-of-flight mass spectrometer, *Applied Biosystems*). ESI-MS (negative mode, CH₃CN/H₂O/TEA) data of compounds **1-8** are presented in Table 2.3.

Table 2.3 Mass spectrometry data (molecular formula, calc. average mass, and obtained).

Oligo.		Molecular formula	Calc. aver.mass	Found
1	(5') AGC TCG GTC ATC GAG AGT GCA	C ₂₀₅ H ₂₅₇ N ₈₃ O ₁₂₃ P ₂₀	6471.3	6472
2	(3') TCG AGC CAG TAG CTC TCA CGT	C ₂₀₃ H ₂₅₈ N ₇₆ O ₁₂₅ P ₂₀	6382.2	6383
3	(5') AGC TCG GTC ASC GAG AGT GCA	C ₂₁₉ H ₂₆₇ N ₈₃ O ₁₂₂ P ₂₀	6633.5	6632
4	(3') TCG AGC CAG TSG CTC TCA CGT	C ₂₁₇ H ₂₆₉ N ₇₃ O ₁₂₆ P ₂₀	6535.4	6534
5	(5') AGC TCG GTC SSC GAG AGT GCA	C ₂₃₃ H ₂₇₈ N ₈₀ O ₁₂₃ P ₂₀	6786.7	6785
6	(3') TCG AGC CAG SSG CTC TCA CGT	C ₂₃₁ H ₂₇₉ N ₇₃ O ₁₂₅ P ₂₀	6697.7	6696
7	(5') AGC TCG GTS SSC GAG AGT GCA	C ₂₄₈ H ₂₈₉ N ₇₉ O ₁₂₃ P ₂₀	6964.0	6963
8	(3') TCG AGC CAS SSG CTC TCA CGT	C ₂₄₅ H ₂₉₀ N ₇₀ O ₁₂₅ P ₂₀	6834.9	6834

Thermal denaturation experiments (1.0 μM oligonucleotide concentration (each strand), 10 mM Tris·HCl buffer (pH 7.4), and 100 mM NaCl) were carried out on *Varian Cary-100 Bio-UV/VIS* spectrophotometer equipped with a *Varian Cary-block* temperature controller and data were collected with *Varian WinUV* software at 245, 260 and 354nm (cooling-heating-cooling cycles in the temperature range of 20-90°C, temperature gradient of 0.5°C/min). Data were analyzed with *Kaleidagraph*[®] software from ©*Synergy Software*. Temperature melting (T_m) values were determined as the maximum of the first derivative of the smoothed (window size 3) melting curve.

Temperature dependent UV-VIS spectra were collected over the range of 210-500nm at 10-90°C with a 10°C interval on *Varian Cary-100 Bio-UV/VIS* spectrophotometer equipped with a *Varian Cary-block* temperature controller. All experiments were carried out at a 1.0 μM oligonucleotide concentration (each strand) in Tris·HCl buffer (10 mM) and NaCl (100 mM) at pH=7.4. The cell compartment was flushed with N₂ to avoid water condensation at low temperature.

Temperature dependent fluorescence data were collected for 1.0 μM oligonucleotide (1.0 μM of each strand in case of double strands) solutions in Tris·HCl buffer (10 mM)

and NaCl (100 mM) at pH=7.4 on a Varian Cary Eclipse fluorescence spectrophotometer equipped with a Varian Cary-block temperature controller (excitation at 354nm; excitation and emission slit width of 5nm). Varian Eclipse software was used to investigate the fluorescence of the different pyrene-containing oligonucleotides at a wavelength range of 375-700nm in the temperature range of 10-90°C.

CD spectra were recorded on a *JASCO J-715* spectrophotometer using quartz cuvettes with an optic path of 1 cm.

2.6 References

1. Verma, S.; Jager, S.; Thum, O.; Famulok, M. *Chem. Rec.* **2003**, *3*, 51-60.
2. Kohler, O.; Jarikote, D. V.; Singh, I.; Parmar, V. S.; Weinhold, E.; Seitz, O. *Pure Appl. Chem.* **2005**, *77*, 327-338.
3. Seeman, N. C. *Nature* **2003**, *421*, 427-431.
4. Samori, B.; Zuccheri, G. *Angew. Chem. Int. Ed.* **2005**, *44*, 1166-1181.
5. Shih, W. M.; Quispe, J. D.; Joyce, G. F. *Nature* **2004**, *427*, 618-621.
6. Mirkin, C. A. *Inorg. Chem.* **2000**, *39*, 2258-2272.
7. Chworos, A.; Severcan, I.; Koyfman, A. Y.; Weinkam, P.; Oroudjev, E.; Hansma, H. G.; Jaeger, L. *Science* **2004**, *306*, 2068-2072.
8. Claridge, S. A.; Goh, S. L.; Frechet, J. M. J.; Williams, S. C.; Micheel, C. M.; Alivisatos, A. P. *Chem. Mater.* **2005**, *17*, 1628-1635.
9. Wengel, J. *Org. Biomol. Chem.* **2004**, *2*, 277-280.
10. Eschenmoser, A. *Chimia* **2005**, *59*, 836-850.
11. Herdewijn, P. *Biochim. Biophys. Acta, Gene Struct. Expr.* **1999**, *1489*, 167-179.
12. Langenegger, S. M.; Häner, R. *Helv. Chim. Acta* **2002**, *85*, 3414-3421.
13. Langenegger, S. M.; Bianke, G.; Tona, R.; Häner, R. *Chimia* **2005**, *59*, 794-797.
14. Langenegger, S. M.; Häner, R. *ChemBiochem* **2005**, *6*, 2149-2152.
15. Winnik, F. M. *Chem. Rev.* **1993**, *93*, 587-614.

16. (a) Langenegger S. M.; Häner, R. *Chem Commun.* **2004**, 2792-2793; (b) Langenegger, S. M.; Häner, R. *Bioorg. Med. Chem. Lett.* **2006**, *16*, [Epub ahead of print].
17. Nielsen, C. B.; Petersen, M.; Pedersen, E. B.; Hansen, P. E.; Christensen, U. B. *Bioconjug. Chem.* **2004**, *15*, 260-269.
18. Gueron, M.; Leroy, J. L. *Curr. Opin. Struct. Biol.* **2000**, *10*, 326-331.
19. Mayer-Enthart, E.; Wagenknecht, H. A. *Angew. Chem. Int. Ed.* **2006**, *45*, 3372-3375.
20. Nakamura, M.; Ohtoshi, Y.; Yamana, K. *Chem Commun.* **2005**, 5163-5165.
21. Malakhov, A. D.; Skorobogaty, M. V.; Prokhorenko, I. A.; Gontarev, S. V.; Kozhich, D. T.; Stetsenko, D. A.; Stepanova, I. A.; Shenkarev, Z. O.; Berlin, Y. A.; Korshun, V. A. *Eur. J. Org. Chem.* **2004**, 1298-1307.
22. Filichev, V. V.; Vester, B.; Hansen, L. H.; Pedersen, E. B. *Nucleic Acids Res.* **2005**, *33*, 7129-7137.
23. Balakin, K. V.; Korshun, V. A.; Mikhalev, I. I.; Maleev, G. V.; Malakhov, A. D.; Prokhorenko, I. A.; Berlin, Y. A. *Biosens. Bioelectron.* **1998**, *13*, 771-778.
24. Yamana, K.; Iwai, T.; Ohtani, Y.; Sato, S.; Nakamura, M.; Nakano, H. *Bioconj. Chem.* **2002**, *13*, 1266-1273.
25. Michel, J.; Bathany, K.; Schmitter, J. M.; Monti, J. P.; Moreau, S. *Tetrahedron* **2002**, *58*, 7975-7982.
26. Dioubankova, M. N.; Malakhov, A. D.; Stetsenko, D. A.; Gait, M. J.; Volynsky, P. E.; Efremov, R. G.; Korshun, V. A. *ChemBioChem* **2003**, *4*, 841-847.
27. Hedlicka, P. J.; Babu, B. R.; Sorensen, M. D.; Wengel, J. *Chem. Commun.* **2004**, 1478-1479.
28. Fujimoto, K.; Shimizu, H.; Inouye, M. *J. Org. Chem.* **2004**, *69*, 3271-3275.
29. Okamoto, A.; Ichiba, T.; Saito, I. *J. Am. Chem. Soc.* **2004**, *126*, 8364-8365.
30. Kosuge, M.; Kubota, M.; Ono, A. *Tetrahedron Lett.* **2004**, *45*, 3945-3947.
31. Yamana, K.; Fukunaga, Y.; Ohtani, Y.; Sato, S.; Nakamura, M.; Kim, W. J.; Akaike, T.; Maruyama, A. *Chem. Commun.* **2005**, 2509-2511.
32. Okamoto, A.; Ochi, Y.; Saito, I. *Chem. Commun.* **2005**, 1128-1130.
33. Cho, Y. J.; Kool, E. T. *ChemBioChem* **2006**, *7*, 669-672.

34. Kashida, H.; Asanuma, H.; Komiyama, M. *Chem. Commun.* **2006**, 2768-2770.
35. Barbaric, J.; Wagenknecht, H. A. *Org. Biomol. Chem.* **2006**, *4*, 2088-2090.
36. Langenegger, S. M.; Häner, R. *Tetrahedron Lett.* **2004**, *45*, 9273-9276.
37. Langenegger, S. M.; Häner, R. *ChemBioChem* **2005**, *6*, 848-851.
38. Saenger, W. *Principles of Nucleic Acid Structure*; Springer-Verlag: New York, **1984**.
39. Kool, E. T. *Chem. Rev.* **1997**, *97*, 1473-1487.
40. Farwer, J.; Packer, M. J.; Hunter, C. A. *Biopolymers* **2006**, *81*, 51-61.
41. For a recent example of a redshift in absorbance upon DNA duplex formation and pyrene intercalation by oligonucleotides containing a single pyrene modification see: Nakamura, M.; Fukunaga, Y.; Sasa, K.; Ohtoshi, Y.; Kanaori, K.; Hayashi, H.; Nakano, H.; Yamana, K. *Nucleic Acids Res.* **2005**, *33*, 5887-5895.
42. See e.g.: Donho, C.; Saito, I. in: *Charge Transfer in DNA - From Mechanism to Application*; Wagenknecht, H. A., ed. Chapter 7 - Chemical Approach to Modulating Hole Transport Through DNA, pp. 153-174; Wiley-VCH; Weinheim, Germany, 2005.
43. It should be noted that, principally, the same observations are possible at the other major pyrene absorbance band around 245nm; since interpretations of this region is complicated by the overlap with the spectrum of the natural bases, however, only the region of 300-400nm is described here.

Chapter 3: Helical Arrangement of Interstrand Stacked Pyrenes in a DNA Framework

Published in:

V. L. Malinovskii, F. Samain, R. Häner, *Angew. Chem. Int. Ed.* **2007**, *46*, 4464-4467.

3.1 Abstract

DNA mimics containing extended stretches of non-nucleosidic pyrene building blocks are described. The modified oligomers form stable hybrids. The nature of the interaction between the pyrene residues in single and double stranded oligomers is analyzed spectroscopically. Furthermore helical self-organization between oligopyrene strands with 14 consecutive achiral pyrene building blocks embedded in a DNA strand leads to an artificial double helix.

3.2 Introduction

DNA takes an eminent role in the construction of well-defined nanostructures and – devices.¹ The unique feature of self-organization, combined with the ease of automated oligonucleotide synthesis² has driven the rapid progress in DNA nanotechnology.³ On the other hand, possible applications in the medical and materials sciences may be limited by the chemical and physical properties of the natural DNA building blocks. Not surprisingly, the quest for modified building blocks matching the special needs is continued with high intensity.⁴ Ever since the discovery of the DNA double helix, the generation of helical structures that are not based on the hydrogen bond mediated pairing scheme of the nucleobases or related derivatives has been a highly competitive aspect in the field of *molecular self-organization*.⁵ While reports on the construction and study of single stranded folded or helical structures are relatively numerous, descriptions of double helices are, in comparison, less abundant. The recognition motifs utilized so far for

creating double stranded assemblies can be grouped into ligand-to-metal coordination, hydrogen bonding, aromatic stacking and electrostatic interactions.⁶ While a range of reports describe the formation of foldamers with aromatic building blocks in organic media, the number of accounts on such systems in aqueous conditions is limited.⁷ The development of complex and functional artificial double helical structures is, thus, still a major challenge.⁸ Replacement of two, four, and six base pairs by non-nucleosidic pyrene building blocks has been reported. Absorbance, emission spectra, and circular dichroism spectra have provided insight into the interactions among pyrenes or between pyrene and neighbouring nucleic acid bases.⁹ Here is described the first example of an interstrand helical organization within an entirely artificial section embedded in a double-stranded DNA molecule. Moreover, the observed double-helical structure is formed under physiologically compatible conditions.

3.3 Results and discussion

The construct is composed of achiral, non-nucleosidic pyrene building blocks (**S**), which are embedded in a DNA as illustrated in Figure 3.1. The incorporation of non-nucleosidic building blocks into oligonucleotides was pioneered by *Letsinger and Lewis*, who described the incorporation of stilbene as well as other aromatic residues into oligodeoxynucleotides.^{10, 11}

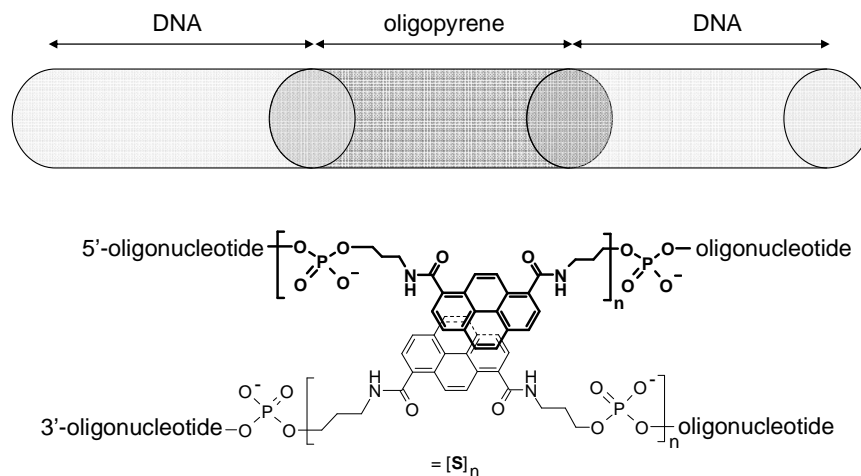


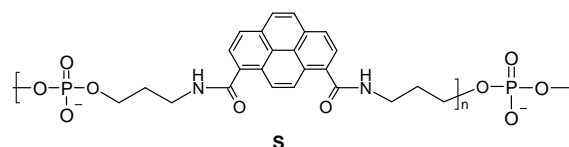
Figure 3.1 Schematic representation of oligopyrene stacks embedded in a DNA duplex

Over the past several years, our own efforts involved the assembly of DNA-like structures with polyaromatic derivatives, such as phenanthrene, phenanthroline and pyrene with alkyl chains and phosphodiester groups linking the individual units.¹² Based on spectroscopic data, a model of interstrand-stacked polyaromatic residues was derived.¹³ We have subsequently expanded the studies to extended stacks of pyrene building blocks.

The corresponding oligomeric compounds **1-10** are shown in Table 3.1. The pyrene residues are contained in the middle of a DNA duplex. The number of pyrenes ranges from two (duplex **3*4**) to fourteen (duplex **9*10**). Duplex **1*2** serves as the reference. The influence of pyrene incorporation on the stability of the hybrids was tested by thermal denaturation. Table 3.1 shows the experimental T_m (melting temperature) values as well as the theoretical values for the corresponding hybrids without the contribution of the pyrene residues.

Table 3.1 Influence of multiple pyrene residues on the thermal stability of hybrids.

Oligo #	duplex ^[a]	T _m (°C) exp. ^[b]	T _m calc. ^[c]	ΔT _m , °C ^[d]
1	(5') AGC TCG GTC ATC GAG AGT GCA	70.5	70.5	-
2	(3') TCG AGC CAG TAG CTC TCA CGT			
3	(5') AGC TCG GTC ASC GAG AGT GCA	70.1	69.5	+0.6
4	(3') TCG AGC CAG TSG CTC TCA CGT			
5	(5') AGC TCG GTC SSC GAG AGT GCA	68.0	68.1	+0.1
6	(3') TCG AGC CAG SSG CTC TCA CGT			
7	(5') AGC TCG GTS SSC GAG AGT GCA	65.1	47.1	+18.0
8	(3') TCG AGC CAS SSG CTC TCA CGT			
9	(5') AGC TCS SSS SSS GAG AGT GCA	56.5	33.6	+22.9
10	(3') TCG AGS SSS SSS CTC TCA CGT			

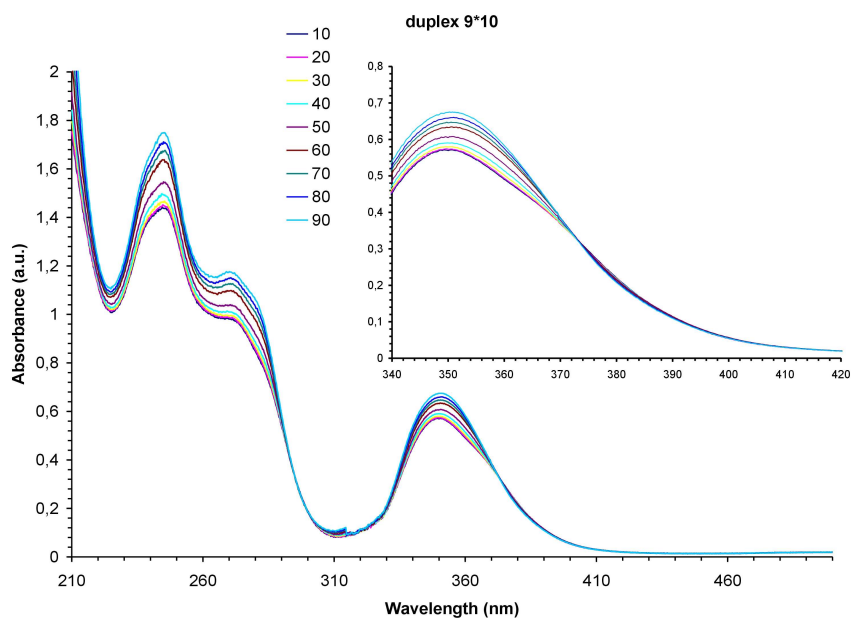


[a] 1.0 μM each strand, 10 mM phosphate buffer, pH 7.0); [b] experimental value; average of three independent experiments; exp. error 0.5°C; [c] T_m value calculated for the corresponding hybrid formed by the two strands without contribution of the unnatural building blocks according to the method described by *Markham and Zuker*¹⁴; [d] difference between experimental and calculated T_m value; this number corresponds to the contribution of the pyrene residues to the overall duplex stability.

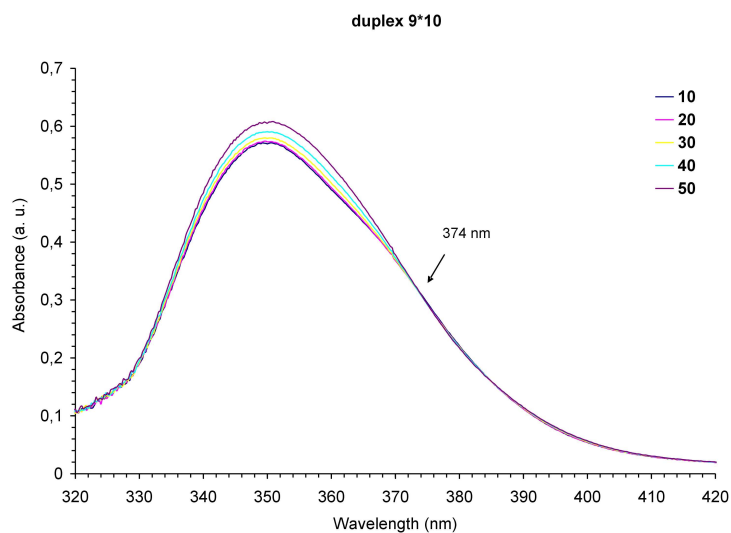
The latter value, which was calculated according to the method described by *Markham and Zuker*,¹⁴ allows an estimation of the contribution by the pyrenes to the overall stability (ΔT_m). While two and four pyrene residues add little to the hybrid stability, six and fourteen pyrenes have a rather large positive effect on the T_m of the respective hybrids. This indicates that interstrand interactions between the pyrenes lead to a significant stabilization of the duplex. Moreover, intrastrand folding of single strands *via* pyrene stacking can facilitate duplex formation by reducing the entropy change in a

manner similar to single strand preorganization in natural oligonucleotides.¹⁵ The occurrence of inter- and intrastrand pyrene stacking interactions is supported by temperature dependent UV-VIS spectroscopy showing the presence of two isosbestic points upon duplex melting. Furthermore, signal broadening and hypochromicity, both of which serve as evidence for face-to-face aggregates,¹⁶ were observed upon duplex formation¹⁷ (Figure 3.2).

a)



b)



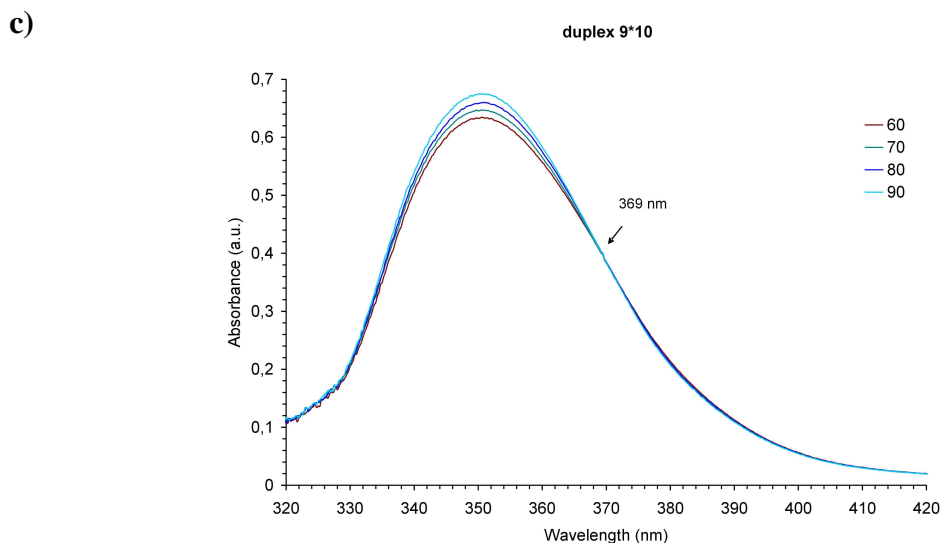
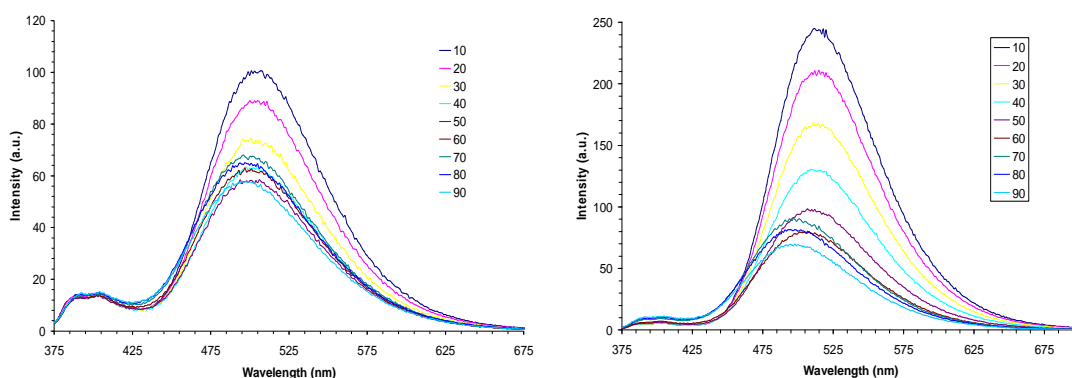


Figure 3.2 Temperature dependent UV-VIS of a) duplex **9*10** (210-500 nm, 10-90 °C); b) isosbestic point at 374 nm (320-420 nm, 10-40 °C); c) isosbestic point at 369 nm (320-420 nm, 60-90 °C).

Then, the oligomers were analyzed for their fluorescence properties. The single strands containing more than one pyrene (**5-10**) and the hybrids formed between them exhibited mainly excimer emission over a temperature range from 10-90°C showing - well in agreement with our expectations - that pyrenes are strongly aggregated in single as well as double strands (Figure 3.3).



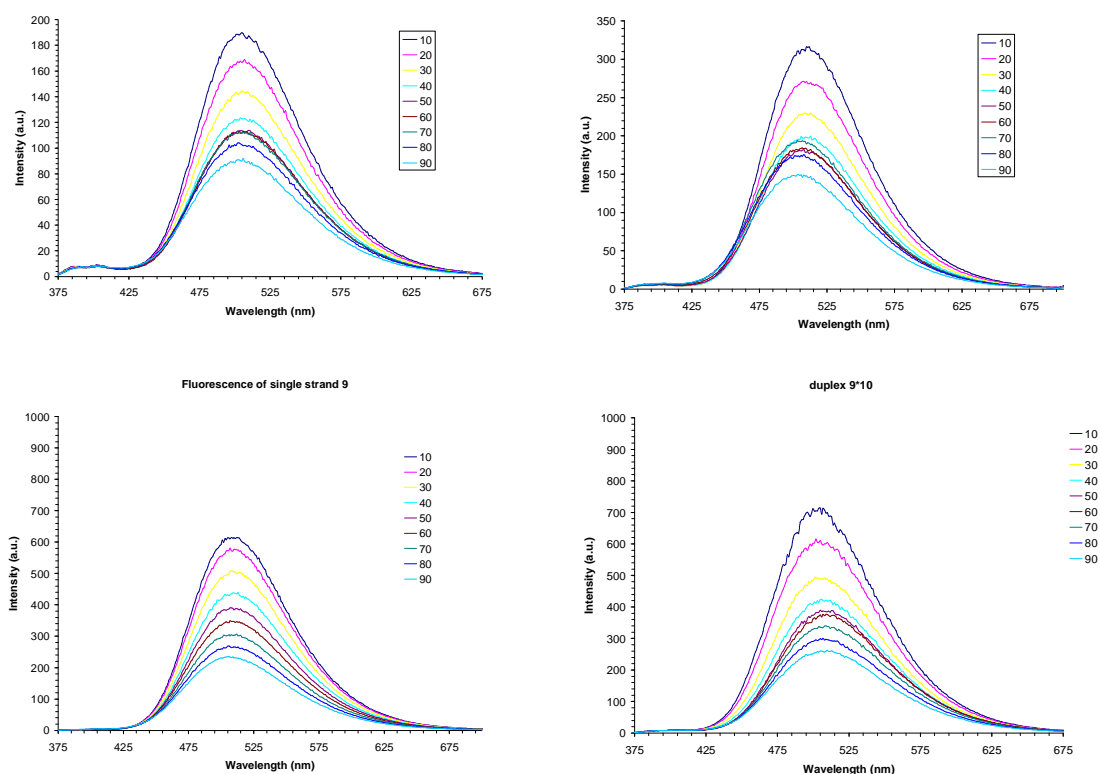


Figure 3.3 Fluorescence spectra of single strands a) **5**; b) **7**; c) **9** (left column) and duplexes d) **5*6**, e) **7*8**, f) **9*10** (right column).

Some exceptional behavior, however, was observed in the emission spectra of hybrid **9*10**. While hybrids **5*6** and **7*8** show a red shift in the excimer emission upon hybrid formation, hybrid **9*10** behaves in an opposite way. As can be seen in Figure 3.4, duplex formation leads to a significant blue shift (511 to 504 nm), when going from 90→10°C.

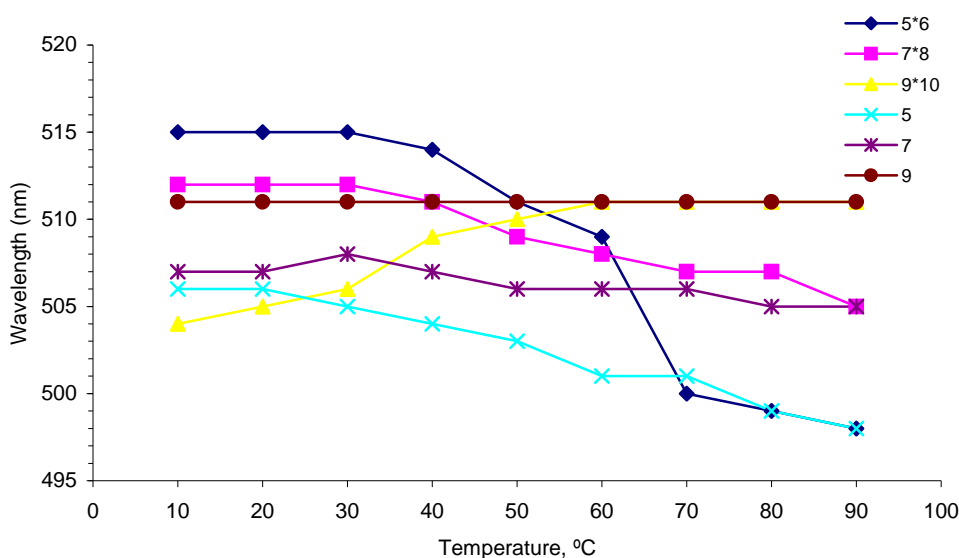


Figure 3.4 Trends of fluorescence maximum shifts upon melting of duplexes **5*6**, **7*8**, **9*10** and single strands **5**, **7**, **9**.

Aggregation of pyrenes and the resulting changes in the fluorescence properties were studied in detail and summarized by Winnik.¹⁷ The inverse behavior of hybrid **9*10** is an indication that *sandwich-type* pyrene aggregation is restricted within the duplex. With increasing temperature and flexibility and furthermore upon strand dissociation, the possibility of adopting the preferred *sandwich-type* aggregation is opened. Blue shifted fluorescence as a result of only partially overlapping excimer geometries has e.g. been observed in crystalline pyrene derivatives, pyrenophanes, bis-pyrenyl systems and polymers with twisted or strained pyrene conformations.^{17,18} An intriguing interpretation of this inverse behavior is the occurrence of a helical arrangement of the pyrenes in hybrid **9*10**, triggered by the unmodified DNA parts. The twisting of the pyrenes upon adoption of a helical conformation would explain the blue-shifted emission. Moreover broadening of excitation spectra compared to pyrene-1,8-dicarboxylic acid bis-[(3-hydroxypropyl)amide] (PU) upon increasing number of pyrene per single strand is clearly observed (**5**, **7** and **9**, respectively). In addition, duplex formation is accompanied with a further increase of this broadening (Figures 3.5 and 3.6). The broadening is accompanied with a decrease of the Intensity Peak/Intensity Valley ratio, which also serves as a qualitative indication on the extent of pyrene aggregation.¹⁷

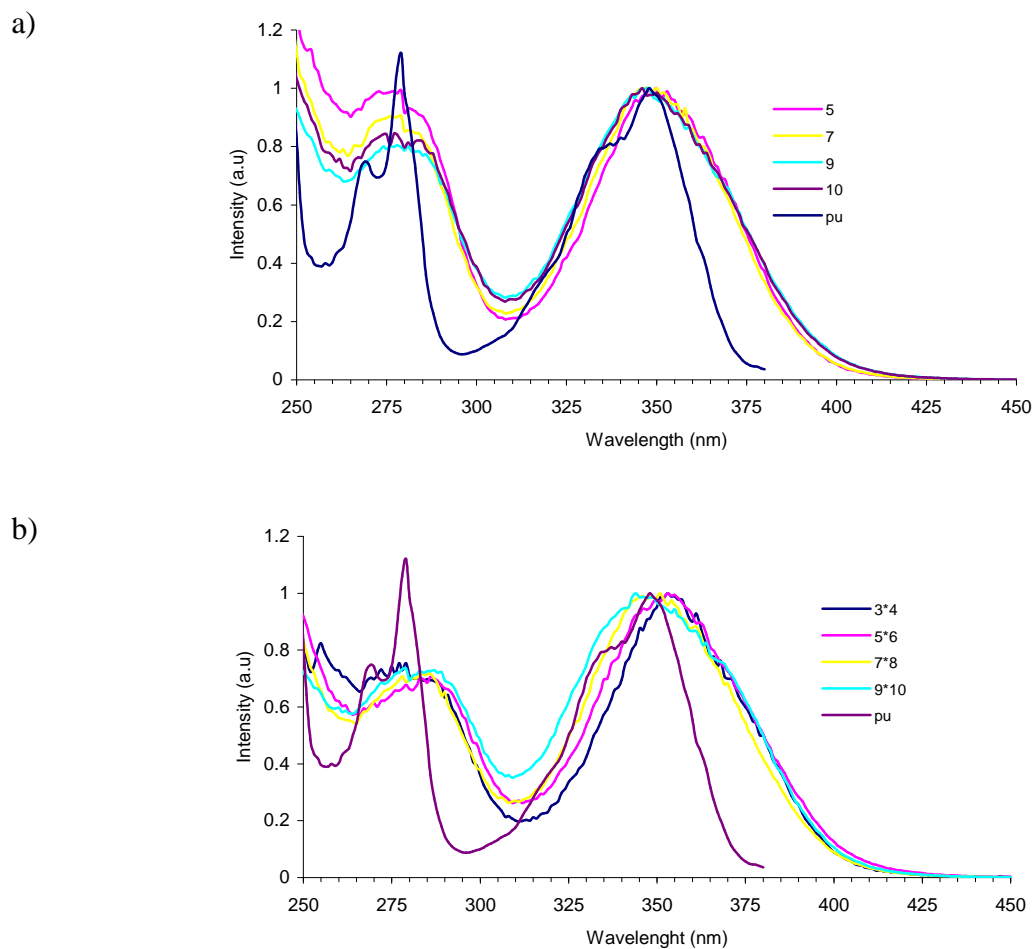
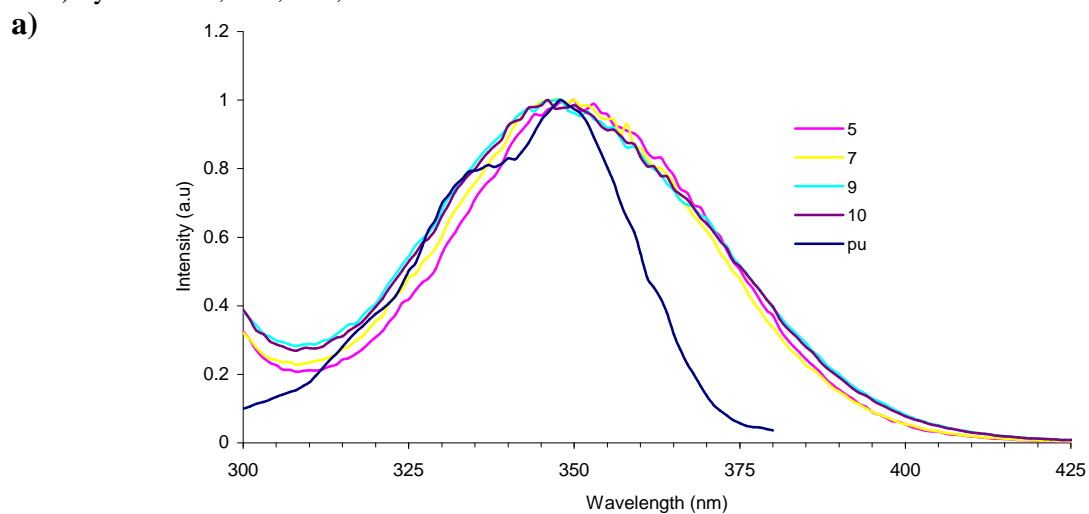


Figure 3.5 Normalized excitation spectra a) single strands **5**, **7**, **9**, **10** and pyrene-1,8-dicarboxylic acid bis-[(3-hydroxy-propyl)amide] (PU, used as reference of monomeric pyrene), and b) hybrids **3*4**, **5*6**, **7*8**, **9*10**.



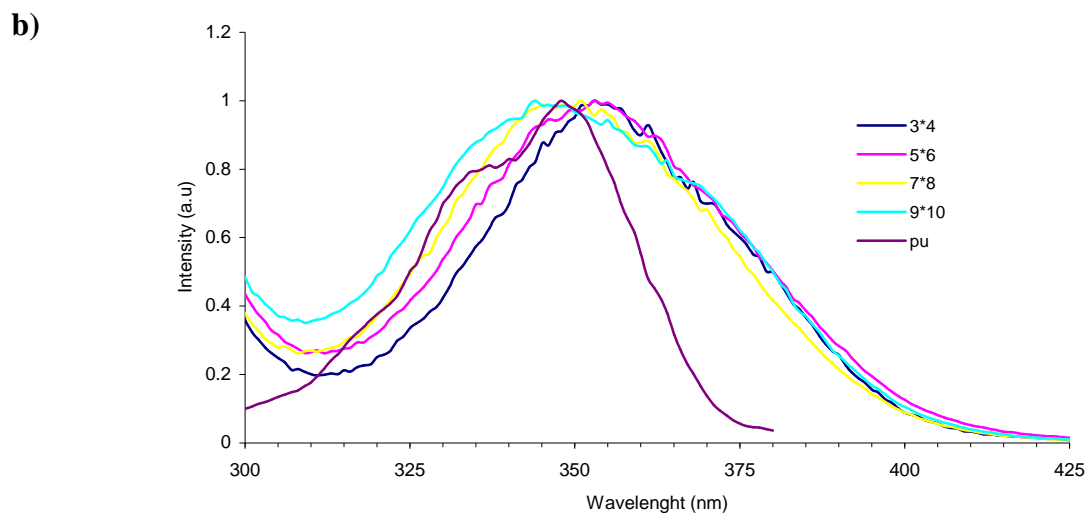


Figure 3.6 Normalized excitation spectra a) single strands **5**, **7**, **9**, **10** and PU, and b) hybrids **3*4**, **5*6**, **7*8**, **9*10** in the pyrene area.

Indeed, confirmation of a helical arrangement of the interstrand stacked pyrenes was obtained by circular dichroism (CD) spectroscopy (Figure 3.7).

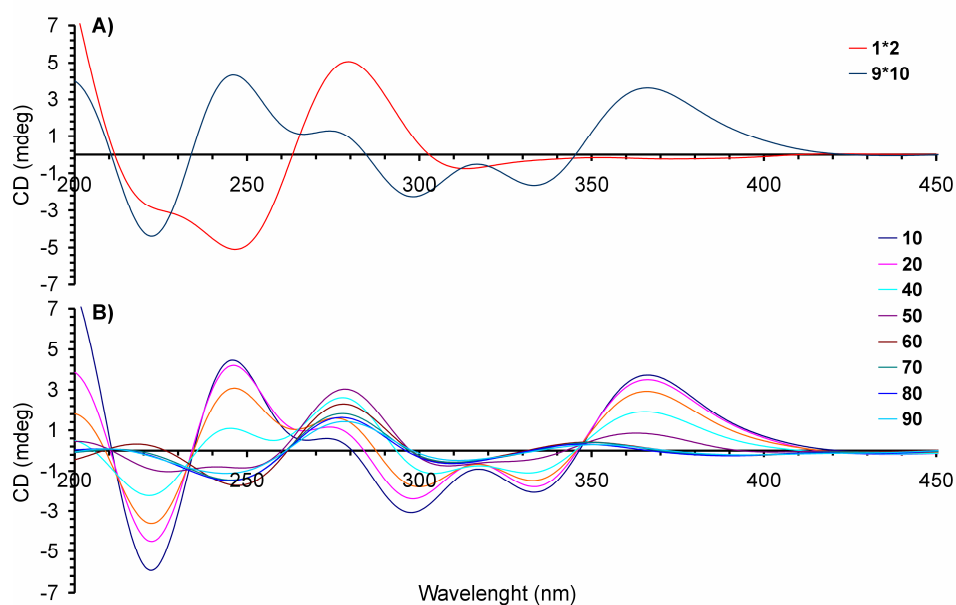


Figure 3.7 a) CD spectra of natural duplex **1*2** and modified duplex **9*10** at 25 °C; b) temperature dependent CD spectra of duplex **9*10** (10→90°C; 1.0 μ M solution in phosphate buffer, pH = 7.0).

The CD spectra of the pyrene modified hybrid **9*10** and the unmodified DNA duplex **1*2** at room temperature are shown in Figure 3.7a. Evidently, the spectrum of **9*10** in the 200-315 nm range is very different from the one observed for B-DNA (**1*2**). The spectrum is dominated by strong dichroism of the pyrene bands indicating a well ordered structure in the oligopyrene part of the duplex. Further evidence for this comes from the very intense bisignate signal for the pyrene band centered at 348 nm with a positive Cotton effect at $\lambda = 365$ nm ($\Delta\epsilon = +113 \text{ M}^{-1}\text{cm}^{-1}$) followed by a minimum at $\lambda = 332$ nm ($\Delta\epsilon = -62 \text{ M}^{-1}\text{cm}^{-1}$). Since there is no interference with the nucleobases in this area of the spectrum, the shape of this signal provides valuable insight into the stacking arrangement of the pyrenes. Thus, a positive amplitude ($A = +175$) obtained from exciton coupled CD reveals a positive chirality.^{19, 20} These data suggest that the pyrenes are arranged in a right-handed helical orientation within the oligopyrene stack. Upon increasing the temperature from 10 to 90°C, the CD couplet in the pyrene 350nm region gradually disappears and the remaining part of the spectrum adopts the features of a normal B-DNA (Figure 3.7b). It is remarkable that bisignate signals of pyrene are not present in CD spectra of single strands **9** and **10** revealing a random aggregation of pyrene units (Figure 3.8). The band at 350 nm corresponding to the maximum of pyrene absorbance is not split. Therefore it represents ICD (induced CD) of pyrene induced by chiral environment of the oligonucleotides.

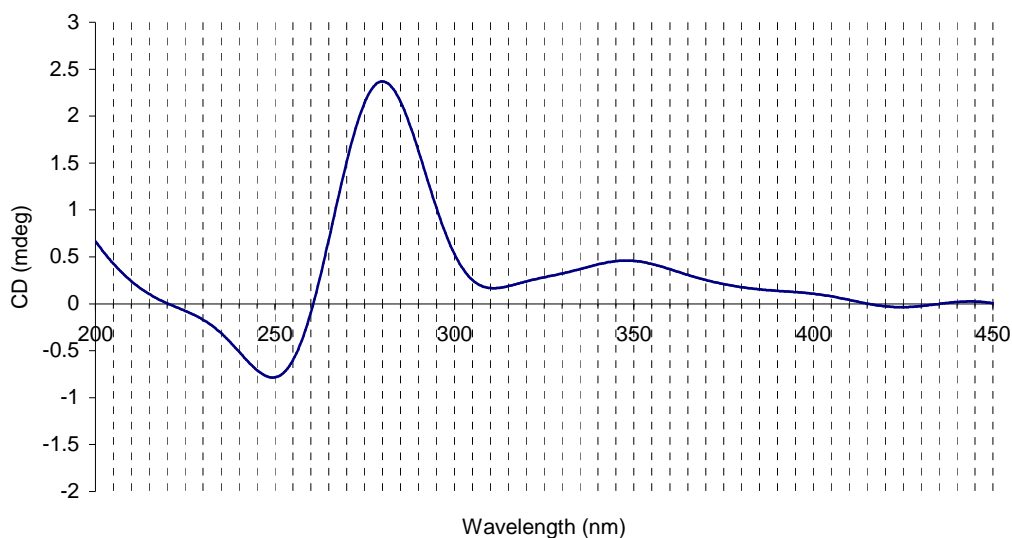


Figure 3.8 CD spectra of single strand **9** (1.0 μM , pH 7, 10 °C).

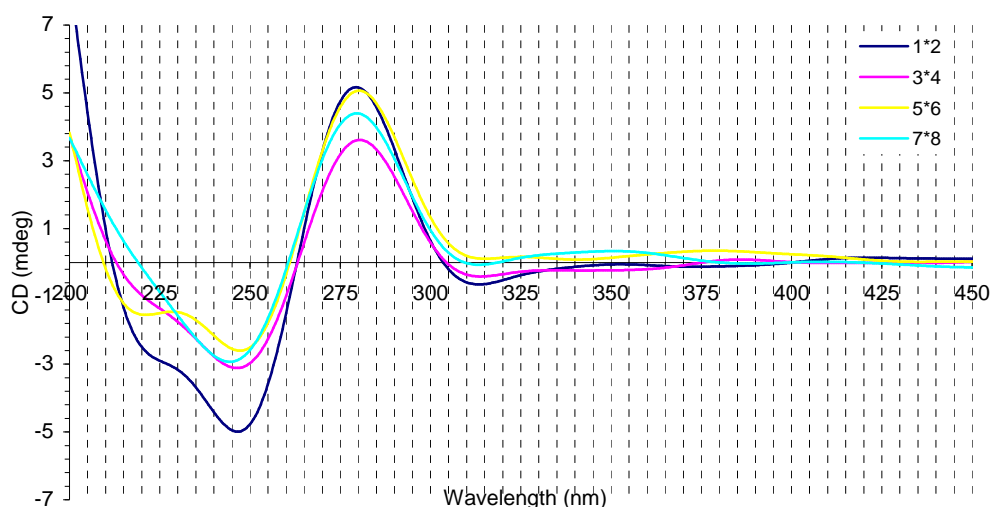


Figure 3.9 CD spectra of duplexes **1*2**, **3*4**, **5*6** and **7*8**.

Furthermore, also the CD spectra of duplexes **3*4**, **5*6** and **7*9** were very similar to normal B-DNA, showing no signs of helicity in the oligopyrene part (Figure 3.9). Duplex **9*10** represents a system composed of 28 natural nucleotides and 14 pyrene units. Therefore, the question of the cooperativity of duplex melting is an important issue. To determine if the duplex-to-single strand transition follows a two-state model, the melting process was additionally monitored at different wavelengths.²¹ For this purpose, temperature-dependent absorbance was recorded at 354 nm (pyrene absorbance only) and 245nm (pyrene and oligonucleotides absorbance). Comparison of these data, together with the already described values obtained at 260nm, showed an excellent agreement (Table 3.2), suggesting a high degree of cooperativity between the different parts.

Table 3.2 Melting temperatures determined at 245, 260, 354 nm.

Hybrids	T _m °C	T _m °C	T _m °C
	245 nm ^[a]	260 nm ^[a]	354 nm ^[b]
1*2	70.2	70.5	-
3*4	69.9	70.1	70.1
5*6	68.7	68.0	68.0
7*8	65.1	65.1	65.9
9*10	56.3	56.5	55.4

[a] Oligonucleotide and pyrene absorbance; [b] pyrene absorbance.

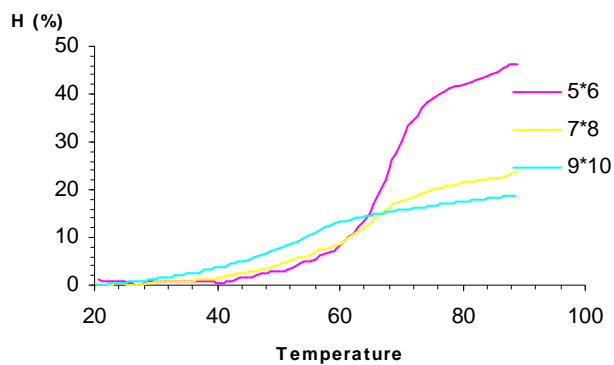


Figure 3.10 Hyperchromicity of hybrids at 354 nm.

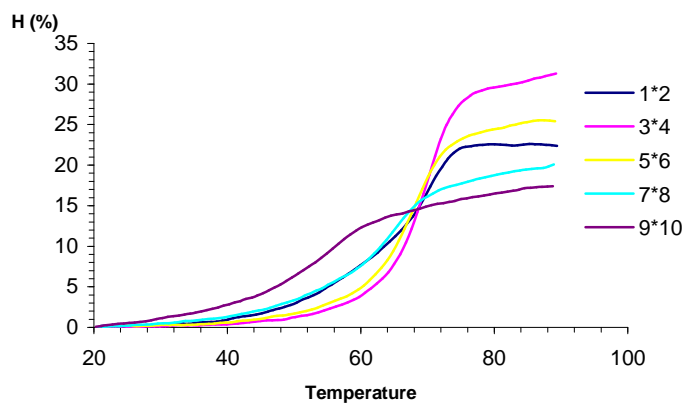


Figure 3.11 Hyperchromicity of hybrids at 245 nm.

The arrangement of pyrene molecules covalently linked to the sugar backbone in RNA²² or to base residues in DNA²³ was published recently. In these studies, DNA or RNA were used as structural scaffolds for the helical arrangement of pyrenes. In contrast to these intrastrand helical stacks along a DNA or RNA backbone,^{22, 23} the present system describes the self-organization of two non-nucleosidic oligopyrene strands in an interstrand helical stack. Since the experiments were carried out in aqueous conditions, stacking of the pyrenes will be largely driven by hydrophobic interactions. However, due to the presence of an amide-type linker, hydrogen bond formation may also play a significant role for the stability as well as for the organization of the helical structure.²⁴ A crystal structure obtained from the building block *pyrene-1,8-dicarboxylic acid bis-[(3-hydroxy-propyl)-amide]* shows the existence of hydrogen bonds between the amide groups of adjacent pyrenes. Furthermore, the pyrene units are stacked in a twisted, face-to-face orientation in the crystal (see Annex V).²⁵

3.4 Conclusion

In summary, a self-organizing system composed of two oligopyrene strands leading to the formation of an *interstrand helical stack* embedded in a double stranded DNA has been reported. Helical organization, as shown with fluorescence and CD spectroscopy, takes place in a hybrid containing fourteen consecutive achiral pyrene building blocks but not within the respective single strands nor in hybrids containing only six or less pyrene residues. Interstrand stacking of the pyrenes within the duplex is supported by high duplex stability as well as by UV-VIS and fluorescence spectroscopy. The findings are important for the design of artificial molecular double stranded helices for applications in nanotechnology.

3.5 Experimental Part

The required pyrene building block was synthesized according to a published procedure (S. M. Langenegger, R. Häner, *Chem. Commun.* **2004**, 2792-2793.) Nucleoside phosphoramidites from *Transgenomic* (Glasgow, UK) were used for oligonucleotide synthesis. Oligonucleotides **1-10** were prepared *via* automated oligonucleotide synthesis by a standard synthetic procedure ('trityl-off' mode) on a 394-DNA/RNA synthesizer (*Applied Biosystems*). Cleavage from the solid support and final deprotection was done by treatment with 30% NH₄OH solution at 55°C overnight. All oligonucleotides were purified by reverse phase HPLC (LiChrospher 100 *RP-18*, 5µm, Merck), *Bio-Tek Instruments Autosampler 560*); eluent A = (Et₃NH)OAc (0.1 M, pH 7.4); eluent B = MeCN; elution at 40°C; gradient 5 – 20% B over 30 min.

Mass spectrometry of oligonucleotides was performed with a Sciex QSTAR pulsar (hybrid quadrupole time-of-flight mass spectrometer, *Applied Biosystems*). ESI-MS (negative mode, CH₃CN/H₂O/TEA) data of compounds **1-10** are presented in Table 3.3.

Table 3.3 Mass spectrometry data (molecular formula, calc. average mass, and obtained).

Oligo.		Molecular formula	Calc. aver.mass	Found
1	(5') AGC TCG GTC ATC GAG AGT GCA	C ₂₀₅ H ₂₅₇ N ₈₃ O ₁₂₃ P ₂₀	6471.3	6472
2	(3') TCG AGC CAG TAG CTC TCA CGT	C ₂₀₃ H ₂₅₈ N ₇₆ O ₁₂₅ P ₂₀	6382.2	6383
3	(5') AGC TCG GTC ASC GAG AGT GCA	C ₂₁₉ H ₂₆₇ N ₈₃ O ₁₂₂ P ₂₀	6633.5	6632
4	(3') TCG AGC CAG TSG CTC TCA CGT	C ₂₁₇ H ₂₆₉ N ₇₃ O ₁₂₆ P ₂₀	6535.4	6534
5	(5') AGC TCG GTC SSC GAG AGT GCA	C ₂₃₃ H ₂₇₈ N ₈₀ O ₁₂₃ P ₂₀	6786.7	6785
6	(3') TCG AGC CAG SSG CTC TCA CGT	C ₂₃₁ H ₂₇₉ N ₇₃ O ₁₂₅ P ₂₀	6697.7	6696
7	(5') AGC TCG GTS SSC GAG AGT GCA	C ₂₄₈ H ₂₈₉ N ₇₉ O ₁₂₃ P ₂₀	6964.0	6963
8	(3') TCG AGC CAS SSG CTC TCA CGT	C ₂₄₅ H ₂₉₀ N ₇₀ O ₁₂₅ P ₂₀	6834.9	6834
9	(5') AGC TCS SSS SSS GAG AGT GCA	C ₃₀₅ H ₃₃₂ N ₇₂ O ₁₂₂ P ₂₀	7577.9	7576.1
10	(3') TCG AGS SSS SSS CTC TCA CGT	C ₃₀₃ H ₃₃₄ N ₆₂ O ₁₂₆ P ₂₀	7479.8	7487.1

All the spectroscopic measurements were performed in potassium phosphate buffer (10 mM, 100 mM NaCl, pH 7.0) for 1.0 μ M oligonucleotide concentration (1.0 μ M of each strand in case of duplex), $\epsilon_{260}= 9000$ was used for pyrene units.

Thermal denaturation experiments were carried out on *Varian Cary-100 Bio-UV/VIS* spectrophotometer equipped with a *Varian Cary-block* temperature controller and data were collected with *Varian WinUV* software at 245, 260 and 354 nm (cooling-heating-cooling cycles in the temperature range of 20-90°C, temperature gradient of 0.5°C/min). Temperature melting (T_m) values were determined as the maximum of the first derivative of the smoothed melting curve.

Temperature dependent UV-VIS spectra were collected with an optic path of 1 cm over the range of 210-500 nm at 10-90 °C with a 10 °C interval on *Varian Cary-100 Bio-UV/VIS* spectrophotometer equipped with a *Varian Cary-block* temperature controller. The cell compartment was flushed with N_2 .

Temperature dependent fluorescence data were collected on a *Varian Cary Eclipse* fluorescence spectrophotometer equipped with a *Varian Cary-block* temperature controller (excitation at 354 nm; excitation and emission slit width of 5 nm) using 1 per 1 cm quartz cuvettes. *Varian Eclipse* software was used to investigate the fluorescence of the different pyrene-containing oligonucleotides at a wavelength range of 375-700 nm in the temperature range of 10-90 °C.

CD spectra were recorded on a *JASCO J-715* spectrophotometer using quartz cuvettes with an optic path of 1 cm.

3.6 References

1. a) D. S. Hopkins, D. Pekker, P. M. Goldbart, A. Bezryadin, *Science*, **2005**, 1762-1765; b) N. C. Seeman, *Nature* **2003**, 421, 427-431; c) R. Bashir, *Superlattices and Microstructures*, **2001**, 29, 1-16; d) K. Keren, R. S. Berman, E. Buchstab, U. Sivan, E. Braun, *Science*, **2003**, 1380-1382; e) A. Pike, B. Horrocks, B. Connolly, A. Houlton, *Aust. J. Chem.* **2002**, 55, 191-194.
2. a) M. H. Caruthers, *Science* **1985**, 230, 281-285; b) N. D. Sinha, J. Biernat, J. McManus, H. Köster, *Nucleic Acids Res.* **1984**, 12, 4539-4557.
3. a) J. R. Heath, M. A. Ratner, *Physics Today*, **2003**, 43-49; b) K. V. Gothelf, T. H. LaBean, *Org. Biomol. Chem.* **2005**, 3, 4023-4037; c) G. Maruccio, R. Cingolani, R. Rinaldi, *J. Mater. Chem.* **2004**, 542-554; e) J. Wengel, *Org. Biomol. Chem.* **2004**, 2, 277-280; e) C. M. Niemeyer, M. Adler, *Angew. Chem. Int. Ed.* **2002**, 41, 3779-3783; f) R. Fiammengo, M. Crego-Calama, D. N. Reinhoudt, *Curr. Opin. Chem. Biol.* **2001**, 660-673.
4. a) A. Eschenmoser, *Chimia* **2005**, 59, 836-850; b) B. Samori, G. Zuccheri, *Angew. Chem. Int. Ed.* **2005**, 1166-1181; c) P. Herdewijn, *Biochim. Biophys. Acta, Gene Struct. Expr.* **1999**, 1489, 167-179; d) O. Kohler, D. V. Jarikote, I. Singh, V. S. Parmar, E. Weinhold, O. Seitz, *Pure and Applied Chemistry* **2005**, 77, 327-338.
5. a) C. Piguet, G. Bernardinelli, G. Hopfgartner, *Chem. Rev.* **1997**, 97, 2005-2062; b) D. J. Hill, M. J. Mio, R. B. Prince, T. S. Hughes, J. S. Moore, *Chem. Rev.* **2001**, 101, 3893-4011; c) A. E. Rowan, R. J. M. Nolte, *Angew. Chem. Int. Ed.* **1998**, 37, 63-68; d) S. H. Gellman, *Acc. Chem. Res.* **1998**, 31, 173-180.
6. a) V. Berl, I. Huc, R. G. Khoury, M. J. Krische, J.-M. Lehn, *Nature* **2000**, 407, 720-723; b) K. Tanaka, A. Tengeiji, T. Kato, N. Toyama, M. Shionoya, *Science* **2003**, 299, 1212-1213; c) J.-M. Lehn, A. Rigault, J. Siegel, J. Harrowfield, B. Chevrier, D. Moras, *Proc. Natl. Acad. Sci. USA* **1987**, 84, 2565-2569; d) Y. Tanaka, H. Katagari, Y. Furusho, E. Yashima, *Angew. Chem. Int. Ed.* **2005**, 44, 3867-3870; e) E.C. Constable, *Chem. Soc. Rev.* **2007**, 36, 246-253; f) X. Yang, S. Martinovic, R. D. Smith, B. J. Gong, *Amer. Chem. Soc.* **2003**, 125, 9932-9933.

7. double helix in water solutions: a) G. L. Gabriel, B. L. Iverson, *J. Amer. Chem. Soc.* **2002**, *124*, 15174-15175; b) I. Huc, V. Maurizot, H. Gornitzka, J.-M. Leger, *Chem. Commun.* **2002**, 578-579; c) H. Goto, H. Katagari, Y. Furusho, E. Yashima, *J. Amer. Chem. Soc.* **2006**, *128*, 7176-7178, and references therein.
8. M. Albrecht, *Angew. Chem. Int. Ed.* **2005**, *44*, 6448-6451.
9. F. Samain, V. L. Malinovskii, S. M. Langenegger, R. Häner, *Bioorg. Med. Chem.* **2008**, *16*, 27-33.
10. R. L. Letsinger, T. Wu, *J. Amer. Chem. Soc.* **1995**, *117*, 7323-7328.
11. a) F. D. Lewis, R. L. Letsinger, M. R. Wasielewski, *Acc. Chem. Res.* **2001**, *34*, 159-170; b) Y. Zheng, H. Long, G. C. Schatz, F. D. Lewis, *Chem. Commun.* **2005**, 4795-4797; c) Y. Zheng, H. Long, G. C. Schatz, F. D. Lewis, *Chem. Commun.* **2006**, 3830-3832.
12. a) S. M. Langenegger, R. Häner, *Helv. Chim. Acta* **2002**, *85*, 3414-3421; b) S. M. Langenegger, R. Häner, *Tetrahedron Lett.* **2004**, *45*, 9273-9276; c) S. M. Langenegger, R. Häner, *ChemBioChem* **2005**, *6*, 848-851; d) S. M. Langenegger, R. Häner, *ChemBioChem* **2005**, *6*, 2149-2152.
13. S. M. Langenegger, R. Häner, *Chem. Commun.* **2004**, 2792-2793.
14. N. R. Markham, M. Zuker, *Nucleic Acids Research*, web server issue **2005**, W577-W581.
15. a) D. J. Cram, *Angew. Chem. Int. Ed.* **1988**, *27*, 1009-1020; b) E. T. Kool, *Chem. Rev.* **1997**, *97*, 1473-1487.
16. a) I. Tinoco, Jr., *J. Amer. Chem. Soc.* **1960**, 4785-4790; b) C. R. Cantor, P. R. Schimmel, *Biophysical Chemistry, part II*; W. H. FREEMAN AND COMPANY, New York, **1980**, pp. 349-408.
17. F. M. Winnik, *Chem. Rev.* **1993**, *93*, 587-614.
18. *pyrenophanes*: a) H. A. Staab, N. Riegler, F. Diederich, C. Krieger, D. Schweitzer, *Chem. Ber.* **1984**, *117*, 246-259; b) H. A. Staab, R. G. H. Kirrstetter, *Liebigs Ann. Chem.* **1979**, 886-898; *bis-pyrenyl systems*: c) K. A. Zachariasse, W. Kuhnle, A. Weller, *Chem. Phys. Lett.* **1978**, *59*, 375-380; d) T. Kanaya, K. Goshiki, M. Yamamoto, Y. Nishijima, *J. Am. Chem. Soc.* **1982**, *104*, 3580-3587; e) M. J. Snare, P. J. Thistlethwaite, K. P. Ghiggino, *J. Am. Chem. Soc.*, **1983**, *105*,

- 3328-3332; f) P. Wahl, C. Krieger, D. Schweitzer, H. A. Staab, *Chem. Ber.* **1984**, *117*, 260-276; other examples with strained pyrene movement: g) O. Shoji, D. Nakajima, M. Annaka, M. Yoshikuni, T. Nakahira, *Polymer* **2002**, *43*, 1711-1714; h) I. Suzuki, M. Ui, A. Yamauchi, *J. Am. Chem. Soc.* **2006**, *128*, 4498-4499.
19. *Positive exciton chirality* is defined as a right handed twist of the electric transition dipole moments of two chromophores, see N. Berova, K. Nakanishi, in *Circular dichroism: principles and applications* (Eds: N. Berova, K. Nakanishi, R. W. Woody), WILEY-VCH, New York, **2000**, pp. 337-382.
20. *exciton coupled method applied to pyrene system*, e.g.: a) A. Ueno, I. Suzuki, T. Osa, *J. Am. Chem. Soc.* **1989**, *111*, 6391-6397; b) H. Mihara, J. Hayashida, H. Hasegawa, H. I. Ogawa, T. Fujimoto, N. Nishino, *J. Chem. Soc. Perkin. Trans. 2*, **1997**, 517-522; c) S. Yagi, H. Kitayama, T. Takagishi, *J. Chem. Soc. Perkin. Trans. 1*, **2000**, 925-932; d) O. Shoji, D. Nakajima, M. Ohkawa, Y. Fujiwara, M. Annaka, M. Yoshikuni, T. Nakahira, *Macromolecules* **2003**, *36*, 4557-4566.
21. a) R. Lumry, R. Biltonen *Biopolymers* **1966**, *4*, 917-944; b) J. SantaLucia, Jr. in *Spectrophotometry and spectrofluorimetry, a practical approach* (Ed: M. G. Gore), OXFORD, New York **2000**, pp. 329-356.
22. M. Nakamura, Y. Ohtoshi, K. Yamana, *Chem. Commun.* **2005**, 5163-5165.
23. a) E. Mayer-Enthart, H.-A. Wagenknecht, *Angew. Chem. Int. Ed.* **2006**, *45*, 3372-3375; b) J. Barbic, H.-A. Wagenknecht, *Org. Biomol. Chem.* **2006**, *4*, 2088-2090.
24. for recent review on amide bond directed foldamers see: I. Huc, *Eur. J. Org. Chem.* **2004**, 17-29.
25. CCDC 636616 contains the supplementary crystallographic data for pyrene-1,8-dicarboxylic acid bis-[(3-hydroxy-propyl)amide]. These data can be obtained free of charge from *The Cambridge Crystallographic Data Centre* http://www.ccdc.cam.ac.uk/data_request/cif.

Chapter 4: DNA Containing Extended Stretches of Pyrene Building Blocks

4.1 Abstract

We have shown in *Chapter 3* a highly ordered structure within a hybrid containing 14 consecutive achiral pyrene residues. In addition to giving insight into the intrastrand and interstrand interactions, DNA mimics containing 8, 10, 12 pyrene building blocks placed in opposite positions in the middle of the DNA duplex have been investigated. Thermal denaturation experiments and spectroscopic investigation of pyrene-containing double strands attempt to clarify the origin of the interstrand helical organization within an entirely artificial section embedded in a double-stranded DNA molecule.

4.2 Introduction

The unique feature of DNA (and modified DNA) for self-organization is one of the main characteristics that are practically used in developments of new therapeutic agents or construction of diagnostic tools.¹ More recently, because of predictability of self organization, simplicity of synthesis, and a wide range of possible modification, DNA was proposed as a very promising building block for the needs of nanotechnology.² DNA building blocks may serve both as real components of nanochemistry devise or as a template for nanostructures.³ However it is recognized that natural DNA building blocks have predefined physical properties which can limit the possible applications. Expanding of genetic alphabet is believed to be one of required tools in DNA based developments in medicinal and materials chemistry.⁴

Since the discovery of the double helix of DNA, folded and helical structures have attracted increasing attention as synthetic targets.⁶ Affords in this direction can be simply

divided in development of single strand and double stranded folded/helical structures. In meantime a formation of single strand folded systems is more developed^{5,6} and for some of them helical secondary structure was established.⁷ Double helices formed from synthetic single strands are relatively rare when compared to synthetic single strands.⁸ We have described in *Chapter 3* a high ordered structure based on non-nucleosidic pyrene building blocks embedded in a DNA framework. The construct which has been described, represents the first example of interstrand-formed helical organization within fully artificial part (fourteen pyrene units) of modified DNA.⁹ In addition to giving insight into the intrastrand and interstrand interactions, DNA mimics containing 8, 10, 12 pyrene building blocks placed in opposite positions in the middle of the DNA duplex have been investigated. In the following, the description of results will be divided into two parts, that is, the thermal denaturation experiments and spectroscopic investigation of pyrene-containing double strands.

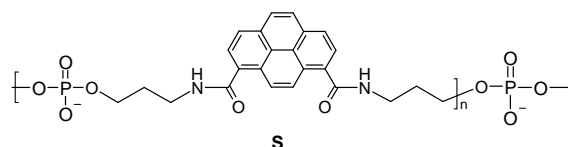
4.3 Results and discussion

4.3.1 Thermal denaturation experiments

Before investigation of the spectroscopic properties of pyrene containing oligomers, the stability of hybrids was tested by thermal denaturation. The data are summarized in Table 4.1. Oligonucleotides **1** and **2** serve as controls and oligomers **3-10** contain between four and seven pyrene building blocks per single strand. T_m values are in agreement with previous findings with one, two, three and seven pyrene building blocks per single strand. Table 4.1 shows the experimental T_m values as well as the calculated values for the corresponding hybrids without any contribution from the pyrene residues. The latter value, which was calculated according to the method described by *Markham and Zuker*¹⁰, allows an estimation of the contribution of the pyrene groups to the overall stability (ΔT_m). Pyrene residues (8, 10 and 12 units) have a large positive effect on the T_m value of the respective hybrids. This finding confirms that interstrand interactions between the pyrene units lead to a significant stabilization of the duplex from four to seven pyrene residues per single strand

Table 4.1 Influence of non-nucleosidic pyrene building blocks on hybrid stability

Oligo #	duplex ^[a]	T _m (°C) exp. ^[b]	ΔT _m calc. ^[c]	ΔT _m , °C ^[d]
1	(5') AGC TCG GTC ATC GAG AGT GCA	71.3	71.3	-
2	(3') TCG AGC CAG TAG CTC TCA CGT			
3	(5') AGC TCG GSS SSC GAG AGT GCA	63.5	46.0	+17.5
4	(3') TCG AGC CSS SSG CTC TCA CGT			
5	(5') AGC TCG SSS SSC GAG AGT GCA	60.8	43.3	+16.7
6	(3') TCG AGC SSS SSG CTC TCA CGT			
7	(5') AGC TCG SSS SSS GAG AGT GCA	60.4	36.9	+23.5
8	(3') TCG AGC SSS SSS CTC TCA CGT			
9	(5') AGC TCS SSS SSS GAG AGT GCA	54.1	32.9	+21.2
10	(3') TCG AGS SSS SSS CTC TCA CGT			



[a] 1.0 μM each strand, 10 mM phosphate buffer, pH 7.0); [b] experimental value; average of three independent experiments; exp. error +/-0.5°C; [c] T_m value calculated for the corresponding hybrid formed by the two strands without contribution of the unnatural building blocks according to the method described by *Markham and Zuker*¹⁰; [d] difference between experimental and calculated T_m value; this number corresponds to the contribution of the pyrene residues to the overall duplex stability.

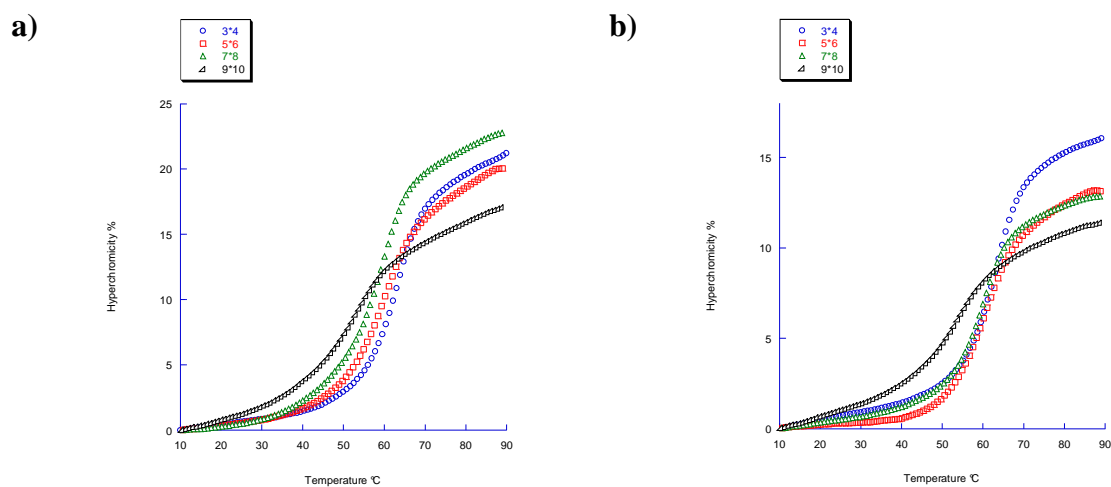
To address the question of the cooperativity of duplex melting, temperature-dependent experiments were recorded at 354 nm (pyrene absorbance only) and 245 nm (pyrene and nucleobase absorbance). Comparison of these data, together with the described values obtained at 260 nm, showed excellent agreement (Table 4.2), suggesting a high degree of cooperativity among the different sections of the hybrid.¹¹

Table 4.2 Melting temperatures determined at 245, 260, and 354 nm.

Hybrids	T _m °C 245 nm ^[a]	T _m °C 260 nm ^[a]	T _m °C 354 nm ^[b]
1*2	71.1	71.3	-
3*4	63.5	63.5	63.8
5*6	60.2	60.8	60.8
7*8	59.5	60.4	59.3
9*10	53.5	54.1	-

[a] Oligonucleotide and pyrene absorbance; [b] pyrene absorbance.

In addition all hybrids investigated in the study showed a single, cooperative transition at the three wavelengths as can be seen in Figure 4.1.



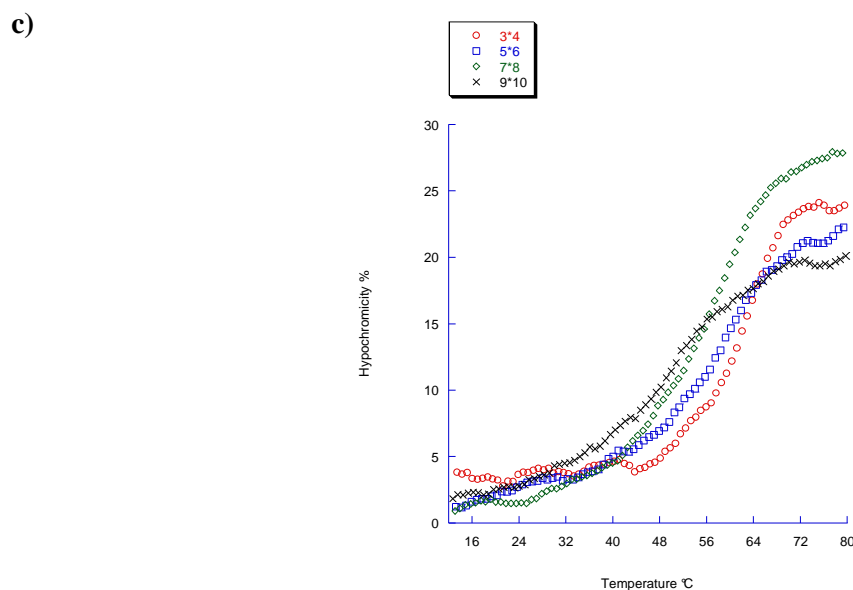


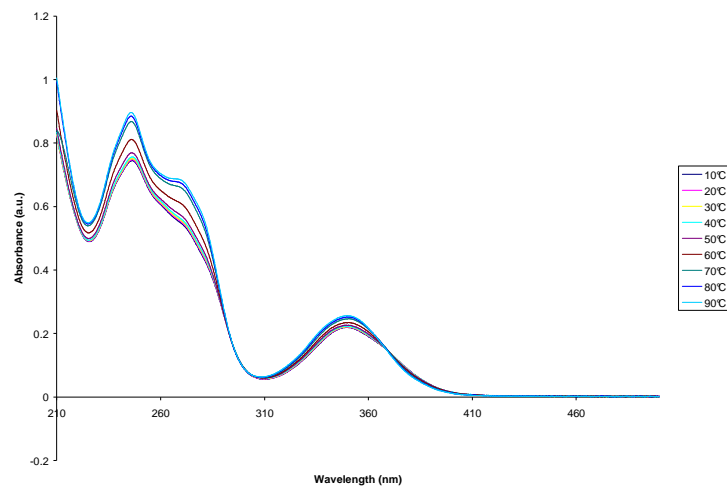
Figure 4.1 Thermal melting curves of hybrids at a) 245 nm; b) 260 nm; c) 350 nm.

The occurrence of inter- and intrastrand pyrene stacking interactions as well as the changes in conformation which lead to the helical organization in hybrids containing 12 and 14 pyrene units are supported by spectroscopic studies.

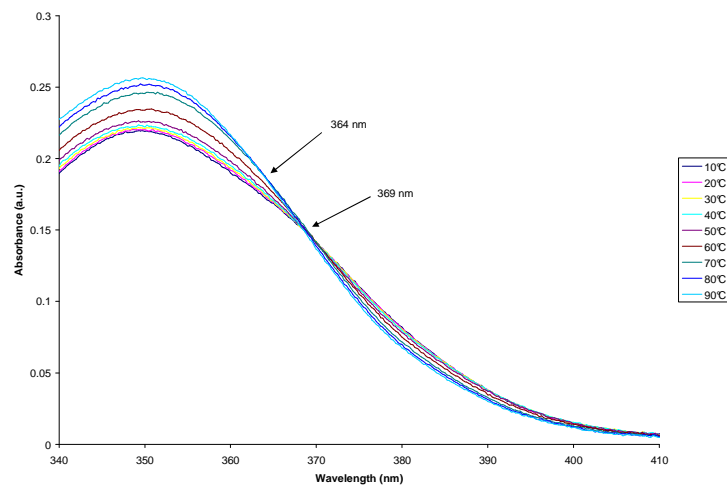
4.3.2 Spectroscopic Studies

The temperature-dependent UV-VIS spectra of hybrid **3*4**, **5*6**, **7*8**, and **9*10** are in agreement with previous findings. Two isosbestic points are present, indicating two different types of interaction between the pyrenes (Figure 4.2). One (at longer wavelength) is attributed to interstrand stacking in the hybrid and the second from intrastrand stacking in the single strands. Furthermore, signal broadening and hypochromicity, both of which serve as evidence for face-to-face aggregates,¹² were observed upon duplex formation. While this question has been partially answered previously in *Chapter 2*, we investigated temperature dependent fluorescence to attempt to clarify whether the behavior of **9*10** within double strand, described in *Chapter 3*, occurs linearly when the number of incorporated pyrenes rises up to seven.

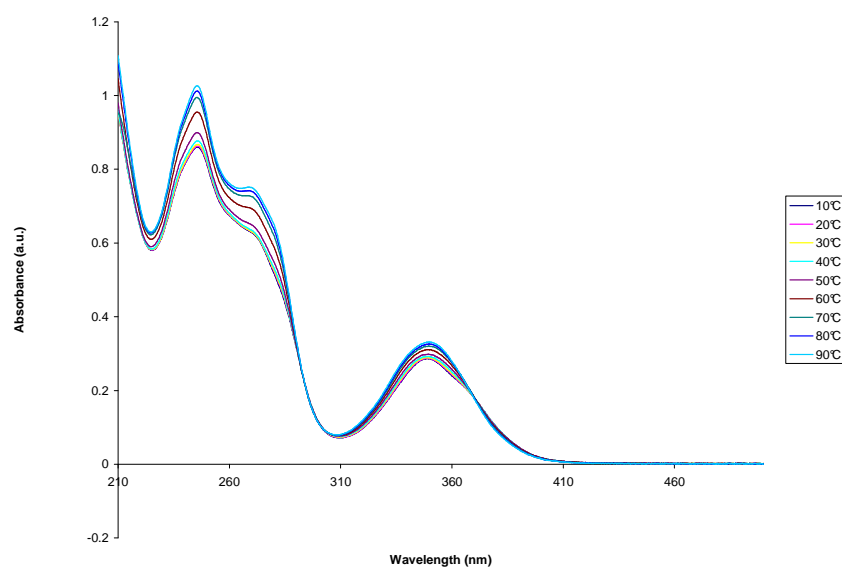
a)



b)



c)



d)

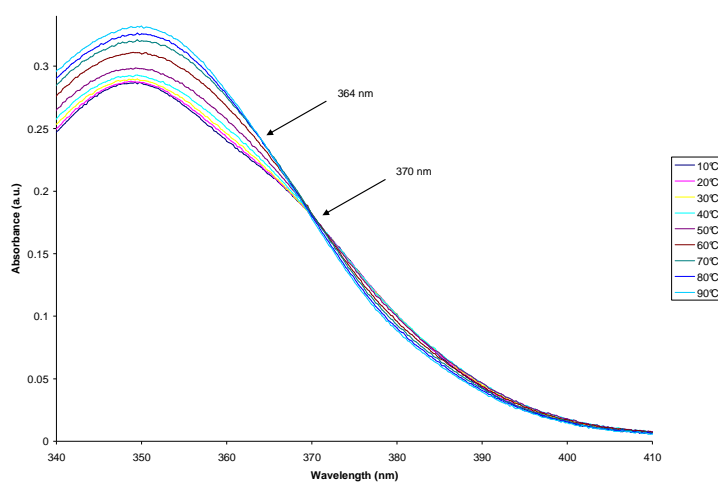
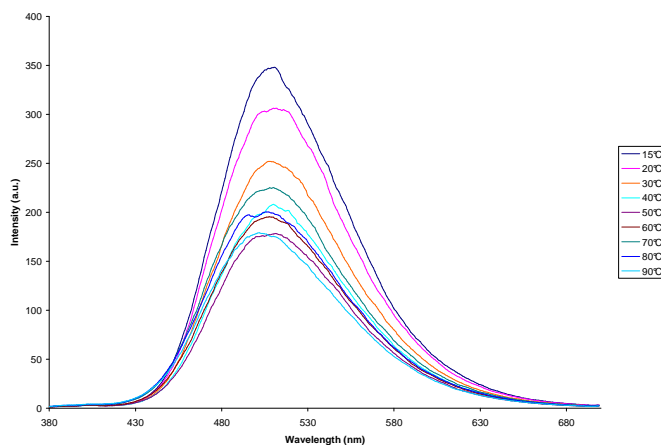


Figure 4.2 Temperature dependent UV-VIS of a) duplex **3*4** (210-500 nm, 10-90 °C); b) duplex **3*4**: isosbestic points at 369 and 364 nm; c) duplex **5*6** (210-500 nm, 10-90 °C); d) duplex **5*6**: isosbestic points at 370 and 364 nm.

The temperature dependent fluorescence spectra of hybrids show, in good agreement with our expectations, that pyrene units are strongly aggregated in double strand (Figure 4.3).

a)



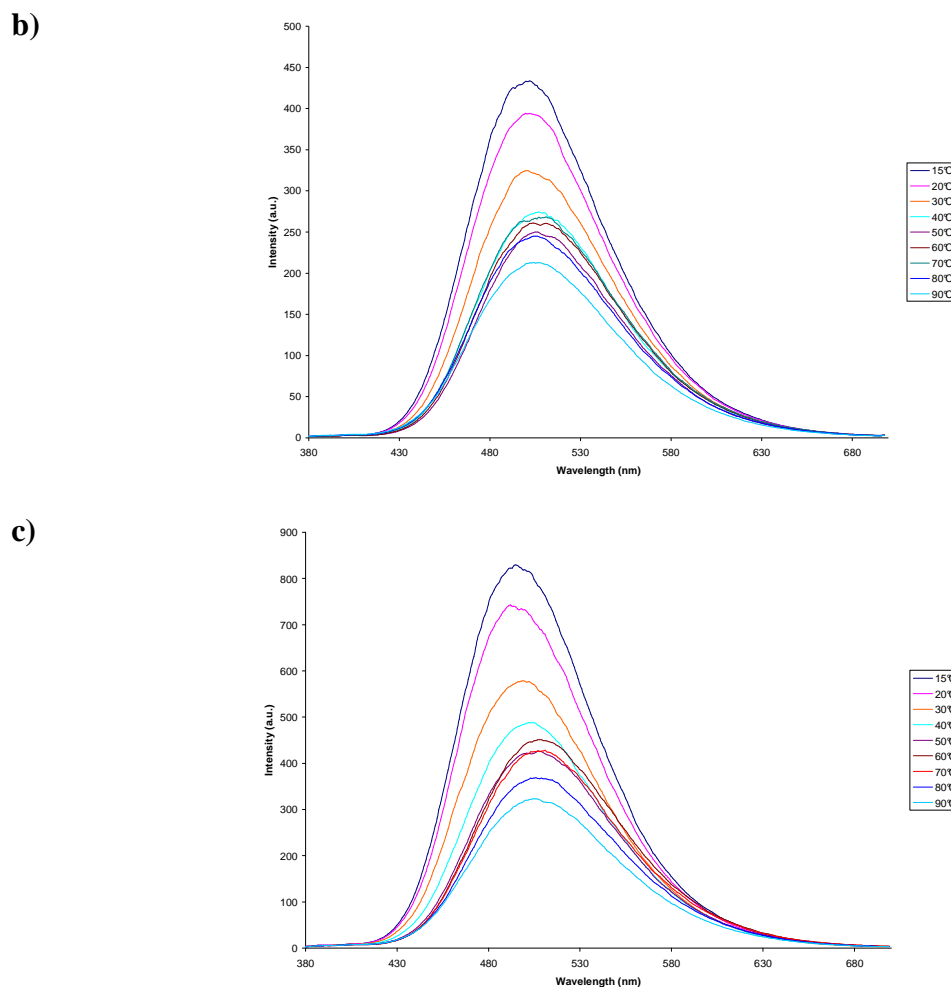


Figure 4.3 Fluorescence spectra of duplexes a) **3*4**, b) **5*6**, c) **7*8**.

Below the T_m , the emission intensity is decreasing with increasing temperature, indicating a geometrical change in the association of the pyrenes. In addition, the intensity is increasing upon melting and then is decreasing again above T_m . As can be seen in Figure 4.4, duplex formation of the hybrid **3*4** leads to a significant red shift (504 nm to 512 nm) when going from 90 \rightarrow 10 $^{\circ}$ C. However, the hybrid **5*6** shows a slight red shift (506 nm to 508 nm) and a stabilization of the maximum upon hybridization 90 \rightarrow 40 $^{\circ}$ C (T_m : 63.5 $^{\circ}$ C). When going from 40 \rightarrow 15 $^{\circ}$ C, the duplex formation leads to a blue shift (508 nm to 501 nm). The hybrid **7*8** shows a significant blue shift upon hybridization (509 nm to 497 nm). The behavior (helical arrangement of interstrand stacked pyrenes) of hybrid **9*10** has been described in *Chapter 3* showing that a sandwich-type aggregation of pyrene units is restricted within the duplex.¹³ Here is shown the transition between the

sandwich –type aggregation and twisted type structure leading to the helical arrangement. The twisting of the pyrene units upon adoption of the helical conformation explains the blue shift in the excimer emission that was already observed for other pyrene containing systems.¹⁴

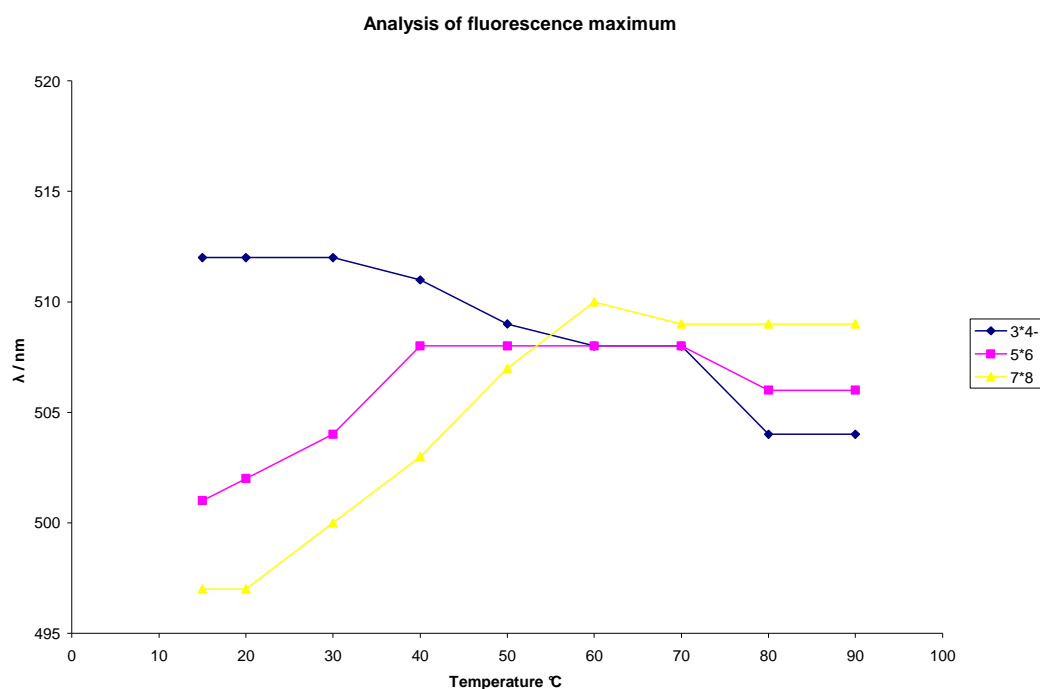


Figure 4.4 Trends of the excimer fluorescence maxima upon melting of hybrids. For conditions see Table 1.

So, compared to the hybrid **9*10**, the hybrid **7*8** adopts already a helical conformation upon duplex formation which would explain the blue-shifted emission (510 nm to 497 nm; 60→10°C) below melting temperature. Confirmation of changes in conformation of pyrene units when strands contain more than four pyrene moieties is supported by circular dichroism (CD) spectroscopy.

The CD spectrum of the hybrid **9*10** in the 200-315 nm range is completely different from the natural hybrid **1*2**. The spectrum indicates a well-ordered structure in the oligopyrene region of the duplex. Furthermore, a very intense bisignate signal for the pyrene band is centered at 348 nm showing the evidence for the helical arrangement.⁹ The CD spectra of the pyrene-modified hybrids **3*4**, **5*6**, **7*8**, **9*10** and the unmodified

DNA duplex are shown in Figure 4.5. Clearly, the spectrum of hybrids **7*8** at 25°C is in agreement with previous study of hybrid **9*10**. In the 200-315 nm range, the spectrum is dominated by strong dichroism of the pyrene bands, which indicates a well-ordered structure in the oligopyrene region of the duplex. Moreover further evidence for a helical arrangement comes from the very intense bisignate signal for the pyrene band centered at 347 nm. The CD spectrum of hybrid **3*4** is very similar to that of normal B-DNA with no signs of helicity in the oligopyrene region. However, the CD spectrum of hybrid **5*6** shows a slight negative band in the pyrene area (360 nm) and in the 200-250 nm range a new band at 235 nm.

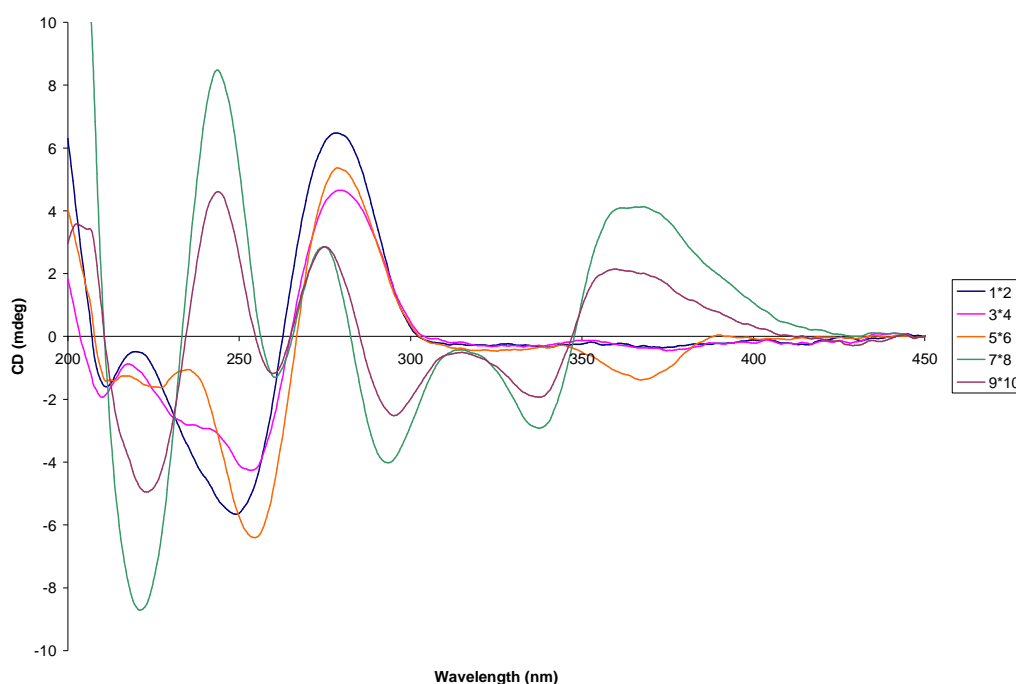


Figure 4.5 CD spectra of natural duplex **1*2** and hybrids **3*4**, **5*6**, **7*8**, and **9*10**. Conditions: 1.0 μM each strand, 10 mM phosphate buffer, pH 7.0.

In addition, the CD spectrum T° dependent of **5*6** provides further informations (Figure 4.6). The changes occur at wavelengths where the electronics transitions of achiral pyrene moieties arise. CD observed in the absorption band of achiral pyrene is the result of their electronic transition with the one of the DNA framework.¹⁵

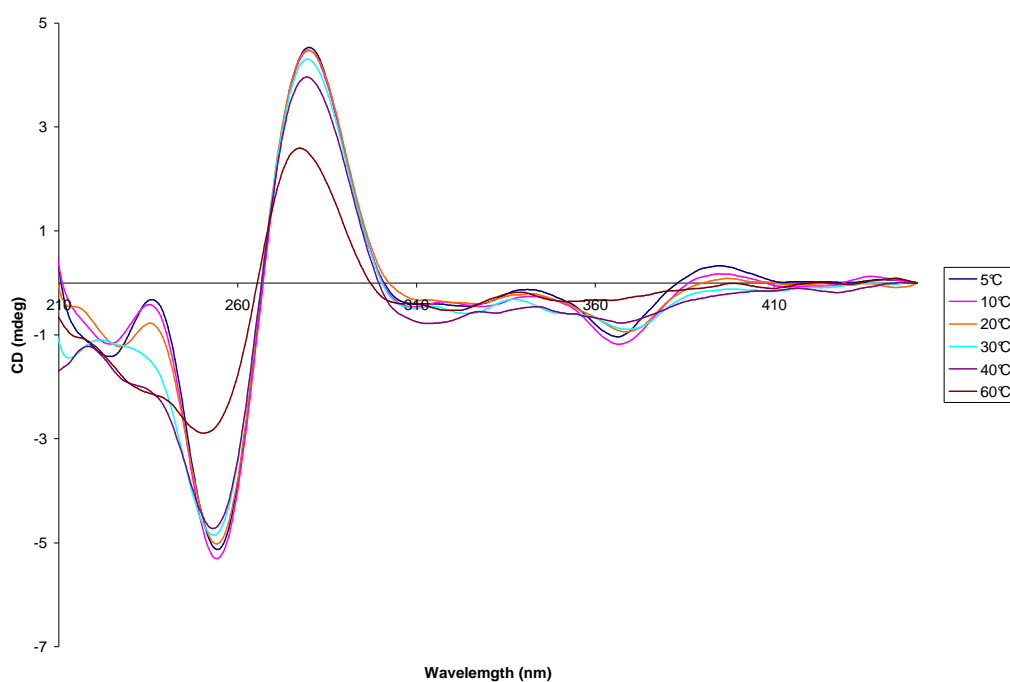


Figure 4.6 Temperature-dependent CD spectra of hybrid **5*6** (5→60°C; 1.0 μ M solution in phosphate buffer, pH 7.0).

The question arises whether pyrene are still face-to-face aggregated or if the rise of incorporated pyrene building blocks force already them to twist. To attempt to clarify this question, CD spectra of **3*4** and **5*6** have been recorded depending of NaCl concentrations (Figure 4.7). The data of hybrid **3*4** suggest that pyrenes do not organize upon rise of NaCl concentration. In addition data of hybrid **5*6** indicate no changes when NaCl concentration rises from 0.1 M NaCl up to 4M NaCl.

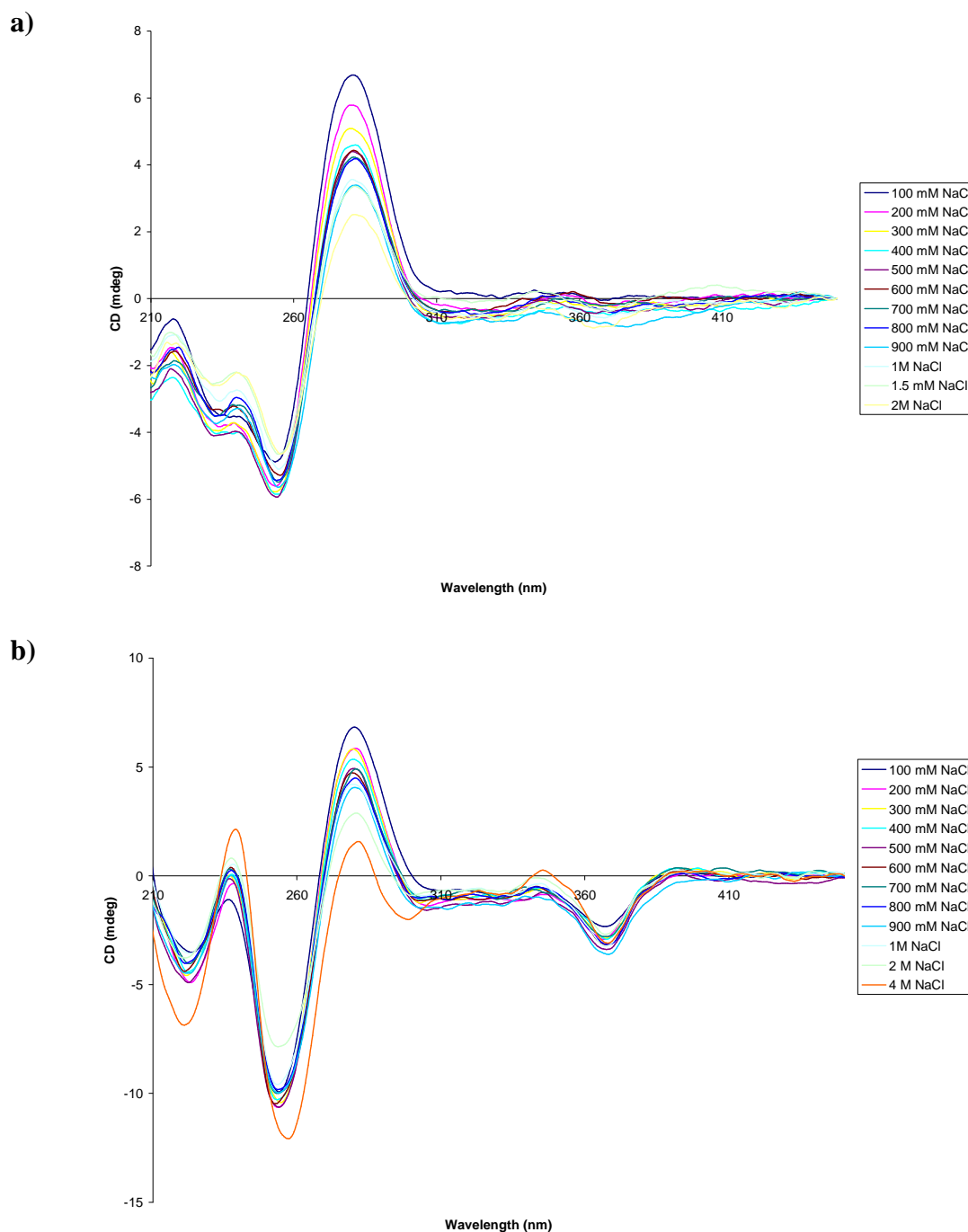


Figure 4.7 CD spectra of hybrids NaCl concentrations dependent, 10 °C: a) 3*4; b) 5*6

The CD spectra of the pyrene-modified single strands reveal a random aggregation of the pyrene units. Nonetheless, by raising the concentration to 2.0 μM , bisignate signals of pyrene are present in the CD spectra of single strands. These data suggest that adjacent

bases and pyrene units containing single strands are stabilized in a helical orientation. The single strands **3** and **7** show a bisignate signal for the pyrene band centered respectively at 352 nm and 350 nm, with a negative cotton effect at $\lambda = 371$ nm and $\lambda = 365$ nm. The negative cotton effect is then followed by a maximum at $\lambda = 341$ nm $\lambda = 338$ nm (Figure 4.8). They indicate a left-handed helical orientation within the oligopyrene stack. However, the single strand **5** shows a positive Cotton effect at $\lambda = 363$ nm.

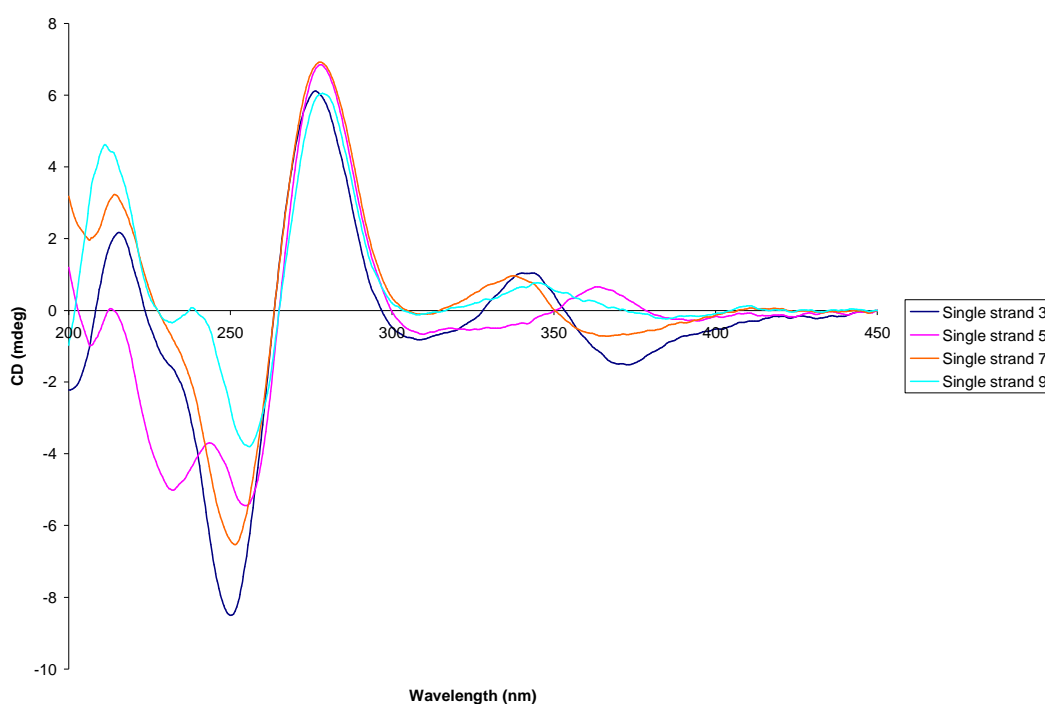


Figure 4.8 CD spectra of single strands 3, 5, 7, and 9 Conditions: 2.0 μM each strand, 10 mM phosphate buffer, pH 7.0.

Single strands containing oligopyrene part are quite flexible. Stacking interactions occur between adjacent bases and pyrene residues. The rise of concentration up to 2 μM allowed us to detect signal for pyrene bands, not visible at 1 μM . In addition the artificial part contains amides connected by phosphodiester bonds. Even if amide has restricted rotational freedom, the combination of amide and phosphodiester bonds plays a key role in helical arrangement within single strand.¹⁶

4.4 Conclusion

In summary, we have described the properties of DNA mimics containing extended stretches of pyrene building blocks. This system composed of two oligopyrene strands (4 to 7 pyrene units per strand) shows that the helical arrangement takes already place in the hybrid containing 12 consecutive achiral pyrene building blocks and not in hybrids containing less pyrene building blocks. However the hybrid **5*6** shows changes in fluorescence emission and CD spectra compared to those of hybrids containing less pyrene residues. But new bands observed in CD spectra as well as trend of the excimer fluorescence maxima upon hybridization exclude well defined arrangement of oligopyrene. Therefore we assume that organization within double strand is not linear with a number of units involved. However the CD spectra of single strands reveal that oligomers containing 2 to 7 pyrene units already involve in an intrastrand helical stack. Adjacent bases and pyrenes are involved in intrastrand stacking interactions which form a stable single stranded helix without any base pairing partners. These findings are important for the design of alternative DNA scaffold containing an artificial section of consecutive achiral pyrene residues.

4.5 Experimental Section

The required pyrene building block was synthesized according to a published procedure¹⁷. Nucleoside phosphoramidites from *Transgenomic* (Glasgow, UK) were used for oligonucleotide synthesis. Oligonucleotides **1-10** were prepared *via* automated oligonucleotide synthesis by a standard synthetic procedure ('trityl-off' mode) on a 394-DNA/RNA synthesizer (*Applied Biosystems*). Cleavage from the solid support and final deprotection was done by treatment with 30% NH₄OH solution at 55°C overnight. All oligonucleotides were purified by reverse phase HPLC (LiChrospher 100 *RP-18*, 5µm, Merck), *Bio-Tek Instruments Autosampler 560*); eluent A = (Et₃NH)OAc (0.1 M, pH 7.4); eluent B = MeCN; elution at 40°C; gradient 5 – 20% B over 30 min.

Mass spectrometry of oligonucleotides was performed with a Sciex QSTAR pulsar (hybrid quadrupole time-of-flight mass spectrometer, *Applied Biosystems*). ESI-MS (negative mode, CH₃CN/H₂O/TEA) data of compounds **1-10** are presented in Table 3.

Table 4.3 Mass spectrometry data (molecular formula, calc. average mass, and obtained).

Oligo.		Molecular formula	Calc. aver.mass	Found
1	(5') AGC TCG GTC ATC GAG AGT GCA	C ₂₀₅ H ₂₅₇ N ₈₃ O ₁₂₃ P ₂₀	6471.3	6472
2	(3') TCG AGC CAG TAG CTC TCA CGT	C ₂₀₃ H ₂₅₈ N ₇₆ O ₁₂₅ P ₂₀	6382.2	6383
3	(5') AGC TCG GSS SSC GAG AGT GCA	C ₂₆₂ H ₂₉₉ N ₇₉ O ₁₂₂ P ₂₀	7126.2	7128.0
4	(3') TCG AGC CSS SSG CTC TCA CGT	C ₂₅₉ H ₃₀₁ N ₆₇ O ₁₂₆ P ₂₀	6988.1	6989.0
5	(5') AGC TCG SSS SSC GAG AGT GCA	C ₂₇₆ H ₃₁₀ N ₇₆ O ₁₂₂ P ₂₀	7263.5	7264.0
6	(3') TCG AGC SSS SSG CTC TCA CGT	C ₂₇₄ H ₃₁₂ N ₆₆ O ₁₂₆ P ₂₀	7165.4	7166.0
7	(5') AGC TCG SSS SSS GAG AGT GCA	C ₂₉₁ H ₃₂₁ N ₇₅ O ₁₂₂ P ₂₀	7440.7	7441.0
8	(3') TCG AGC SSS SSS CTC TCA CGT	C ₂₈₈ H ₃₂₃ N ₆₃ O ₁₂₆ P ₂₀	7302.6	7303.0
9	(5') AGC TCS SSS SSS GAG AGT GCA	C ₃₀₅ H ₃₃₂ N ₇₂ O ₁₂₂ P ₂₀	7577.9	7576.1
10	(3') TCG AGS SSS SSS CTC TCA CGT	C ₃₀₃ H ₃₃₄ N ₆₂ O ₁₂₆ P ₂₀	7479.8	7487.1

All the spectroscopic measurements were performed in potassium phosphate buffer (10 mM, 100 mM NaCl, pH 7.0) for 1.0 μM oligonucleotide concentration (1.0 μM of each strand in case of duplex), ε₂₆₀= 9000 was used for pyrene units.

Thermal denaturation experiments were carried out on *Varian Cary-100 Bio-UV/VIS* spectrophotometer equipped with a *Varian Cary-block* temperature controller and data were collected with *Varian WinUV* software at 245, 260 and 354 nm (cooling-heating-cooling cycles in the temperature range of 20-90°C, temperature gradient of 0.5°C/min). Temperature melting (T_m) values were determined as the maximum of the first derivative of the smoothed melting curve.

Temperature dependent UV-VIS spectra were collected with an optic path of 1 cm over the range of 210-500 nm at 10-90 °C with a 10 °C interval on *Varian Cary-100 Bio-UV/VIS* spectrophotometer equipped with a *Varian Cary-block* temperature controller. The cell compartment was flushed with N₂.

Temperature dependent fluorescence data were collected on a *Varian Cary Eclipse* fluorescence spectrophotometer equipped with a *Varian Cary-block* temperature controller (excitation at 354 nm; excitation and emission slit width of 5 nm) using 1 per 1 cm quartz cuvettes. *Varian Eclipse* software was used to investigate the fluorescence of the different pyrene-containing oligonucleotides at a wavelength range of 375-700 nm in the temperature range of 10-90 °C.

CD spectra were recorded on a *JASCO J-715* spectrophotometer using quartz cuvettes with an optic path of 1 cm.

4.6 References

1. N.C. Seeman, *Nature* **2003**, 421, 427-431.
2. a) Heath, J. R., Ratner, M. A. *Physics Today*, 2003, 43-49; b) Gothelf, K. V., LaBean, T. H. *Org. Biomol. Chem.* **2005**, 3, 4023-4037; c) Maruccio, G., Cingolani, R., Rinaldi, R. *J. Mater. Chem.* **2004**, 542-554; d) Wengel, J. *Org. Biomol. Chem.* **2004**, 2, 277-280; e) Niemeyer, C. M., Adler, M. *Angew. Chem. Int. Ed.* **2002**, 41, 3779-3783.
3. e. g. a) Hopkins, D. S., Pekker, D., Goldbart, P. M., Bezryadin, A. *Science*, **2005**, 1762-1765; b) Bashir, R. *Superlattices and Microstructures*, Vol. 29, No. 1, **2001**, 1-16; c) Keren, K., Berman, R. S., Buchstab, E., Sivan, U., Braun, E. *Science*, **2003**, 1380-1382; d) Pike, A., Horrocks, B., Connolly, B., Houlton, A. *Aust. J. Chem.* **2002**, 55, 191-194.
4. a) Eschenmoser, A. *Chimia* 2005, 59, 836-850; b) Vasella, A. T. *Chimia* 2005, 785-793; c) Samori, B., Zuccheri, G. *Angew. Chem. Int. Ed.* **2005**, 1166-1181; c) Herdewijn, P. *Biochim. Biophys. Acta, Gene Struct. Expr.* **1999**, 1489, 167-179.
5. a) Piguet, C., Bernardinelli, G., Hopfgartner, G. *Chem. Rev.* **1997**, 97, 2005-2062; b) Hill, D. J., Mio, M. J., Prince, R. B., Hughes, T. S., Moore, J. S. *Chem. Rev.*

- 2001, 101, 3893-4011; c) Rowan, A. E., Nolte, R. J. M. *Angew. Chem. Int. Ed.* **1998**, 37, 63-68; d) Gellman, S. H. *Acc. Chem. Res.* **1998**, 31, 173-180.
6. a) Huc, I. *Eur. J. Org. Chem.* **2004**, 17-29; b) Hu, Z.-Q., Hu, H.-Y., Chen, Ch.-F. *J. Org. Chem.* **2006**, 1131-1138.
7. a) Rowan A. E., Nolte R. J. M., *Angew chem. Int. Ed.* **1998**, 37, 63; b) Hill D. J., Mio M. J., Prince R. B., Hughes T. S., Moore J. S., *Chem Rev.* **2001**, 101, 3893; c) Albrecht M., *Angew. Chem.* **2005**, 117, 6606; *Angew. Chem. Int. Ed.* **2005**, 44, 6448; d) Prince R. B., Saven J. G., Wolynes P. G., Moore J. S., *J. Am. Chem. Soc.* **1999**, 121, 3114.
8. a) Huc I., *Eur. J. Org. Chem.* **2004**, 17; b) Berl V., Huc I., Khoury R., Krische M., Lehn J.-M., *Nature* **2000**, 407, 720.
9. V. L. Malinovskii, F. Samain, R. Häner, *Angew. Chem. Int. Ed.* **2007**, 46, 4464-4467.
10. N. R. Markham, M. Zuker, *Nucleic Acids Research*, web server issue **2005**, W577-W581.
11. a) R. Lumry, R. Biltonen *Biopolymers* **1966**, 4, 917-944; b) J. SantaLucia, Jr. in *Spectrophotometry and spectrofluorimetry, a practical approach* (Ed: M. G. Gore), OXFORD, New York **2000**, pp. 329-356.
12. a) I. Tinoco, Jr., *J. Amer. Chem. Soc.* **1960**, 4785-4790; b) C. R. Cantor, P. R. Schimmel, *Biophysical Chemistry, part II*; W. H. FREEMAN AND COMPANY, New York, **1980**, pp. 349-408.
13. F. M. Winnik, *Chem. Rev.* **1993**, 93, 587-614.
14. *pyrenophanes*: a) H. A. Staab, N. Riegler, F. Diederich, C. Krieger, D. Schweitzer, *Chem. Ber.* **1984**, 117, 246-259; b) H. A. Staab, R. G. H. Kirrstetter, *Liebigs Ann. Chem.* **1979**, 886-898; *bis-pyrenyl systems*: c) K. A. Zachariasse, W. Kuhnle, A. Weller, *Chem. Phys. Lett.* **1978**, 59, 375-380; d) T. Kanaya, K. Goshiki, M. Yamamoto, Y. Nishijima, *J. Am. Chem. Soc.* **1982**, 104, 3580-3587; e) M. J. Snare, P. J. Thistlethwaite, K. P. Ghiggino, *J. Am. Chem. Soc.*, **1983**, 105, 3328-3332; f) P. Wahl, C. Krieger, D. Schweitzer, H. A. Staab, *Chem. Ber.* **1984**, 117, 260-276; *other examples with strained pyrene movement*: g) O. Shoji, D. Nakajima, M.

- Annaka, M. Yoshikuni, T. Nakahira, *Polymer* **2002**, *43*, 1711-1714; h) I. Suzuki, M. Ui, A. Yamauchi, *J. Am. Chem. Soc.* **2006**, *128*, 4498-4499.
15. N. Berova, K. Nakanishi, in *Circular dichroism: principles and applications* (Eds: N. Berova, K. Nakanishi, R. W. Woody), WILEY-VCH, New York, **2000**, pp. 337-382.
16. E.T. Kool, *Chem. Rev.* **1997**, *97*, 1473-1487.
17. S. M. Langenegger, R. Häner, *Chem. Commun.* **2004**, 2792-2793.

Chapter 5: Helical Arrangement in Alternative Systems

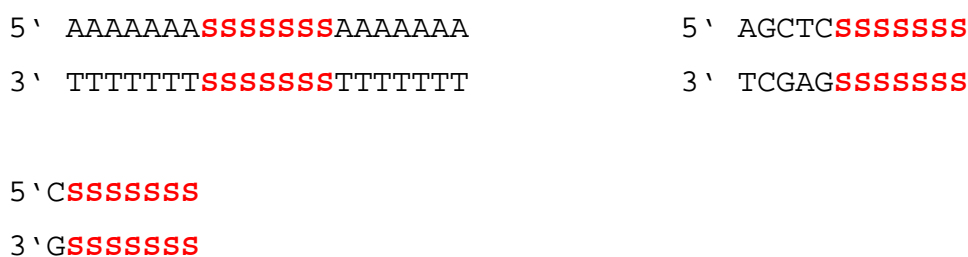
5.1 Abstract

Interstrand and intrastrand stacked pyrenes in a DNA framework have been described in previous chapters. In addition, an artificial section composed of seven achiral pyrene moieties which self-arranges in a helical structure along DNA has been shown in *Chapter 3*. We set out to expand these studies to alternative systems such as a poly (dA)·(dT) and a short DNA scaffold consisting of five bases per strand and one base per strand.

5.2 Introduction

Double helix DNA can be considered as a natural polymer that has a *folded* structure because of stacking of natural bases within separate single strands, and has a *helical* arrangement due to interstrand hydrogen bonding and stacking.¹ The unique feature of DNA for self-organization is one of the main characteristics that are practically used in developments of new therapeutic agents or construction of diagnostic tools.² More recently, because of predictability of self organization, simplicity of synthesis, and a wide range of possible modification, DNA was proposed as a very promising building block for the needs of nanotechnology.³ DNA building blocks may serve both as real components of nanochemistry, or as a template for nanostructures.⁴ Since the discovery of DNA double helix, the generation of helical structures that are not based on the hydrogen-bond-mediated pairing scheme of the nucleobases or related derivatives has been a highly competitive aspect in the field of molecular self-organisation.⁵⁻⁸ Chemists have been looking for new molecules with the ability to form helical structures through non covalent interactions, and hydrogen bonds.⁷ Thus a large variety of synthetic foldamers or oligomers exist that are able to fold into well-defined conformations in

solution. There are two classes of foldamers: single-stranded foldamers that only fold and multiple-stranded foldamers that both associate and fold.⁹ Previously in *Chapter 3* a well-organized helical arrangement of non-nucleosidic pyrene building blocks embedded in a DNA framework has been described.¹⁰ The constructs are composed of achiral pyrene building blocks in a DNA scaffold. We set out to expand these studies to alternative systems such as a poly (dA)·(dT) framework and a short DNA scaffold. Poly (dA)·(dT) is a DNA where one strand consists of only adenine and the other strand consists of only thymine. Moreover this type of nucleotide is well described in literature and can easily serve as a new scaffold for probing interstrand helical conformation of oligopyrenes.¹¹ Furthermore two short DNA scaffolds have been designed which consist of five or one consecutive bases followed by an oligopyrene as the stem. The description of results will be divided into two parts, that is, the thermal denaturation experiments and spectroscopic investigation of pyrene-containing single and double strands.



5.3 Results and discussion

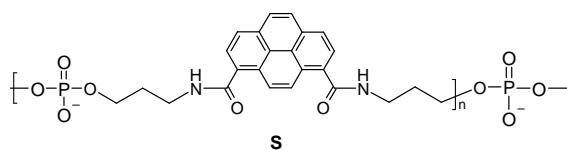
5.3.1 Thermal Denaturation Experiments

Before investigation of the spectroscopic properties of pyrene containing oligomers, the stability of hybrids was tested by thermal denaturation. The data are summarized in Table 5.1. Oligonucleotides **1*2** and **9*10** serve as controls and oligomers **9-14** contain seven consecutive achiral pyrene building blocks per single strand. Furthermore the hybrid **15*16** serves as reference to determine the contribution of achiral pyrene in a poly (dA)·(dT) scaffold. Table 5.1 shows the experimental T_m values as well as the calculated

values for the corresponding hybrids without any contribution from the pyrene residues. The latter value, which was calculated according to the method described by *Markham and Zuker*¹², allows an estimation of the contribution of the pyrene groups to the overall stability (ΔT_m).

Table 5.1 Influence of non-nucleosidic pyrene building blocks on hybrid stability

Oligo #	duplex ^[a]	T_m (°C) exp. ^[b]	T_m calc. ^[c]	ΔT_m , °C ^[d]
1	5' AGC TCG GTC ATC GAG AGT GCA	70.7	70.7	-
2	3' TCG AGC CAG TAG CTC TCA CGT			
9	5' AGC TCS SSS SSS GAG AGT GCA	55.8	32.6	+23.2
10	3' TCG AGS SSS SSS CTC TCA CGT			
11	5' AAA AAA ASS SSS SSA AAA AAA	29.0	-6.6	(+ 35.6)
12	3' TTT TTT TSS SSS SST TTT TTT			
13	5' AGC TCS SSS SSS	31.2 (245 nm)	-15.3	(+ 46,5)
14	3' TCG AGS SSS SSS			
15	5' AAA AAA AAA AAA AAA AAA AAA	47.4	47.4	-
16	3' TTT TTT TTT TTT TTT TTT TTT			



[a] 1.0 μ M each strand, 10 mM phosphate buffer, pH 7.0); [b] experimental value; average of three independent experiments; exp. error $\pm 0.5^\circ\text{C}$; [c] T_m value calculated for the corresponding hybrid formed by the two strands without contribution of the unnatural building blocks according to the method described by *Markham and Zuker*¹²; [d] difference between experimental and calculated T_m value; this number corresponds to the contribution of the pyrene residues to the overall duplex stability.

T_m values of hybrids **1*2** and **9*10** are in agreement with previous findings. T_m values calculated for hybrid **11*12** and **13*14** show that these hybrids should not form if

pyrenes were not present at conditions used (20°C). However all hybrids investigated in the study showed a single, cooperative transition which indicate that oligopyrenes within the duplex have a rather large positive effect on the T_m value (Figure 5.1). This finding indicates that interstrand interactions between the pyrene units lead to a significant stabilization of the duplex.

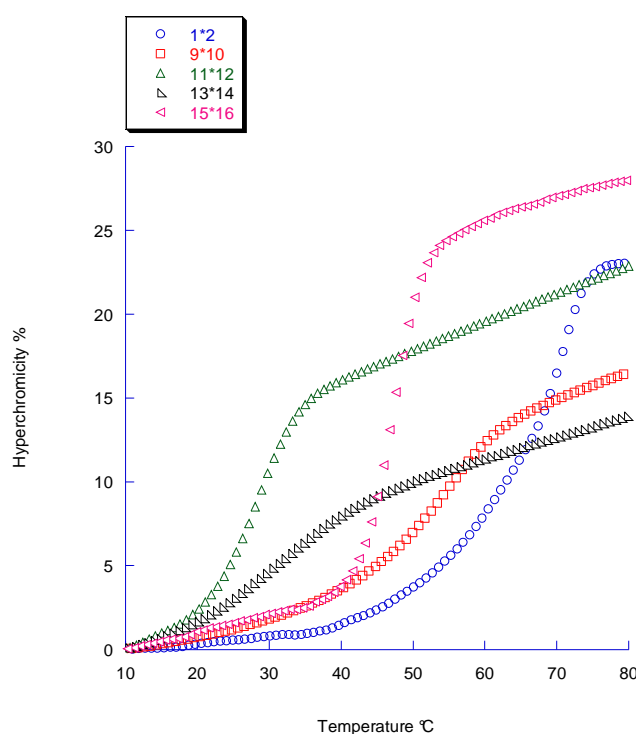


Figure 5.1 Thermal melting curves of hybrids at 245 nm.

In addition, in an attempt to go into more details, two achiral oligopyrene strands containing each only one chiral base (G and C) were synthesized. Their stability within single and double strands have been tested and summarized in Table 5.2. Thermal stability experiments were performed at 1M NaCl. Complementary strands showed a single and cooperative transition whereas the calculated T_m values indicate that this system should again not hybridize in the absence of the pyrenes (Figure 5.2). When melting experiments were carried out with oligopyrene single strands, experiment data showed similar transition than duplexes.

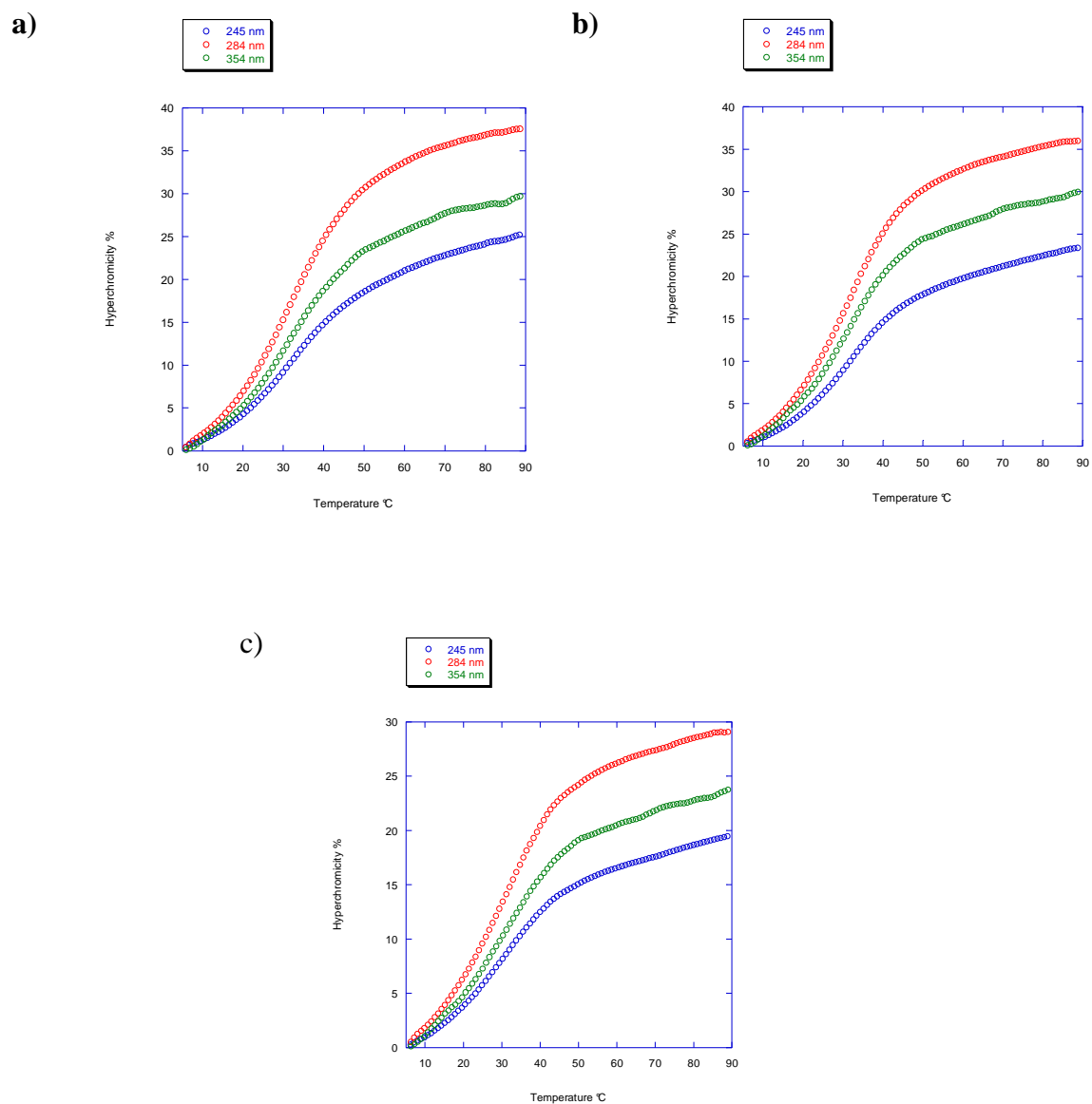
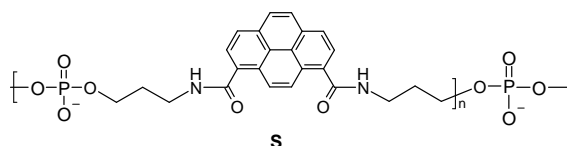


Figure 5.2 Thermal melting curves of a) 17*18; b) 17; c) 18.

Table 5.2 Melting experiments of hybrid **17*18**, oligopyrene single strand **17**, and **18**.

Oligo	Oligonucleotides ^[a]	T _m (°C) exp. ^[b]	T _m calc. ^[c]	ΔT _m , °C ^[d]
17	5' CS SSS SSS	31.7	[e]	-
18	3' GS SSS SSS			
17	5' CS SSS SSS	31.8	[e]	-
18	3' GS SSS SSS	30.0	[e]	-



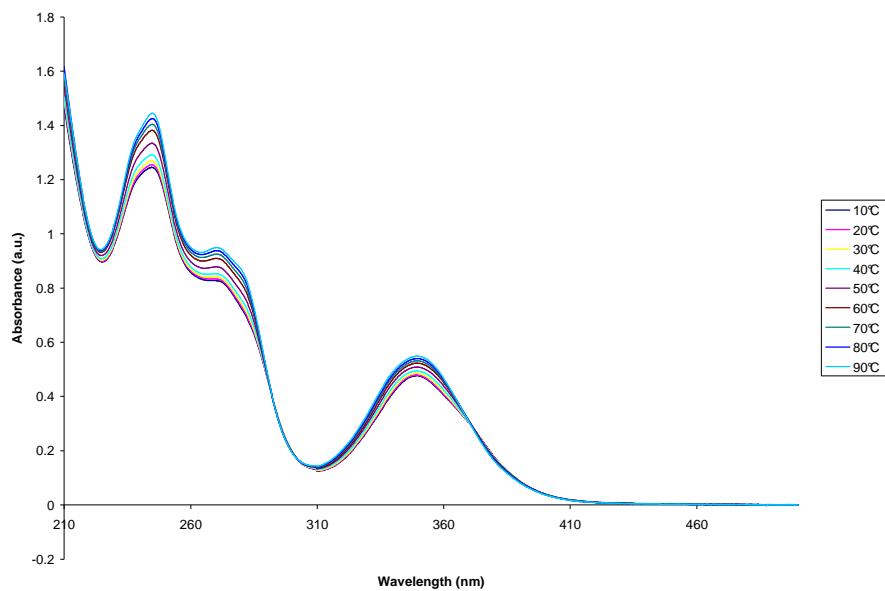
[a] 1.0 μM each strand, 10 mM phosphate buffer, 1M NaCl, pH 7.0); [b] experimental value at 245 nm; average of three independent experiments; exp. error +/-0.5°C; [c] T_m value calculated for the corresponding hybrid formed by the two strands without contribution of the unnatural building blocks according to the method described by *Markham and Zuker*¹²; [d] difference between experimental and calculated T_m value; this number corresponds to the contribution of the pyrene residues to the overall duplex stability; [e] negative values.

Then, spectroscopic properties of single and double strand were analyzed. Interstrand and intrastrand interactions are monitored by temperature dependent UV/VIS spectroscopic studies.

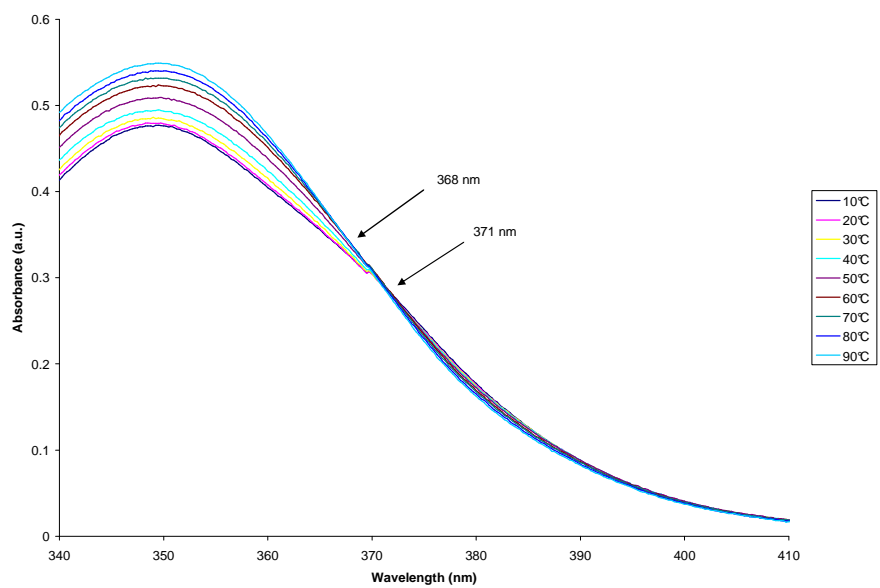
5.3.2 Spectroscopic Studies

The temperature-dependent UV-VIS spectra of hybrid **9*10**, **11*12**, and **13*14** are in agreement with previous findings. Two isosbestic points are present, indicating two different types of interaction between the pyrenes (Figure 5.3). One (at longer wavelength) is attributed to interstrand stacking in the hybrid and the second from intrastrand stacking in the single strands.

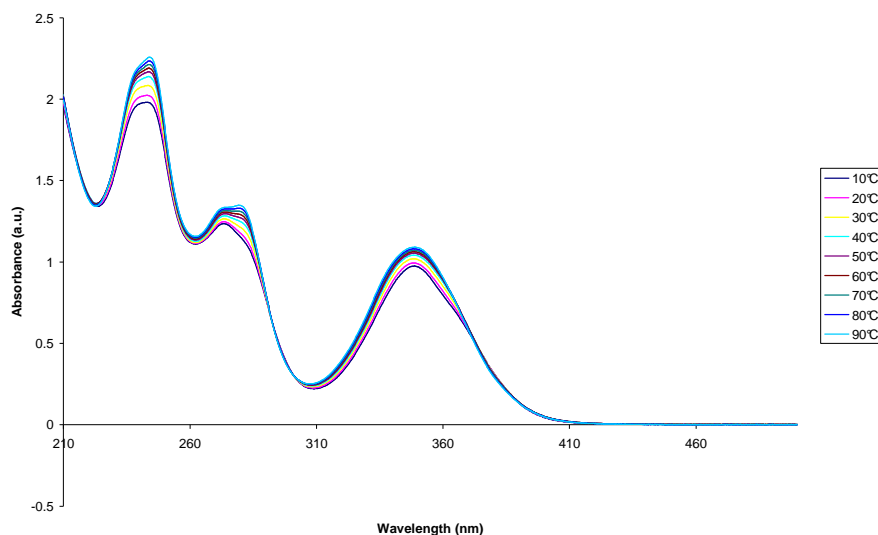
a)



b)



c)



d)

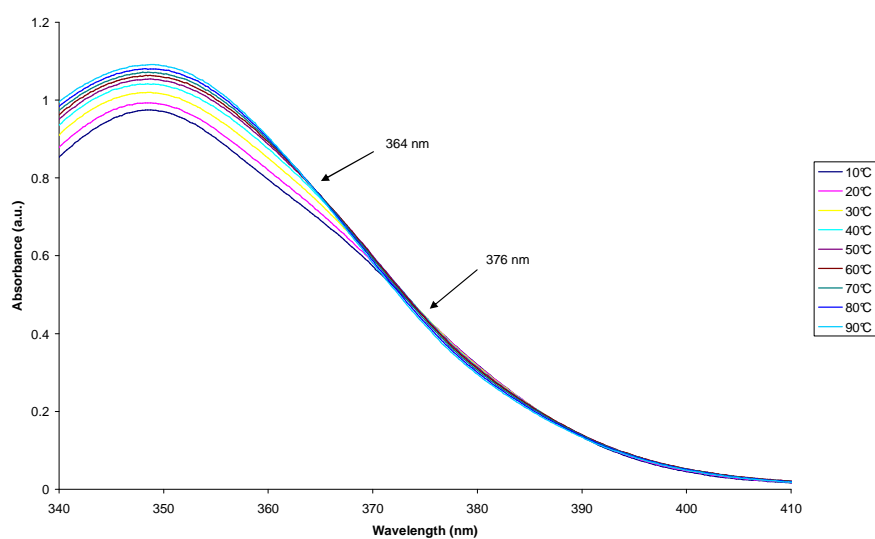


Figure 5.3 Temperature dependent UV-VIS of a) duplex **9*10** (210-500 nm, 10-90 °C); b) duplex **9*10**: isosbestic points at 371 and 368 nm; c) duplex **13*14** (210-500 nm, 10-90 °C); d) **13*14**: isosbestic points at 376 and 364 nm.

If one natural section of the oligonucleotide is taken off, the hybrid **13*14** exhibits also the two isosbestic points which show that pyrene interact within double strand as well as within single strands. The finding indicates that contributions of the pyrene units lead to a significant stabilization of the system. As can be seen in Figure 5.4, duplex formation of

hybrid **13*14** as well as hybrid **11*12**, lead to a significant red shift which is in good agreement with the findings described in *Chapter 3*.

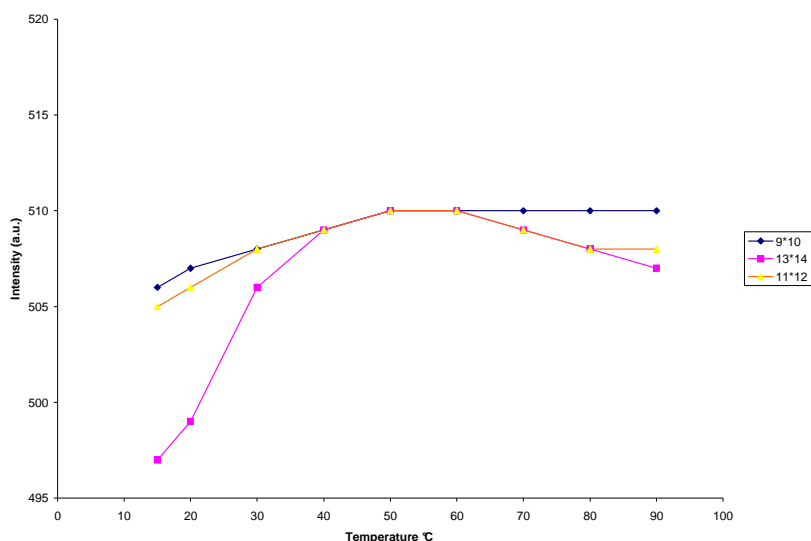


Figure 5.4 Trends of the excimer fluorescence maxima upon melting of hybrids

The confirmation of helical arrangement of interstrand-stacked pyrenes was obtained by CD spectroscopy of hybrids **11*12** and **13*14** (Figure 5.5). Clearly, the spectra of the hybrids are in agreement with the previous study of hybrid **9*10**. In the 200-315 nm range, the spectrum of **13*14** is dominated by strong dichroism of the pyrene bands, which indicates a well-ordered structure in the oligopyrene region of the duplex. Moreover further evidence for a helical arrangement comes from the very intense bisignate signal for the pyrene band centered at 347 nm.

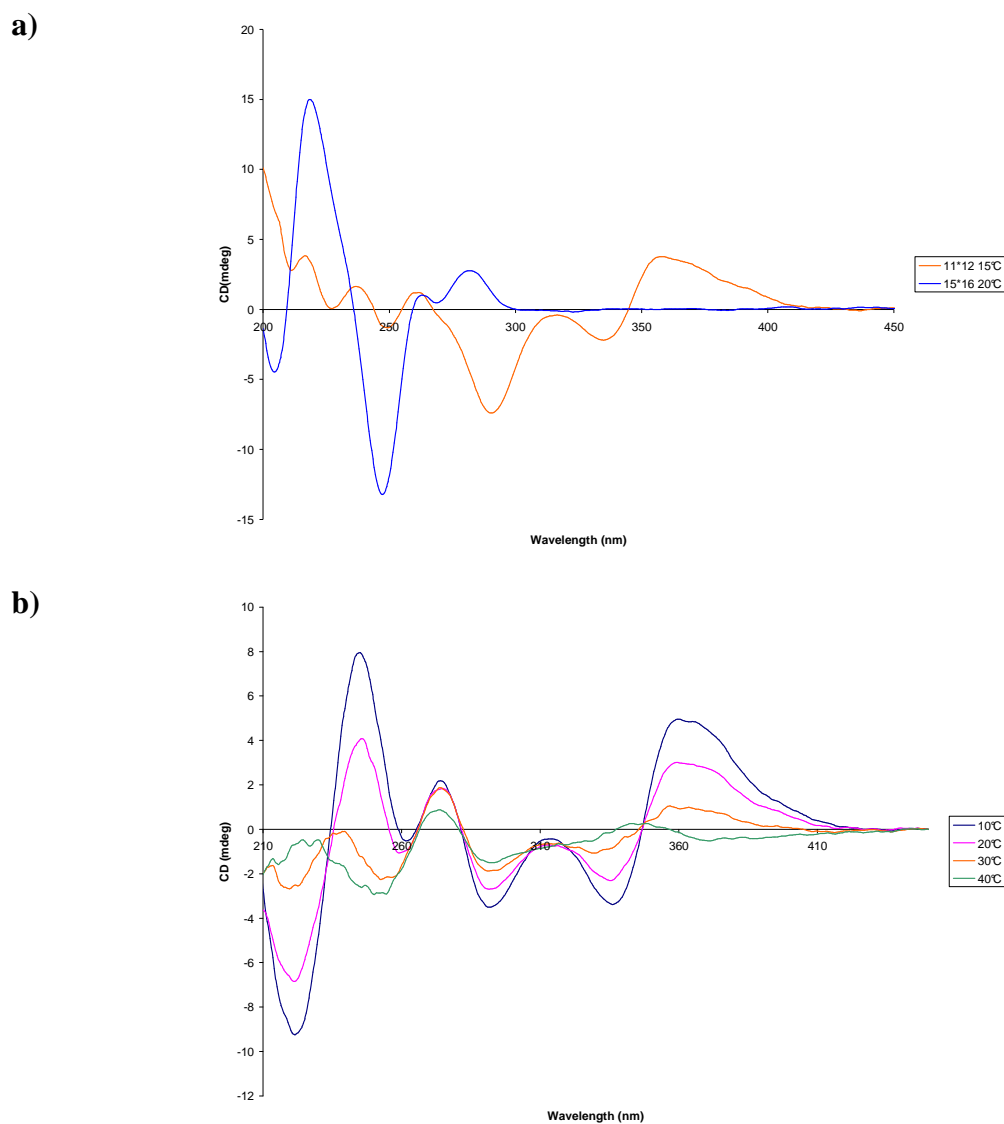
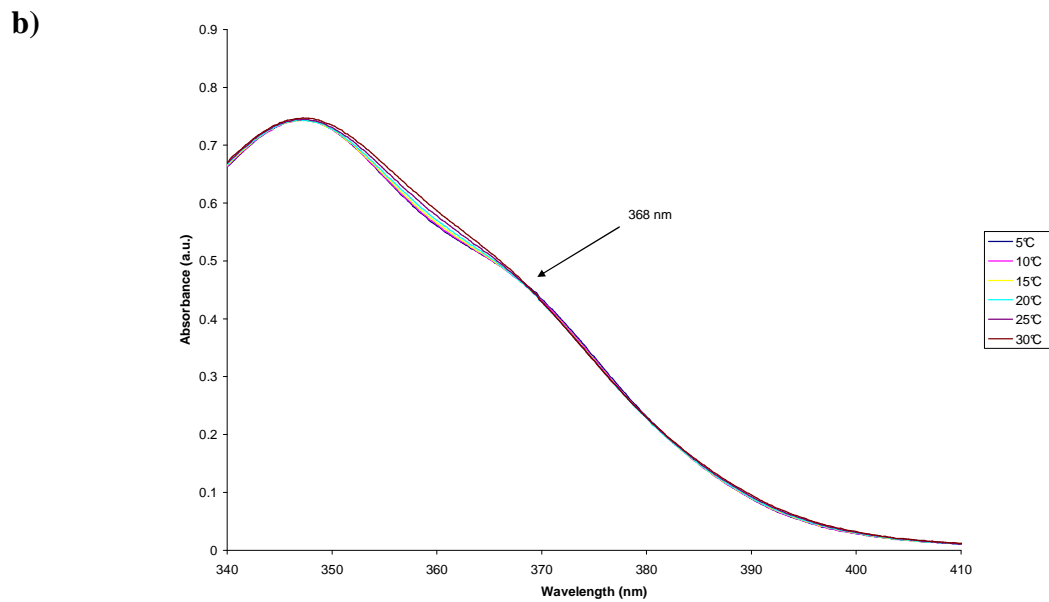
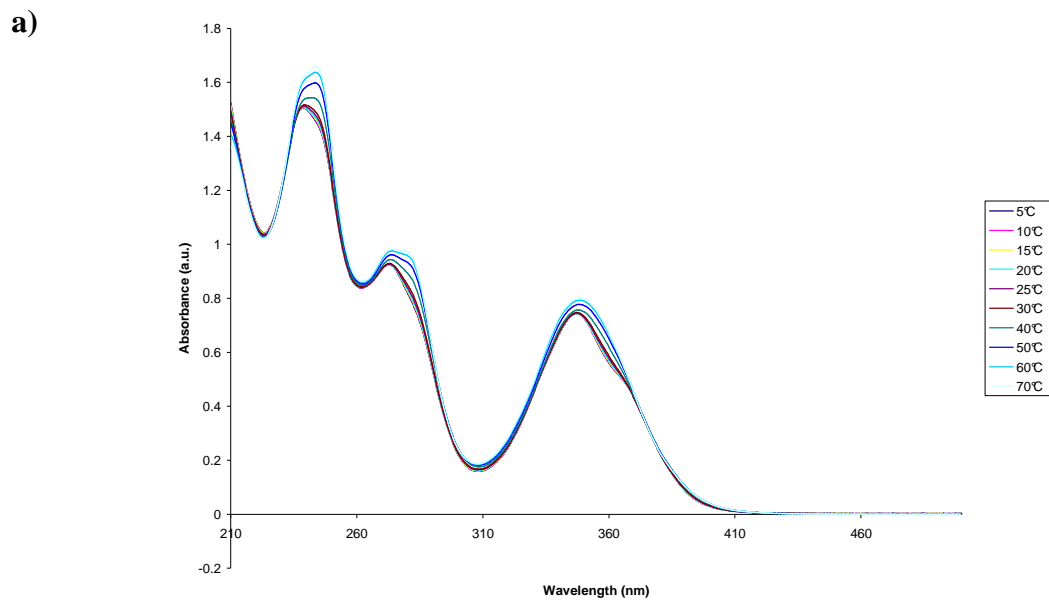


Figure 5.5 CD spectra temperature dependent of hybrid: a) **11*12**; b) **13*14**.

However the CD spectrum of **11*12** undergoes a change in the 200-280 range. The pyrene bands interfere with nucleobases bands in this area of the spectrum and the shape arises from the sum of those bands.

In addition, the behavior of hybrid **17*18** has been followed by temperature-dependent UV/VIS experiments. Whereas pyrenes interact randomly at normal conditions (10mM phosphate buffer, 100 mM NaCl and 500 mM NaCl), the system undergoes a change when NaCl concentration rises up to 1M NaCl and shows a transition. Curves taken

below the T_m as well as those taken above ($31,7\text{ }^\circ\text{C}$) form, respectively, two isosbestic point at 368 nm and 370 nm (Figure 5.6).



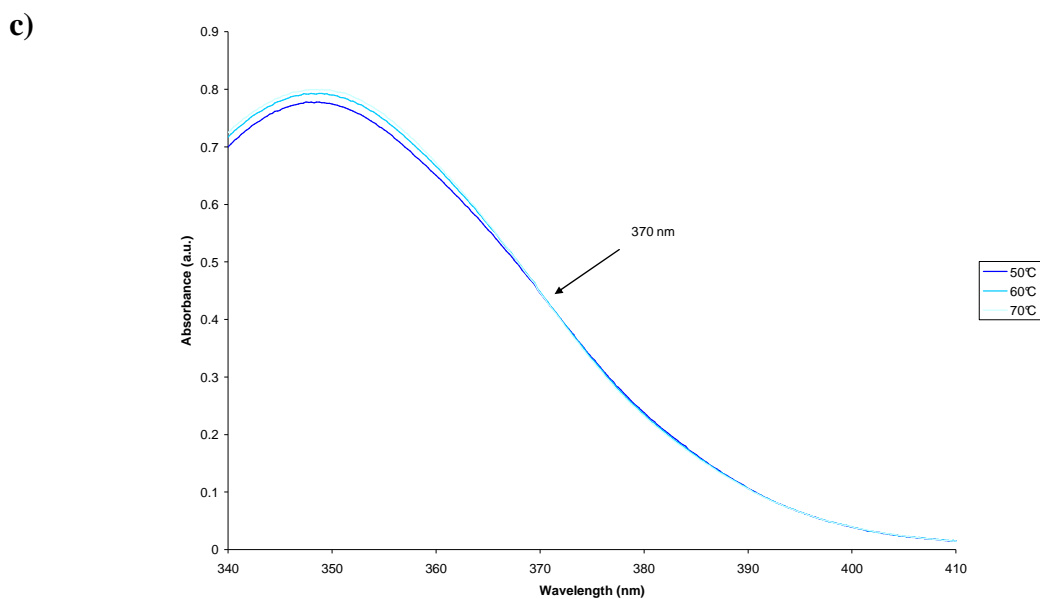


Figure 5.6 Temperature dependent UV-VIS of **17*18** a); b) isosbestic 368 nm (5-30°C); c) isosbestic point (50-70°C).

Temperature-dependent UV/VIS (not shown) as well as melting experiments of single strands **17**, **18** exhibit one transition (see Figure 5.2). Pyrenes are involved in intrastrand interaction in agreement with previous studies and probably pyrenes from one strand interact with those from another strand to form interstrand helical organization. Next, temperature dependent fluorescence experiments of oligopyrene within complementary strands and single strands were performed. They are in agreement with previous findings described in *Chapter 3* and *4* and exhibit clearly a blue shift in their maxima upon hybridization (Figure 5.7).

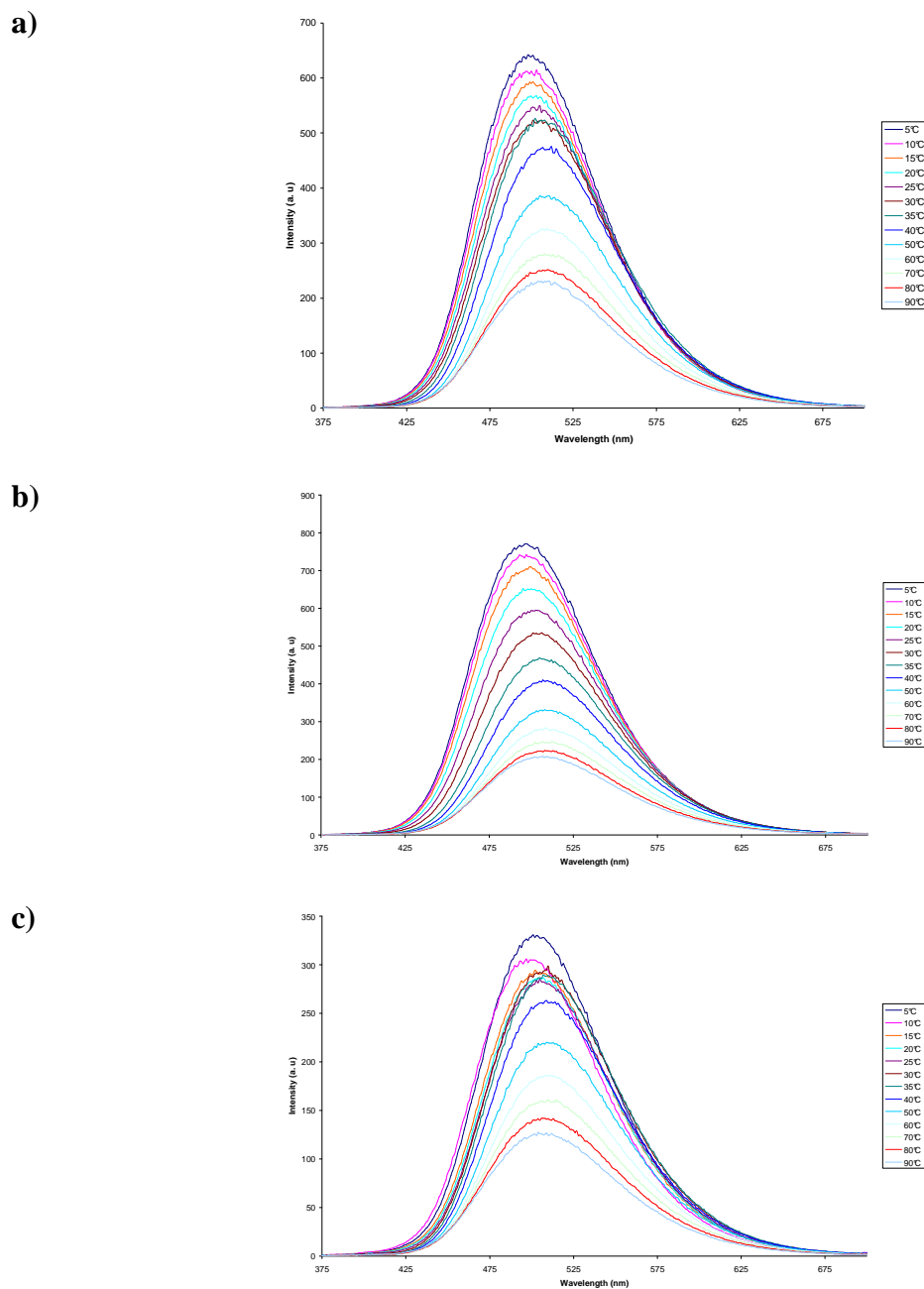


Figure 5.7 Fluorescence spectra of hybrid a) **17*18**; b) strand **17**; strand **18**, conditions: 1.0 μM each strand, 10 mM phosphate buffer, 1M NaCl, pH 7.0.

Below the T_m , the emission intensity of the hybrid **17*18** is decreasing with increasing temperature, indicating a geometrical change in the association of the pyrenes. In addition, the intensity is increasing upon melting and then is decreasing again above T_m . The duplex formation of the hybrid **17*18** leads to a significant blue shift (511 nm to 500 nm) when going from 70 \rightarrow 5 $^{\circ}\text{C}$. The strands **17** and **18** show a significant blue shift when

temperature decreases (511 nm to 497 nm) and (512 nm to 498 nm), respectively. In *Chapter 3* is shown the transition between the sandwich-type aggregation and twisted type structure leading to the helical arrangement. The twisting of the pyrene units upon adoption of the helical conformation explains the blue shift in the excimer emission. The chirality of the nucleobase (G or C) seems to be therefore transferred to the oligopyrene chain resulting in the helical folding.¹³ This finding is supported by CD spectra of the hybrid **17*18** and strand **17** and **18**. The oligopyrene double strands folds into a preferred right handed helical arrangement (Figure 5.8).

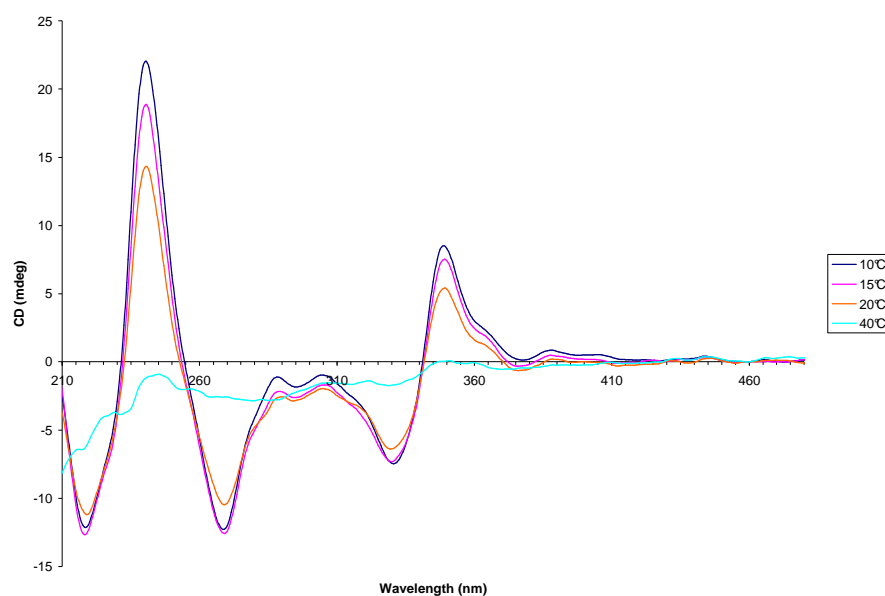


Figure 5.8 CD spectra of hybrid **17*18**, conditions see Table 5.2.

Clearly, the spectra of hybrids **17*18** are in agreement with the previous study of hybrid **9*10** in *Chapter 3*. In the 200-400 nm range, the spectrum is dominated by strong dichroism of the pyrene bands (see page 121, Annex IV: absorbance spectrum of pyrene), which indicates a well-ordered structure in the oligopyrene region of the duplex. Further evidence for a helical arrangement comes from the very intense bisignate signal for the pyrene band centered at 342 nm. In addition the CD spectra of the strand **17** as well the strand **18** reveal that a single stranded oligopyrene folds in a helical arrangement at conditions used (Figure 5.9).

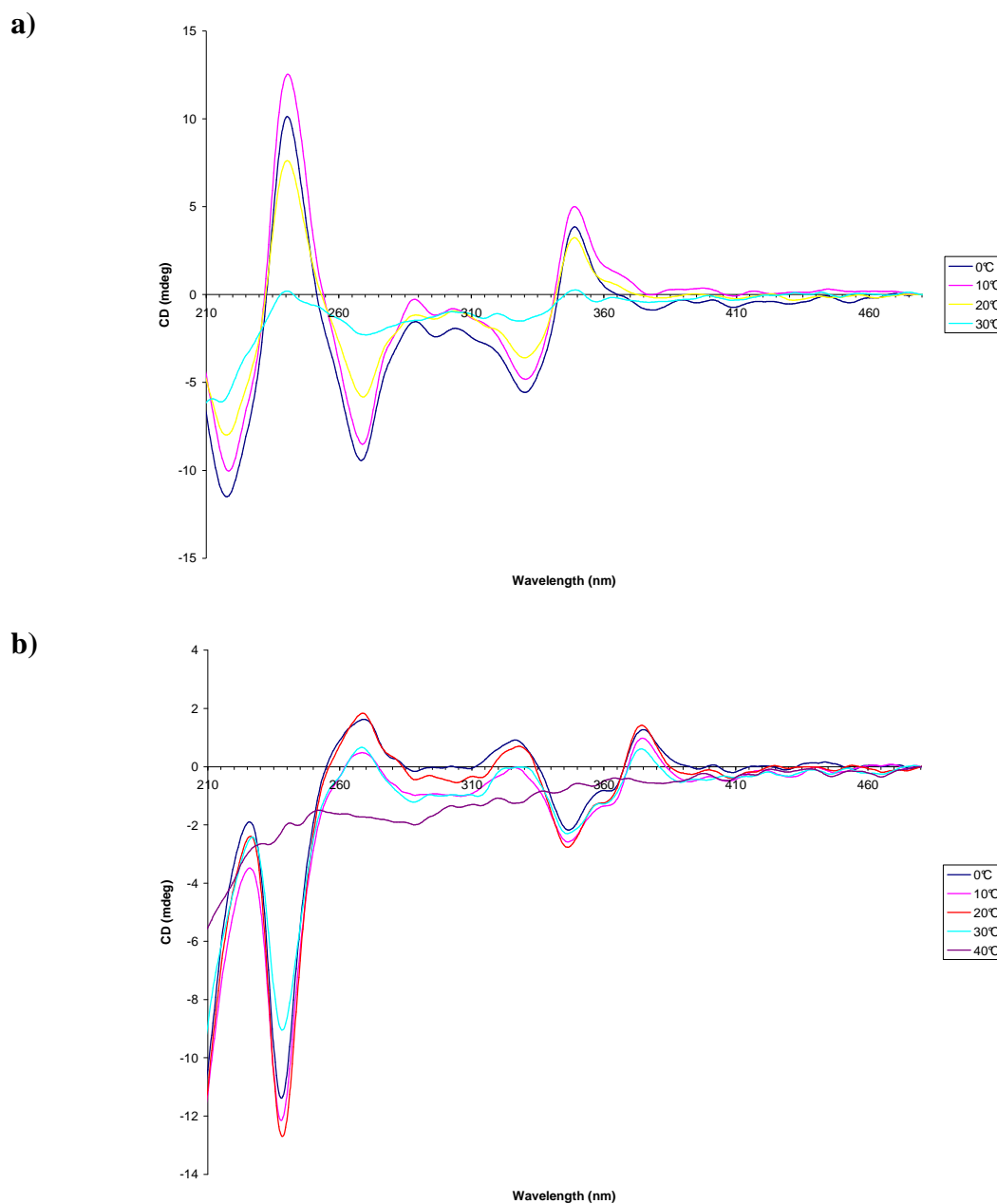


Figure 5.9 CD spectra of a) strand 17; b) strand 18.

The question arises whether the oligopyrenes within one strand self-arrange as single strands or if two identical oligopyrenes intertwine to form a double helical structure which allows much more extensive intermolecular stacking interactions.¹⁴⁻¹⁷ The thermal stability experiments of strands separately exhibit a transition around 30°C and would support this behavior. However when the two oligopyrene strands are combined, an

inversion of helicity of the strand **18** or intertwining of the complementary oligopyrene strands are observed, and the strands adopt the right-handed helical.

5.4 Conclusion

In summary, we have investigated the properties of consecutive achiral pyrenes in alternative systems, embedded either in a poly (dA)·(dT) framework or in a short DNA scaffold consisting of five bases per strand. In all systems, oligopyrene strands self-organize and adopt an interstrand helical stack embedded in a double-stranded DNA in agreement with *Chapter 3*. Moreover one hybrid containing 14 achiral pyrene building blocks and only one G≡C base pair has been synthesized. As shown by fluorescence and CD spectroscopy, the chirality is transferred from the nucleotide to the oligopyrene chains which lead to the helical organization of the system. More important one oligopyrene strand adopt a right-handed helical orientation whereas the complementary strand adopt a left-handed helical orientation. When the two complementary oligopyrene strands are mixed, they fold into a stable right-handed helical conformation. Those studies have shown that interstrand helical conformation of oligopyrenes takes place for different types of DNA scaffold. Furthermore the unique feature linked to a G≡C base pair which provides a dynamic helical oligomer is very attractive for the design of novel intelligent materials in nanotechnology.

5.5 Experimental Part

The required pyrene building block was synthesized according to a published procedure¹⁸. Nucleoside phosphoramidites from *Transgenomic* (Glasgow, UK) were used for oligonucleotide synthesis. Oligonucleotides **1-18** were prepared *via* automated oligonucleotide synthesis by a standard synthetic procedure ('trityl-off' mode) on a 394-DNA/RNA synthesizer (*Applied Biosystems*). Oligonucleotides **15**, **16** were obtained from *Microsynth* (Switzerland) and were used without additional purification. Cleavage

from the solid support and final deprotection was done by treatment with 30% NH_4OH solution at 55°C overnight. All oligonucleotides were purified by reverse phase HPLC (LiChrospher 100 *RP-18*, $5\mu\text{m}$, Merck), *Bio-Tek Instruments Autosampler 560*); eluent *A* = $(\text{Et}_3\text{NH})\text{OAc}$ (0.1 M, pH 7.4); eluent *B* = MeCN; elution at 40°C ; gradient 5 – 20% *B* over 30 min.

Mass spectrometry of oligonucleotides was performed with a Sciex QSTAR pulsar (hybrid quadrupole time-of-flight mass spectrometer, *Applied Biosystems*). ESI-MS (negative mode, $\text{CH}_3\text{CN}/\text{H}_2\text{O}/\text{TEA}$) data of compounds **1-18** are presented in Table 5.3

Table 5.3 Mass spectrometry data (molecular formula, calc. average mass and obtained).

Oligo.		Molecular formula	Calc. aver.mass	Found
1	(5') AGC TCG GTC ATC GAG AGT GCA	$\text{C}_{205}\text{H}_{257}\text{N}_{83}\text{O}_{123}\text{P}_{20}$	6471.3	6472
2	(3') TCG AGC CAG TAG CTC TCA CGT	$\text{C}_{203}\text{H}_{258}\text{N}_{76}\text{O}_{125}\text{P}_{20}$	6382.2	6383
9	(5') AGC TCS SSS SSS GAG AGT GCA	$\text{C}_{305}\text{H}_{332}\text{N}_{72}\text{O}_{122}\text{P}_{20}$	7577.9	7576.1
10	(3') TCG AGS SSS SSS CTC TCA CGT	$\text{C}_{303}\text{H}_{334}\text{N}_{62}\text{O}_{126}\text{P}_{20}$	7479.8	7487.1
11	(5') AAA AAA ASS SSS SSA AAA AAA	$\text{C}_{308}\text{H}_{330}\text{N}_{84}\text{O}_{110}\text{P}_{20}$	7588.0	7589.0
12	(3') TTT TTT TSS SSS SST TTT TTT	$\text{C}_{308}\text{H}_{344}\text{N}_{42}\text{O}_{138}\text{P}_{20}$	7461.0	7463.0
13	(5') AGC TCG SSS SSS	$\text{C}_{216}\text{H}_{223}\text{N}_{32}\text{O}_{70}\text{P}_{11}$	4728.0	4728.0
14	(3') TCG AGC SSS SSS	$\text{C}_{217}\text{H}_{223}\text{N}_{34}\text{O}_{70}\text{P}_{11}$	4768.1	4769.0
17	(5') G SSS SSS	$\text{C}_{177}\text{H}_{174}\text{N}_{17}\text{O}_{46}\text{P}_7$	3492.2	3492.0
18	(3') C SSS SSS	$\text{C}_{178}\text{H}_{174}\text{N}_{19}\text{O}_{46}\text{P}_7$	3532.2	3531.0

The spectroscopic measurements were performed in potassium phosphate buffer (10 mM, 100 mM NaCl, pH 7.0) for 1.0 μM oligonucleotide concentration (1.0 μM of each strand in case of duplex), $\epsilon_{260} = 9000$ was used for pyrene units.

The measurements of hybrid **17*18** were performed in potassium phosphate buffer (10 mM, 1 M NaCl, pH 7.0) for 1.0 μM oligonucleotide concentration (1.0 μM of each strand in case of duplex), $\epsilon_{260} = 9000$ was used for pyrene units.

Thermal denaturation experiments were carried out on *Varian Cary-100 Bio-UV/VIS* spectrophotometer equipped with a *Varian Cary-block* temperature controller and data were collected with *Varian WinUV* software at 245, 260 and 354 nm (cooling-heating-cooling cycles in the temperature range of 20-90°C, temperature gradient of 0.5°C/min). Temperature melting (T_m) values were determined as the maximum of the first derivative of the smoothed melting curve.

Temperature dependent UV-VIS spectra were collected with an optic path of 1 cm over the range of 210-500 nm at 10-90 °C with a 10 °C interval on *Varian Cary-100 Bio-UV/VIS* spectrophotometer equipped with a *Varian Cary-block* temperature controller. The cell compartment was flushed with N_2 .

Temperature dependent fluorescence data were collected on a *Varian Cary Eclipse* fluorescence spectrophotometer equipped with a *Varian Cary-block* temperature controller (excitation at 354 nm; excitation and emission slit width of 5 nm) using 1 per 1 cm quartz cuvettes. *Varian Eclipse* software was used to investigate the fluorescence of the different pyrene-containing oligonucleotides at a wavelength range of 375-700 nm in the temperature range of 10-90 °C.

CD spectra were recorded on a *JASCO J-715* spectrophotometer using quartz cuvettes with an optic path of 1 cm.

5.6 References

1. W. Saenger, *Principles of Nucleic Acid Structure*, Springer-Verlag, New York, **1984**.
2. N.C. Seeman, *Nature* **2003**, 421, 427-431.
3. a) Heath, J. R., Ratner, M. A. *Physics Today*, 2003, 43-49; b) Gothelf, K. V., LaBean, T. H. *Org. Biomol. Chem.* **2005**, 3, 4023-4037; c) Maruccio, G., Cingolani,

- R., Rinaldi, R. *J. Mater. Chem.* **2004**, 542-554; d) Wengel, J. *Org.Biomol.Chem.* **2004**, 2, 277-280; e) Niemeyer, C. M., Adler, M. *Angew. Chem. Int. Ed.* **2002**, 41, 3779-3783.
4. e. g. a) Hopkins, D. S., Pekker, D., Goldbart, P. M., Bezryadin, A. *Science*, **2005**, 1762-1765; b) Bashir, R. *Superlattices and Microstructures*, Vol. 29, No. 1, **2001**, 1-16; c) Keren, K., Berman, R. S., Buchstab, E., Sivan, U., Braun, E. *Science*, **2003**, 1380-1382; d) Pike, A., Horrocks, B., Connolly, B., Houlton, A. *Aust. J. Chem.* **2002**, 55, 191-194.
 5. Piguet C., Bernardinelli G., Hopfgartner G., *Chem Rev.* **1997**, 97, 2005.
 6. Gellman S. H., *Acc. Chem. Res.* **1998**, 31, 173.
 7. Rowan A. E., Nolte R. J. M., *Angew chem. Int. Ed.* **1998**, 37, 63.
 8. Hill D. J., Mio M. J., Prince R. B., Hughes T. S., Moore J. S., *Chem Rev.* **2001**, 101, 3893.
 9. Hecht S., Huc I., *Foldamers: Structure, properties, and Applications*, Wiley-VCH, **2007**.
 10. V. L. Malinovskii, F. Samain, R. Häner, *Angew. Chem. Int. Ed.* **2007**, 46, 4464-4467.
 11. D. G. Alexeev, A. A. Lipanov, I. Ya. Skuratovskii, *Nature* **1987**, 325, 821-823.
 12. N. R. Markham, M. Zuker, *Nucleic Acids Research*, web server issue **2005**, W577-W581.
 13. E. Yashima, K. Maeda, *Macromolecules* **2008**, 41, 3-12.
 14. Lam J. W. Y., Tang B. Z., *Acc. Chem. Res.* **2005**, 38, 745.
 15. Zhao H., Sanda F., Masuda T., *J. Polym. Sci., Part A; Polym. Chem.* **2005**, 43, 5168.
 16. Okoshi K., Sakajiri K., Kumaki J., Yashima E., *Macromolecules* **2005**, 38, 4061.
 17. Cheuk K. K. L., Lam J. W. Y., Chen J., Lai L. M., Tang B. Z., *Macromolecules* **2003**, 36, 5947.
 18. S. M. Langenegger, R. Häner, *Chem. Commun.* **2004**, 2792-2793.

Chapter 6: Conclusions and Outlook

This work presents a study of interstrand and intrastrand stacking interactions of DNA containing stretches of pyrene building blocks. Pyrene was an ideal candidate for probing the stacking interactions due to its spectroscopic properties such as long wavelength absorption and fluorescence properties. Replacement of two or more base pairs by non-nucleosidic pyrene building blocks had a positive effect on the stability of hybrids. This has been attributed to favorable stacking interactions within duplex and single strands. In addition replacement of six and seven base pairs by respectively twelve and fourteen consecutive achiral pyrene moieties has given rise to specific interstrand helical arrangement. The observed interstrand helical folding embedded in a double-stranded DNA molecule has been shown by fluorescence and CD spectroscopy. Based on this specific property of an oligopyrene embedded in a DNA scaffold, the focus was then on using it in alternative systems consisting of a poly (dA)·(dT) framework and a short DNA scaffold. In all systems, oligopyrene strands self-organized and adopted an interstrand helical stack showing that the right-handed helical arrangement is largely driven by hydrophobic interactions and likely by the presence of amide-type linkers independently of the kind of DNA framework. Therefore, in order to go in more details, one hybrid containing fourteen achiral pyrene building blocks and only one G≡C base pair has been studied. Supported by fluorescence and CD spectroscopy, it was shown that the oligopyrene strands are highly sensitive to the chiral environment of either G or C or G≡C base pair. One oligopyrene strand adopted a right-handed helical orientation whereas the complementary strand adopted a left-handed helical orientation. However the question still remains whether oligopyrene within one strand self-arranges or if two identical oligomers intertwine to form a double helical structure which allows much more extensive intermolecular stacking interactions.

In conclusion the findings and the unique feature linked to only a G≡C base pair which provide a dynamic helical oligomer are very attractive for the design of novel intelligent materials and might provide the basis for applications in the area of molecular electronics, diagnostics as well as in nanotechnology.

Further studies derived from this work can go in various directions. One possibility is to use the preliminary investigation of stretches of non-nucleosidic phenanthroline building blocks described in *Annex I*, to form heterogeneous hybrids. Firstly the idea is to study the stability of those hybrids and secondly to monitor the influence of phenanthroline on pyrene and then to examine whether this specific combination provides well-ordered arrangement.

The findings described here may serve also to expand the specific well-ordered arrangement of pyrene moieties to the triple helix. One possibility is using poly (dA)·(dT) wherein pyrene building blocks have been already incorporated and studied. Furthermore, it exists a range of reports which describe natural triple-helix (dA)·2(dT) formation induced with MgCl₂ at neutral pH. Therefore, based on those references, the idea is to study the triple-helix (dA)·2(dT) formation and the behavior of twenty one consecutive achiral pyrene building blocks in a triple helix environment. It can be expected that they provide an interstrand helical arrangement which would be monitored by fluorescence and CD spectroscopy.

```
( 5 ' )  TTT  TTT  TSS  SSS  SST  TTT  TTT
( 5 ' )  AAA  AAA  ASS  SSS  SSA  AAA  AAA
( 3 ' )  TTT  TTT  TSS  SSS  SST  TTT  TTT
```

Schematic representation of an *oligopyrene-stack* embedded within a poly-d(A)·2(dT) triplex.

Annexes

Annex I: Properties of DNA Containing Non-nucleosidic Phenanthroline Building Blocks.

1. Abstract

Simple, non-nucleosidic phenanthroline-derivatives have been synthesized and incorporated into DNA. The modified oligomers form stable hybrids. Thermal denaturation experiments show that the double strands containing the phenanthroline-derivatives are more stable in comparison to the unmodified DNA duplex if one or two base pairs are replaced. However replacement of three or seven base pairs shows a slight reduction in hybrid stability. Hybridization of complementary strands is also supported by circular dichroism spectroscopy.

2. Introduction

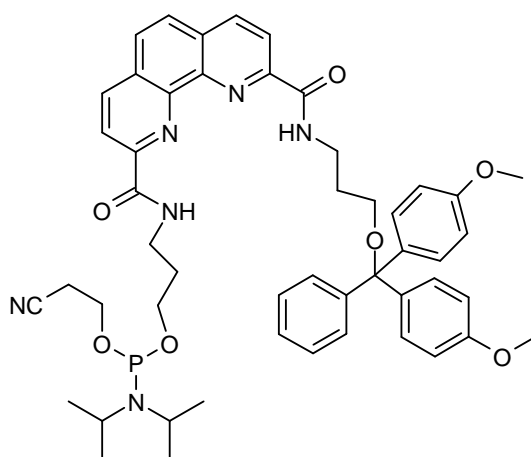
Modified nucleotides enjoy widespread interest as diagnostics and tools.^{1,2} In addition, the generation of defined molecular architectures using nucleic acids as building blocks is a research topic of high interest.³⁻⁸ The repetitive and well defined structural features of nucleic acids and related types of oligomers render them valuable building block for the generation of nanometer sized structures.⁹ The combination of natural oligonucleotide with novel synthetic building blocks lead to a large increase in the number of possible constructs and application.^{10,11} Recently, the synthesis and properties of non-nucleosidic, phenanthrene-based building blocks and their incorporation into DNA were reported.^{12,13} These building blocks can serve as base surrogates allowing hybridization of complementary strands without significant destabilization of the duplex. Replacement of two or more base pairs by non-nucleosidic phenanthrene building blocks was well

tolerated having almost no influence on hybrid stability compared to an unmodified duplex.¹⁴

The attempt of the work described in this report is to further replace two or more base pairs by non-nucleosidic phenanthroline building blocks and to study the stability of the hybrids.

3. Results and discussion

The required phenanthroline building block with a three-carbon linker (Scheme I.1) has been synthesized according to a published procedure.^{15, 16}



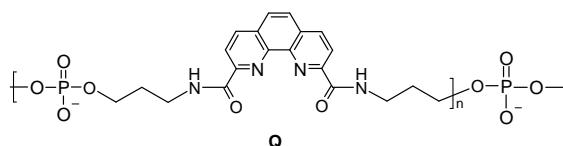
Scheme I.1 Phosphoramidite phenanthroline derivative building block.

Then the phosphoramidite phenanthroline derivative was used for the synthesis of oligonucleotides. Assembly of oligomers involved in automated oligonucleotide synthesis, the crude oligomers were purified by reverse phase HPLC and their identity was verified by mass spectrometry.

The hybrids were tested by thermal denaturation experiments. Oligonucleotides **1** and **2** serve as control and oligomers contain between one and seven phenanthroline building blocks per strand.

Table I.1 Influence of non-nucleosidic phenanthroline building blocks on hybrid stability. ^[a]

Oligo #	duplex ^[a]	T _m (°C) exp. ^[b]	ΔT _m calc. ^[c]	ΔT _m , °C ^[d]
1	(5') AGC TCG GTC ATC GAG AGT GCA	71.0	71.0	-
2	(3') TCG AGC CAG TAG CTC TCA CGT			
3	(5') AGC TCG GTC AQC GAG AGT GCA	73.4	69.9	+3.5
4	(3') TCG AGC CAG TQG CTC TCA CGT			
5	(5') AGC TCG GTC QQC GAG AGT GCA	74.8	68.4	+6.4
6	(3') TCG AGC CAG QQG CTC TCA CGT			
7	(5') AGC TCG GTQ QQC GAG AGT GCA	69.4	52.6	+16.8
8	(3') TCG AGC CAQ QQG CTC TCA CGT			
9	(5') AGC TCQ QQQ QQQ GAG AGT GCA	63.8	32.7	+31.1
10	(3') TCG AGQ QQQ QQQ CTC TCA CGT			



[a] 1.0 μM each strand, 10 mM phosphate buffer, pH 7.0); [b] experimental value; average of three independent experiments; exp. error +/-0.5°C; [c] T_m value calculated for the corresponding hybrid formed by the two strands without contribution of the unnatural building blocks according to the method described by *Markham and Zuker*¹⁹; [d] difference between experimental and calculated T_m value; this number corresponds to the contribution of the phenanthroline residues to the overall duplex stability.

Table I.1 shows the experimental *T_m* (melting temperature) values as well as the theoretical values for the corresponding hybrids without any contribution from the phenanthroline residues. The latter value, which was calculated according Markham and Zuker¹⁹, allows an estimation of the influence of the phenanthroline groups to the overall stability (Δ*T_m*). The phenanthroline residues have a large positive effect on the *T_m* value

of the respective hybrids. Moreover the hybrids show a highly cooperative melting curve (Figure I.1).

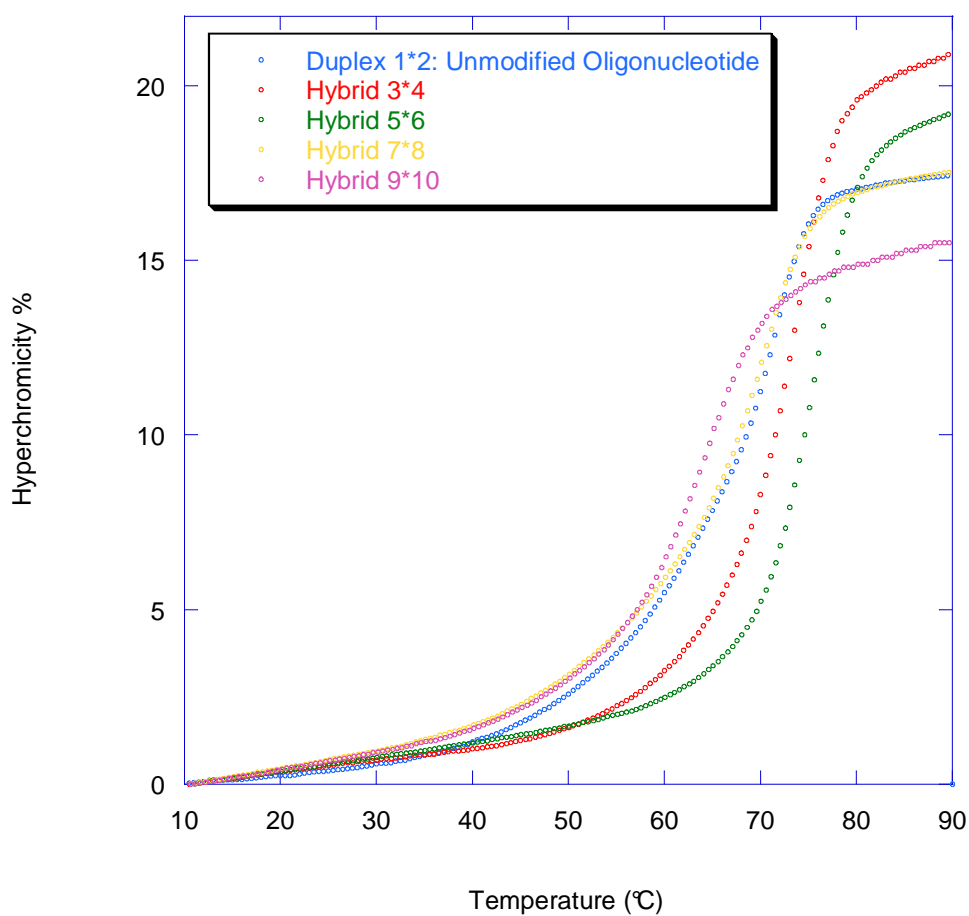


Figure I.1 Representative thermal melting curve of hybrids containing phenanthroline building blocks.

In addition, the circular dichroism spectra (CD) of the hybrids investigated are all in agreement with a B-form duplex. The CD spectra of hybrids are shown in Figure I.2.

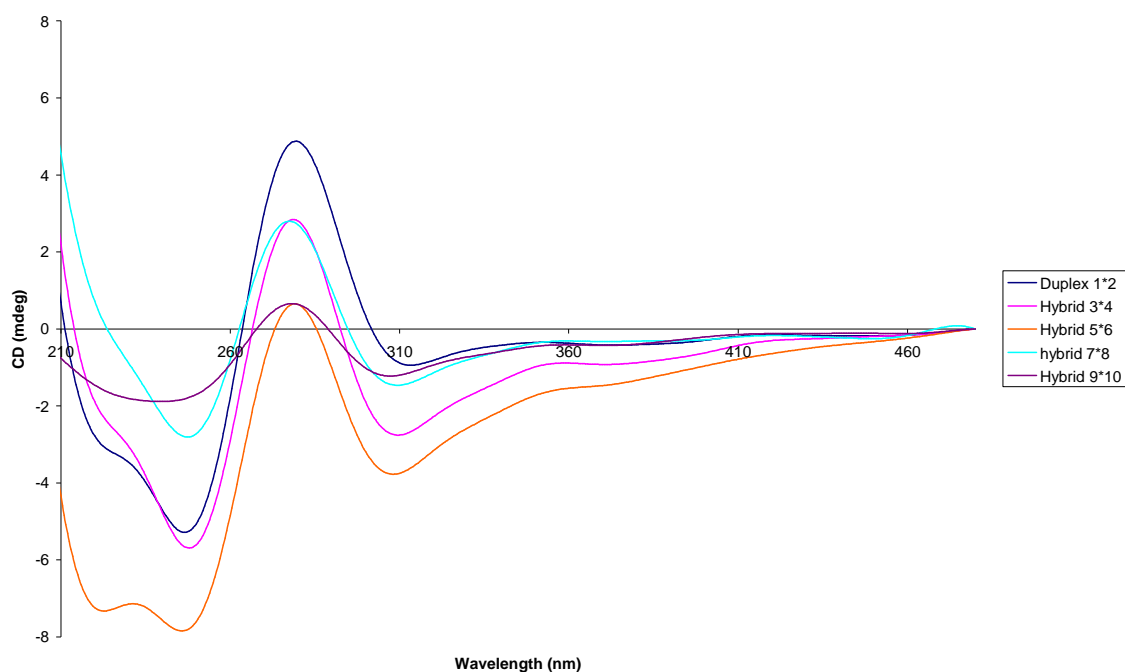


Figure I.2 CD spectra of hybrids containing non-nucleosidic phenanthroline residues

4. Conclusion

In conclusion, non-nucleosidic phenanthroline building blocks are well tolerated in duplex DNA. In agreement with the work reported in our group¹⁶, replacement of one and two base pairs with phenanthroline building blocks lead to the increase in T_m . In addition replacement of three or seven base pairs forms stable duplexes resulting in stronger interstrand stacking interactions. However the spectroscopic properties of phenanthroline are limited. Within the set of building blocks that we have been used¹⁴⁻¹⁶ the pyrene molecule is an ideal candidate for probing the stacking interactions and thus to investigate the self organization of single stranded nucleic acids into double helical structures.¹⁸

5. Experimental Section

The required phenanthroline building block with a three-carbon linker has been synthesized according to a published procedure.¹⁶ Nucleoside phosphoramidites from *Transgenomic* (Glasgow, UK) were used for oligonucleotide synthesis. Oligonucleotides **1-10** were prepared *via* automated oligonucleotide synthesis by a standard synthetic procedure ('trityl-off' mode) on a 394-DNA/RNA synthesizer (*Applied Biosystems*). Cleavage from the solid support and final deprotection was done by treatment with 30% NH₄OH solution at 55°C overnight. All oligonucleotides were purified by reverse phase HPLC (LiChrospher 100 *RP-18*, 5µm, Merck), *Bio-Tek Instruments Autosampler 560*); eluent A = (Et₃NH)OAc (0.1 M, pH 7.4); eluent B = MeCN; elution at 40°C; gradient 5 – 20% B over 30 min.

Molecular mass determinations of oligonucleotides were performed with a Sciex QSTAR pulsar (hybrid quadrupole time-of-flight mass spectrometer, *Applied Biosystems*). ESI-MS (negative mode, CH₃CN/H₂O/TEA) data of compounds **1-10** are presented in Table I.2.

Table I.2 Mass spectrometry data (molecular formula, calc. average mass, and obtained).

Oligo.		Molecular formula	Calc. aver.mass	Found
1	(5') AGC TCG GTC ATC GAG AGT GCA	C ₂₀₅ H ₂₅₇ N ₈₃ O ₁₂₃ P ₂₀	6471.3	6472
2	(3') TCG AGC CAG TAG CTC TCA CGT	C ₂₀₃ H ₂₅₈ N ₇₆ O ₁₂₅ P ₂₀	6382.2	6383
3	(5') AGC TCG GTC AQC GAG AGT GCA	C ₂₁₅ H ₂₆₅ N ₈₅ O ₁₂₂ P ₂₀	6611.5	6612
4	(3') TCG AGC CAG TQG CTC TCA CGT	C ₂₁₃ H ₂₆₇ N ₇₅ O ₁₂₆ P ₂₀	6513.4	6514
5	(5') AGC TCG GTC QQC GAG AGT GCA	C ₂₂₅ H ₂₇₄ N ₈₄ O ₁₂₃ P ₂₀	6742.7	6743
6	(3') TCG AGC CAG QQG CTC TCA CGT	C ₂₂₃ H ₂₇₅ N ₇₇ O ₁₂₅ P ₂₀	6653.6	6654
7	(5') AGC TCG GTQ QQC GAG AGT GCA	C ₂₃₆ H ₂₈₃ N ₈₅ O ₁₂₃ P ₂₀	6897.9	6899
8	(3') TCG AGC CAQ QQG CTC TCA CGT	C ₂₃₃ H ₂₈₄ N ₇₆ O ₁₂₅ P ₂₀	6768.8	6770
9	(5') AGC TCQ QQQ QQQ GAG AGT GCA	C ₂₇₇ H ₃₁₈ N ₈₆ O ₁₂₂ P ₂₀	7423.6	7425
10	(3') TCG AGQ QQQ QQQ CTC TCA CGT	C ₂₇₅ H ₃₂₀ N ₇₆ O ₁₂₆ P ₂₀	7325.5	7324.5

Thermal denaturation experiments (1.0 μM oligonucleotide concentration (each strand), 10 mM Phosphate buffer (pH 7.0), and 100 mM NaCl) were carried out on *Varian Cary-100 Bio-UV/VIS* spectrophotometer equipped with a *Varian Cary-block* temperature controller and data were collected with *Varian WinUV* software at 245, 260 and 354nm (cooling-heating-cooling cycles in the temperature range of 10-90°C, temperature gradient of 0.5°C/min). Data were analyzed with *Kaleidagraph*[®] software from ©*Synergy Software*. Temperature melting (T_m) values were determined as the maximum of the first derivative of the smoothed (window size 3) melting curve.

Temperature dependent UV-VIS spectra were collected over the range of 210-500nm at 10-90°C with a 10°C interval on *Varian Cary-100 Bio-UV/VIS* spectrophotometer equipped with a *Varian Cary-block* temperature controller. All experiments were carried out at a 1.0 μM oligonucleotide concentration (each strand) in Phosphate buffer (10 mM) and NaCl (100 mM) at pH=7.0. The cell compartment was flushed with N_2 to avoid water condensation at low temperature.

CD spectra were recorded on a *JASCO J-715* spectrophotometer using quartz cuvettes with an optic path of 1 cm.

6. References

1. Verma, S.; Jager, S.; Thum, O.; Famulok, M. *Chemical Record* **2003**, *3*, 51-60.
2. Kohler, O.; Jarikote, D. V.; Singh, I.; Parmar, V. S.; Weinhold, E.; Seitz, O. *Pure and Applied Chemistry* **2005**, *77*, 327-338.
3. Seeman, N. C. *Nature* **2003**, *421*, 427-431.
4. Samori, B.; Zuccheri, G. *Angew.Chem.Int.Ed.* **2005**, *44*, 1166-1181.
5. Shih, W. M.; Quispe, J. D.; Joyce, G. F. *Nature* **2004**, *427*, 618-621.
6. Mirkin, C. A. *Inorg.Chem.* **2000**, *39*, 2258-2272.
7. Chworos, A.; Severcan, I.; Koyfman, A. Y.; Weinkam, P.; Oroudjev, E.; Hansma, H. G.; Jaeger, L. *Science* **2004**, *306*, 2068-2072.
8. Claridge, S. A.; Goh, S. L.; Frechet, J. M. J.; Williams, S. C.; Micheel, C. M.; Alivisatos, A. P. *Chemistry of Materials* **2005**, *17*, 1628-1635.
9. Wengel, J. *Org.Biomol.Chem.* **2004**, *2*, 277-280.
10. Eschenmoser, A. *Chimia* **2005**, *59*, 836-850.
11. Herdewijn, P. *Biochim.Biophys.Acta, Gene Struct.Expr.* **1999**, *1489*, 167-179.
12. Langenegger, S. M.; Häner, R. *Helv.Chim.Acta* **2002**, *85*, 3414-3421.
13. Langenegger, S. M.; Bianke, G.; Tona, R.; Häner, R. *Chimia* **2005**, *59*, 794-797.
14. Langenegger, S. M.; Häner, R. *ChemBioChem* **2005**, *6*, 2149-2152.
15. Chandler C. J.; Deady L. W.; Reiss J. A., *J. Heterocycl. Chem.* **1981**, *18*, 599-601.
16. Langenegger, S. M.; Häner, R. *Tetrahedron Lett.* **2004**, *45*, 9273-9276.
17. Langenegger, S. M.; Häner, R. *Chem.Commun.* **2004**, 2792-2793.
18. Samain, F.; Malinovskii, V. L. ; Langenegger, S. M. ; Häner, R. *Bioorg. Med. Chem.* **2008**, *16*, 27-33.
19. Markham, N. R.; Zuker, M.; *Nucl. Acids Res.*, web server issue **2005**, W577-W581.

Annex II: Solid Phase Synthesis of Oligonucleotides

All of the synthesized oligonucleotides were prepared using an automated DNA synthesizer and on a 1.0 μM scale (392 DNA/RNA Synthesizer, *Applied Biosystems*) using standard solid phase phosphoramidite chemistry (Figure II.1).

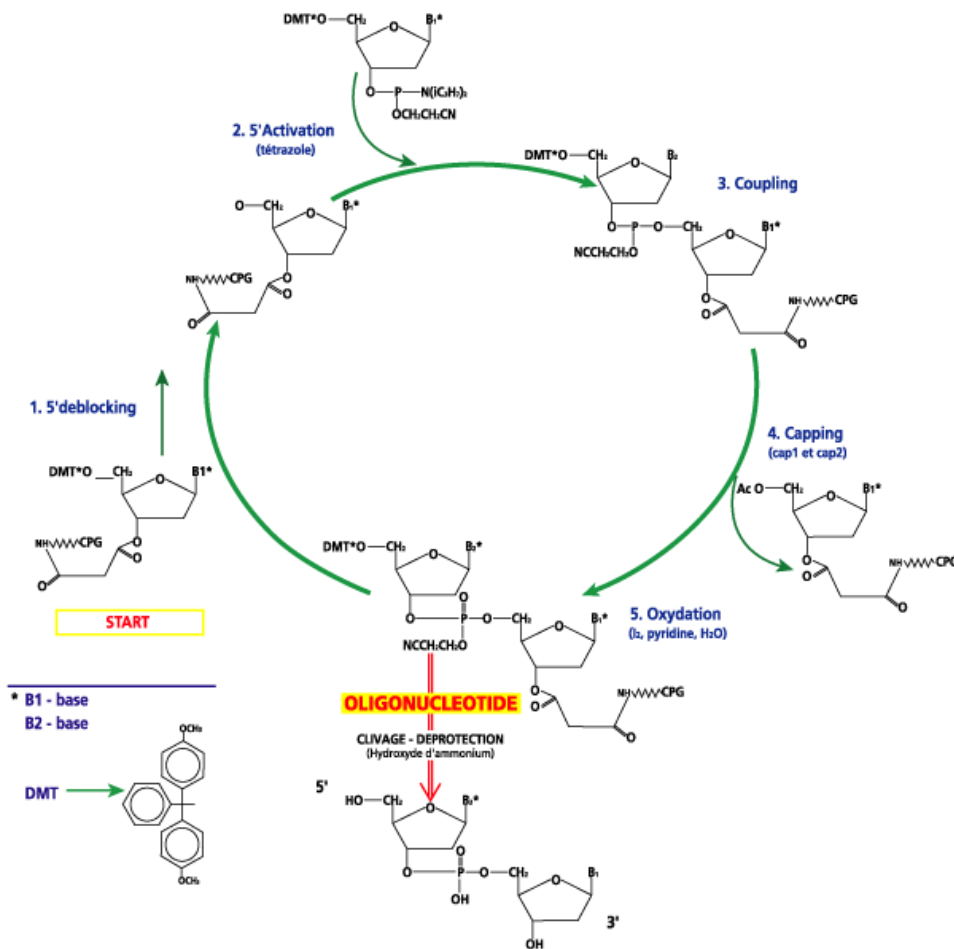


Figure II.1 Solid phase oligonucleotide synthesis cycle with standard phosphoramidite chemistry.

This method for oligonucleotide synthesis is applied in most laboratories due to its high efficiency and rapid coupling, as well as the stability of starting materials.

The first base is linked to the CPG (controlled pore glass) solid support at its 3'-end. The solid support is loaded into the reaction column. In each step, the solutions will be

pumped through the column. The reaction column is attached to the reagent delivery lines and the nucleic acid synthesizer. Each new base is added via computer control of the reagent delivery.

Step 1: De-blocking (Detritylation)

The first base is at first inactive because all the active sites have been blocked or protected. To add the next base, the DMT group protecting the 5'-hydroxyl group must be removed. This is done by adding an acid, in our case 3% of trichloroacetic acid in dichloromethane (DCM), to the reaction column. The 5'-hydroxyl group is now the only reactive group on the base monomer. This ensures that the addition of the next base will only bind to that site. The reaction column is then washed to remove any extra acid and by-products.

Step 2: Base Condensation (Coupling)

The next base monomer cannot be added until it has been activated. This is achieved by adding tetrazole (0.45M in CH₃CN) to the base. Tetrazole cleaves off one of the groups protecting the phosphorus linkage. This base is then added to the reaction column. The active 5'-hydroxyl group of the preceding base and the newly activated phosphorus bind to loosely join the two bases together. This forms an unstable phosphite linkage. The reaction column is then washed to remove any extra tetrazole, unbound base and by-products.

Step 3: Capping

When the activated base is added to the reaction column some does not bind to the active 5'-hydroxyl site of the previous base. If this group is left unreacted in a step it is possible for it to react in later additions of different bases. This would result in an oligonucleotide with a deletion. To prevent this from occurring, the unbound, active 5'-hydroxyl group is capped with a protective group which subsequently prohibits that strand from growing again. This is done by adding acetic anhydride in THF/Pyridine (Cap A solution) and N-

methylimidazole in same solvents (Cap B solution) to the reaction column. These compounds only react with the 5'-hydroxyl group. The base is capped by undergoing acetylation. The reaction column is then washed to remove any extra acetic anhydride or N-methylimidazole.

Step 4: Oxidation

In step 2 the next desired base was added to the previous base, which resulted in an unstable phosphite linkage. To stabilize this linkage a solution of dilute iodine (0.02M in THF/water/pyridine) is added to the reaction column. The unstable phosphite (+III) linkage is oxidized to form a much more stable phosphate (+V) linkage.

Repeat

Steps one through four are repeated until all desired bases have been added to the oligonucleotide. Each cycle is approximately 98/99% efficient.

Post Synthesis

After all bases have been added the oligonucleotide must be cleaved from the solid support and deprotected before it can be effectively used. This is done by incubating the chain in concentrated ammonia (33% in water) at a high temperature for an extended amount of time (55°C over night). All the protecting groups are now cleaved, including the cyanoethyl group, the heterocyclic protection groups, and the DMT group on the very last base. All the oligomers synthesized were purified, mostly by RP-HPLC and their identities are proven by negative electrospray mass spectrometry.

Annex III: Fluorescence Properties of Pyrene

Throughout this work, pyrene has been used as a tool for studying the architecture of the oligonucleotides described. This annex will briefly explain the fundamentals of pyrene monomer and excimer fluorescence.

Upon excitation at 350-360nm, pyrene molecules emit a fluorescent signal with a maximum in the range 390nm-400nm, which is called “monomer fluorescence” since its nature lies in the relaxation of a single excited molecule. The origin of fluorescent signal is described in Figure III.1. Upon absorption of a photon, the molecule is put into an electronically excited state, usually also a state of higher vibrational energy. In this excited state, the molecule can collide with its environment which allows for some shedding of kinetic energy in the form of heat without photon emission. In this way, the molecule ladders down vibrational modes until, at some point, it undergoes a spontaneous emission of a photon (fluorescence) bringing the molecule back to the ground state.

The emitted photon is of a lower energy than the absorbed photon since, as described, some of the absorbed energy is lost through relaxation decay. Therefore the wavelength of the emitted light is higher than the one of the absorbed as shown in Figure III.1a and b.

The special interest of pyrene lies in its ability to form excited dimers (*excimers*). As defined by *Birks*, an excimer is a dimer which is associated in an electronic excited state and which is dissociative in its ground state.¹ This would require for the pyrenes to be sufficiently separated at the point of light absorption so that the excitation is localized to one of them. As

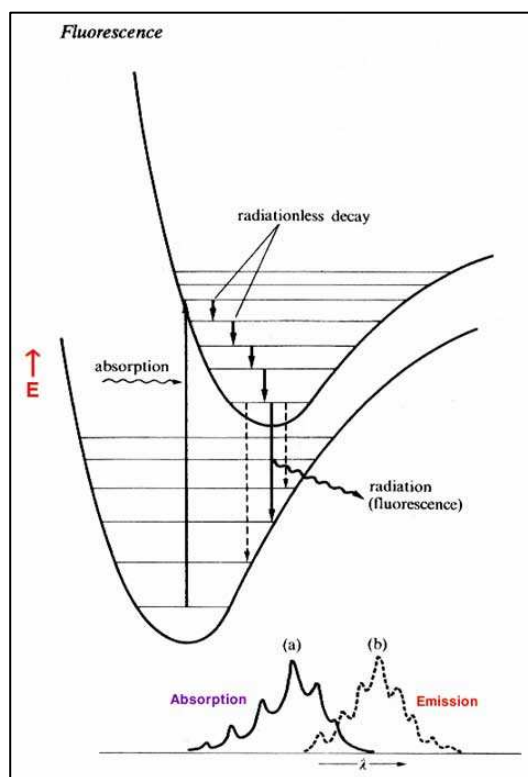


Figure III.1 Energy diagrams of the ground and excited states; a) absorption spectrum b) emission spectrum

described by *Winnik*, this definition refers to what can be described as “dynamic excimers”, where excited dimer formation is possible only through the prior excitation of one of the monomer pyrene units.² In contrast, *Winnik* also defines “static excimers”, characterized by the pre-organization of pyrenes prior to excitation.

Moreover, the term excimer is used to describe excited dimers formed from molecules of the same species, whereas heterodimeric species (like the pyrene and phenanthrene dimer) are referred to as *exciplexes*.

Figure III.2 depicts excimer formation of pyrenes dissolved in ethanol. Depending on concentration of pyrene in ethanol, we observe a rise of the excimer signal with a maximum in the area 460-500 nm. With the decrease of concentration, the likelihood that an excited pyrene molecule will encounter another is reduced.

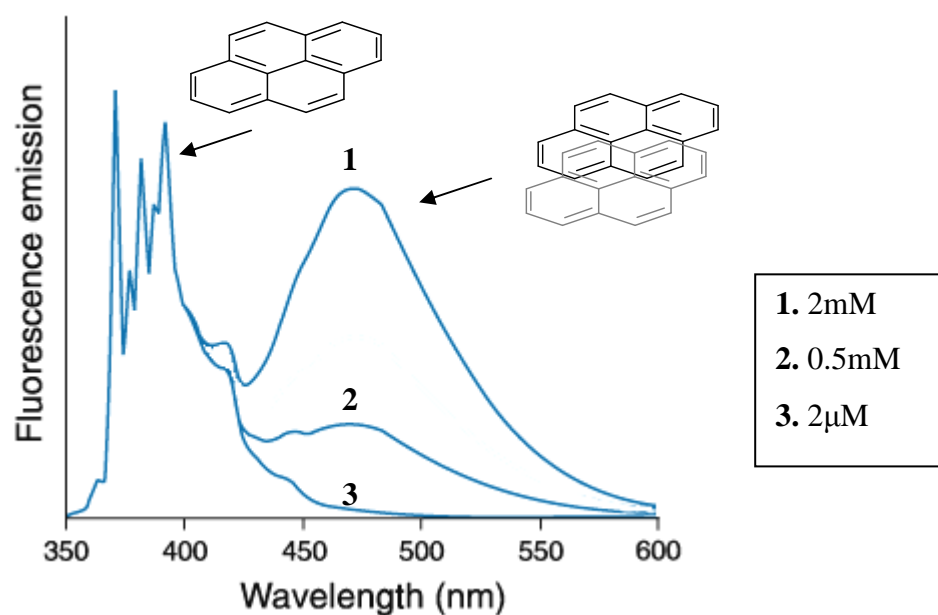


Figure III.2 Formation of pyrene excimers in ethanol. Excitation wavelength: 353nm. (Adopted from³).

The necessity of bringing pyrenes into proximity to give rise to excimer formation renders them very useful for our research. We were able to gain valuable information on the molecular architecture of duplex mimics by monitoring pyrene excimer formation. As shown in Figure III.3, the dissociation of duplex was followed by monitoring the decrease of the excimer signal at 500nm as well as the trend of the maximum of fluorescence intensity.

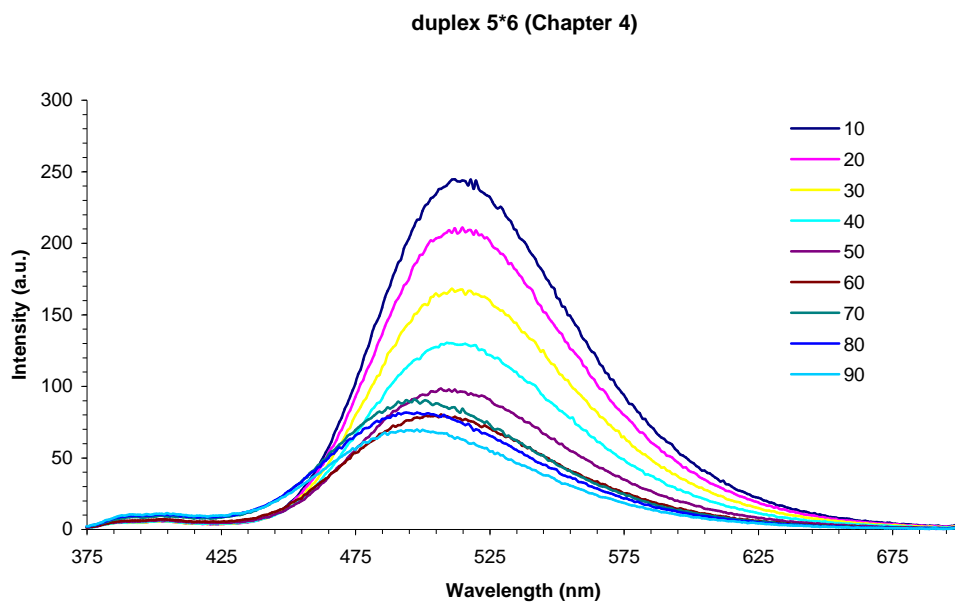


Figure III.3 Fluorescence spectra of duplex 5*6.

References:

1. Birks J.B., Rep. Prog. Phys. **1975**, 38, 903.
2. Winnik F.M., Chem. Rev. **1993**, 93, 587
3. <http://probes.invitrogen.com/handbook/figures/0917.html>

Annex IV: CD Spectroscopy and Study of Duplex Formation

Circular dichroism (CD) measurements are used to determine the conformation of nucleic acids in solution. This technique is based on the difference in absorbance of left and right circularly polarized light that results from the chirality of the molecule we are investigating.

Due to their absorbance properties, pyrene is responsible for a specific CD signal in 350 nm and 245 nm areas. When the CD spectrum of the hybrids is compared to that of the unmodified oligonucleotide, changes can be attributed to a conformational change of the pyrenes into DNA.

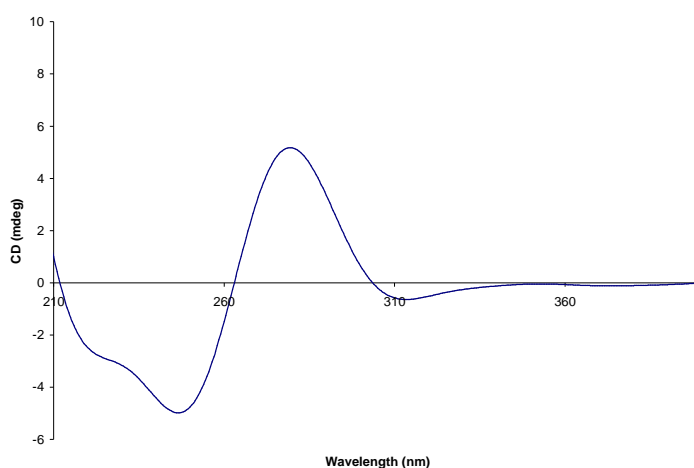


Figure IV.2. CD spectrum of a typical B-DNA

As a consequence, replacement of nucleosides by pyrene building blocks may influence the CD spectrum of hybrids. As shown in Figure IV.2, the arrangement of pyrenes within duplex was followed by monitoring the dichroism of the pyrene bands.

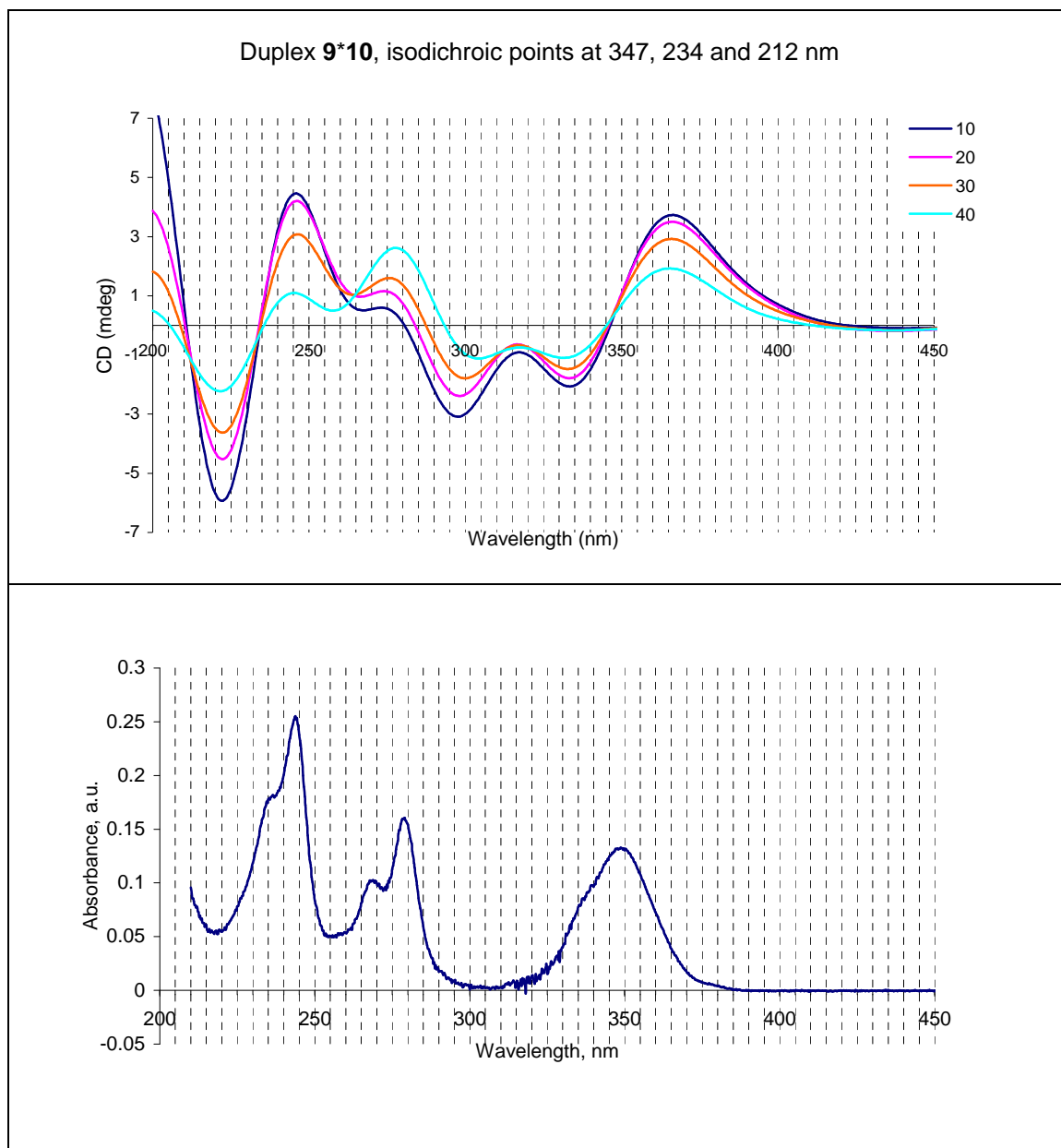
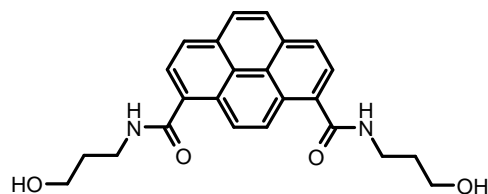


Figure IV.3 a) Isodichroic points for duplex **9*10** (see Chapter 4); 10-40 °C; b) UV-Vis spectrum of the pyrene building block (10^{-6} M) in phosphate buffer solution (pH = 7.0) at 20 °C.

Annex V: X-Ray crystallography

(Dr. Antonia Neels, X-Ray Diffraction Service, Institut de microtechnique, Université de Neuchâtel)



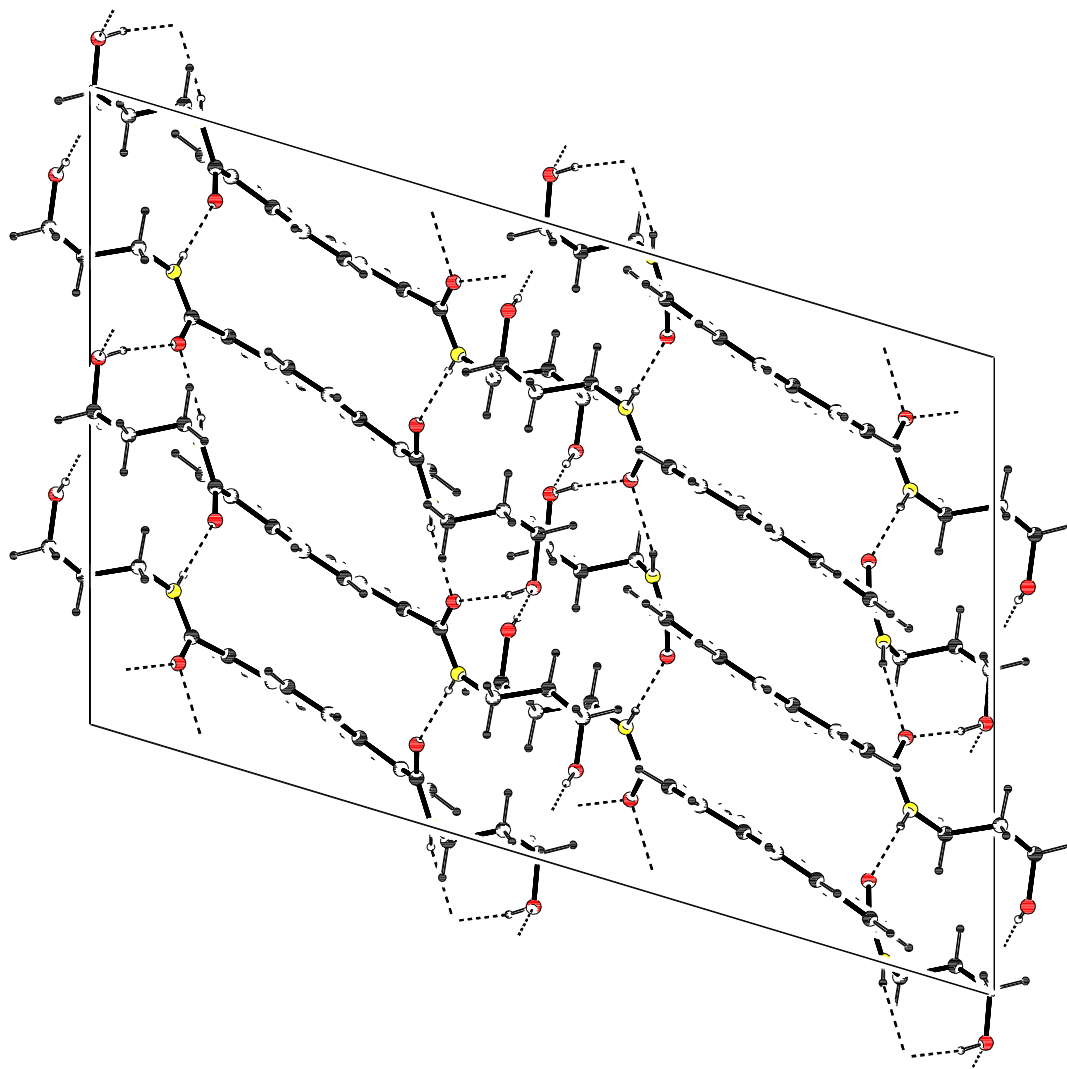
Pyrene-1,8-dicarboxylic acid bis-[(3-hydroxy-propyl)amide]

A light yellow crystal of compound PYRENE was mounted on a Stoe Mark II-Image Plate Diffraction System [1]. The intensity data were collected at 173K (-100°C) using MoK α graphite monochromated radiation, Image plate distance 100mm, ω oscillation scans 0 - 180° at ϕ 0°, 2 θ range 2.29 – 59.53°, d_{\max} - d_{\min} = 17.78 - 0.72 Å.

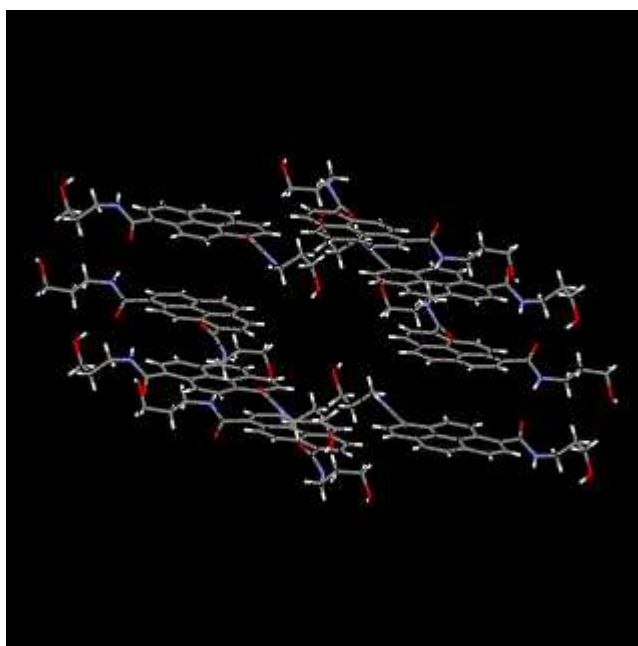
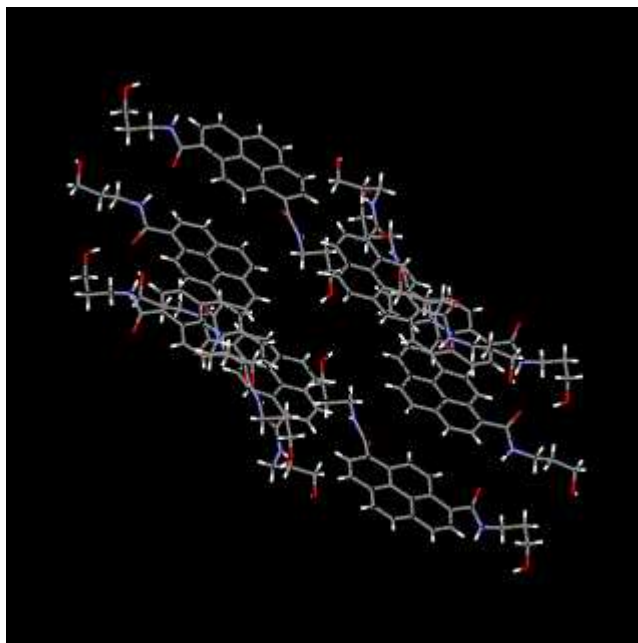
The compound crystallises in the centrosymmetric monoclinic space group C2/c, the molecular formula is [C₂₄H₂₄N₂O₄].

The structure was solved by Direct methods using the programme SHELXS-97 [2]. The refinement and all further calculations were carried out using SHELXL-97 [3]. All hydrogen atoms were included in calculated positions and treated as riding atoms using SHELXL-97 default parameters. The non-H atoms were refined anisotropically, using weighted full-matrix least-squares on F². The program PLATON [4] was used for molecular drawings. No absorption correction was applied.

- 1 Stoe & Cie (2002). *X-Area V1.17 & X-RED32 V1.04 Software*. Stoe & Cie GmbH, Darmstadt, Germany.
- 2 G. M. Sheldrick, (1990) "SHELXS-97 Program for Crystal Structure Determination", *Acta Crystallogr.*, **A46**, 467-473.
- 3 G. Sheldrick, (1999) "SHELXL-97", Universität Göttingen, Göttingen, Germany.
- 4 Spek, A. L. (2003). *J.Appl.Cryst.* **36**, 7-13.



Packing diagram showing hydrogen bonds (N – yellow, O – red),
made by A. Neels, University of Neuchâtel, Switzerland.



Representative pictures of X-ray for the pyrene building block.

Table IV 1. Crystal data table for pyrene.

Identification code	pyrene
Crystal shape	block
Crystal colour	yellow
Crystal size	0.45 x 0.45 x 0.45 mm
Empirical formula	C ₂₄ H ₂₄ N ₂ O ₄
Formula weight	404.45
Crystal system	Monoclinic
Space group	C 2/c
Unit cell dimensions	a = 17.0374(6) Å alpha = 90 deg. b = 9.6090(5) Å beta = 106.742(3) deg. c = 25.1817(10) Å gamma = 90 deg.
Volume	3947.8(3) Å ³
Cell refinement parameters	
Reflections	35752
Angle range	1.69 < theta < 29.63
Z	8
Density (calculated)	1.361 g/cm ³
Radiation used	MoK α
Wavelength	0.71073 Å
Linear absorption coefficient	0.093 mm ⁻¹
Temperature	173(2) K

Florent SAMAIN

Nationality French
Date of Birth June 1st, 1978
Home address Sulgenrain 22, 3C
CH-3007 Bern Switzerland

Phone number Home : +41 31 534 52 19 / Mobil : +41 78 713 53 08
E-Mail florent@samain.com

❖ Work Experience

2005-2008

July to May:

Ph.D under the guidance of Pr. Dr. Robert Häner, Department of Chemistry and Biochemistry, University of Bern, Switzerland.

Self-Assembly of DNA Containing Non-nucleosidic Polyaromatic Building Blocks;

<http://www.dcb-server.unibe.ch/groups/haener/>

2004-2005

September to June

Polyphor Ltd: Laborant position, Basel, Switzerland

2004

April to September

Hoffmann-La-Roche: Industrial studentship in pre-clinical research with the team of Dr E. Kitas, Basel, Switzerland.

2003

April to September

Roche Vitamins Ltd: Industrial studentship in the Chemical Process Technology department with the team of Dr A. Gum, Basel, Switzerland.

❖ Teaching Experience

2008

Supervisor of a M. Sc. Student in organic chemistry, University of Bern.

2005-2007

Teaching assistant first and second year students in organic chemistry, University of Bern, Switzerland.

❖ Education

2005-2008 Ph.D in Organic Chemistry, Department of Chemistry and Biochemistry University of Bern, Switzerland.

2003-2004 DEA (Second year of M. Sc.) in Molecular Chemistry, University of Rennes 1, Rennes, France.

2001-2003 B. Sc. And M.Sc. in Organic Chemistry, University of Rennes 1, Rennes, France.

1999-2000 General University Studies Degree of physics and chemistry, University of Rennes 1, Rennes, France.

1997-1999 Two years in Medicinal Faculty, University of Rennes 1, Rennes, France.

❖ Publications

1. Helical Arrangement of Interstrand Stacked Pyrenes in a DNA Framework; V. Malinovskii, F. Samain, R. Häner; *Angew. Chem. Int. Ed.* **2007**, *46*, 4464-4467.
2. Spectroscopic properties of pyrene-containing DNA mimics; F. Samain, V. Malinovskii, S. M. Langenegger, R. Häner; *Bioorg. Med. Chem.* **2008**, *16*, 27-33.

❖ Skills and Techniques

Synthesis

Organic molecules, automated DNA synthesis.

Purification and characterization of products: (NMR (1D and 2D), MS spectrometry, IR, HPLC reverse phase, Fluorescence spectroscopy, CD spectroscopy, UV-vis spectroscopy.

Communication

Effective oral and written presentation skills developed via regular group meetings and department presentations. Ability to work in a team and in an international environment.

Software

KaleidaGraph, ChemOffice, Isis Draw, Microsoft Office, SciFinder, Beilstein.

❖ Languages

- French : Native language.
- English : Advanced level.
- Spanish : Basic Knowledge.